24. SEDIMENTOLOGY

A. O. Beall, Jr., Continental Oil Company, Ponca City, Oklahoma
and
A. G. Fischer, Department of Geology, Princeton University, Princeton, New Jersey

THE MAIN TYPES OF SEDIMENT

Visual examination of the cores and microscopic examination of smear slides of the wide variety of sediments cored on Leg 1 revealed an equal range of particle origins, modes of transport, and manner of deposition. These sediments may be considered under the following arbitrary headings:

- Organogenic pelagic sediments.
  - Nannoplankton chalks and marls.
  - Radiolarian mudstones and cherts.
  - Diatom and spicule clays.
- Turbidites.
  - Terrigenous turbidites.
  - Organogenic turbidites.
- Pebbly muds.
- Paraglacial terrigenous muds.
- Brown and red deep-sea clay.
- Other sediments–mainly volcanogenic.

These sections will be discussed in order, before considering other matters, such as: texture, mineral composition, sedimentary structures, physical properties, and diagenesis.

Nannoplankton Chalks and Marls

Chalks and marls composed largely of nannofossils (coccoliths, discoasters, etc.) are the most abundant types of sediment cored on Leg 1 (Plate 15, C & D; Plate 18, C-F). In parts of the Cretaceous of Sites 4 and 5, chalks composed largely of coccoliths are associated with chalks composed mainly of coccolith fragments (disaggregated sections of *Braarudosphaera* pentaliths, Plate 6D), and with other chalks in which the constituent particles are anhedral unicrystalline grains of calcite of uncertain origin. Such grains could conceivably be products of Coccolithophoridae; here they are treated along with the definite nannoplankton chalks.

The nannoplankton chalks of the Tithonian and early Cretaceous (Sites 4 and 5) contain moderate to large numbers of Radiolaria, generally calcitized (Plate 18, E & F). Planktonic foraminifera generally occur in the Cretaceous and younger chalks, but rarely (Plate 18, C & D) in quantities that would merit the term globigerina ooze.

The color of these chalks and marls ranges from white through cream to gray, greenish gray and bluish gray, and the deviation from white is generally a fair measure of clay content.

Burrowing of these chalks and marls is generally moderate to intense, but at Sites 4 and 5 parts of the Cretaceous sequence are somewhat carbonaceous, delicately laminated, and unburrowed. The Tithonian and Neocomian chalks here contain some chert.

Whereas some of these chalks and marls appear to have accumulated directly as the result of the normal "rain" of planktonic skeletons, others have been resedimented. The sequences cored contain many beds of calcarenite or calcisilt, which appear to have been derived from shelf or slope areas by turbidity currents, and which are discussed below. Each of these beds normally grades upward into nannoplankton chalk which appears depleted of larger planktonic foraminifera, but may be enriched by fine allochthonous debris such as tunicate spicules and fine skeletal fragments of uncertain origin. In some cases (Site 3) these chalks are cemented, contrasting with the normal pelagic ones; their tops may also be very heavily burrowed. The authors believe that these chalks were formed by the incorporation of pelagic sediment into turbidity currents, and their redeposition from that medium of transport: the coarser pelagic constituents were sedimented in the mainly allochthonous coarse base, while the coccoliths dominate the finer upper part of the turbidite.

The nannoplankton marls and chalks in the Cenozoic of Sites 4, 5, 6 and 7 (Plate 6, E & F; Plate 7, A & B) were almost certainly deposited as such resediments, inasmuch as they occur as interbeds in clayey or siliceous sequences which bear the signs of deposition below the carbonate compensation depth.

Radiolarian Mudstones and Cherts

The existence of radiolarian ooze in the Eocene of the Gulf of Mexico is made evident by clasts of such material in Pleistocene turbidites at Site 3. These are pure white, fluffy oozes; and, how they came to be incorporated in the turbidite remains uncertain.

Radiolarian mudstone and chert were cored in the Albian and Cenomanian of Site 5. These sediments are dark gray to black in hand specimen, and brown in transmitted light, and are quite carbonaceous. They are radiolarian-rich laminae alternating with clear chert bands. (Thin-sections are illustrated in Plate 19.) The cherts consist mainly of opaline material, in part in spheroidal accumulations, and chalcedony, but the radiolarian tests have commonly left pores. Mineralogy and petrology are discussed in more detail under the section on diagenesis.

We believe that the relatively pure radiolarian cherts and mudstones were deposited below the carbonate compensation depth. There are, however, sediments in which radiolarian remains are abundant in nannoplankton chalks (Tithonian and Neocomian of Sites 4 and 5, Plate 18, E & F). In such cases, there has commonly been an exchange of silica and carbonate, producing on the one hand limestones with calcitized Radiolaria, and on the other hand cherts with some Radiolaria in a secondary matrix of silica.

Diatom and Spicule Clays

The Middle Eocene sequence of Sites 6 and 7 contains abundant siliceous remains throughout: namely, sponge spicules, diatoms, Radiolaria and silicoflagellates, in order of abundance. Much of this section consists of silica-rich calcarenites and calcisiltites, and of silica-rich nannoplankton chalks, all of which appear to be of allochthonous (turbidite) origin (Plate 6, E & F; Plate 7, A, B, E & F; Plate 17, A & B; Plate 20) and is discussed below. Such graded units are normally separated by dark greenish clays with abundant diatoms, sponge spicules, radiolarian remains and silicoflagellates (Plate 7, C & D), which represent the finest sediments in the sequence and are non-calcareous (deposited slowly below compensation depth?) and heavily burrowed. These clays are the only beds in the sequence that could possibly be of straightforward pelagic origin.

At first glance, the nature of the diatoms in these beds is not consistent with this view. According to Dr. Lloyd Burkle of Lamont-Doherty Observatory (personal communication) the diatom flora contains an abundance of shallow water benthonic forms (*Melosira* and others). Since both the stratigraphic sequence (interposition of the diatom-bearing sequence between older and younger red deep-sea clays) and the sedimental nature of the Middle Eocene itself (graded beds, allochthonous nannoplankton chalks) essentially rule out an *in situ* shallow water episode, it is then concluded that the diatoms in this section—and specifically those of the turbidites as well as those of the diatomaceous clay units discussed here—were brought in from afar, possibly the North American shelf.

It is possible that these diatom-rich clays are a pelagic type of sediment, representing slow particle-by-particle type deposition, and that the abundance of allochthonous diatoms reflects mainly the ease with which diatom frustules can be carried and dispersed by ocean currents. On the other hand, the possibility cannot be fully ruled out that they represent, instead, the uppermost parts of turbidites, from which carbonate was removed (1) in the process of settling, and (2) by solution on the sea floor (Hollmann's subsolution, 1962).

Terrigenous Turbidites

Graded beds of dominantly terrigenous material were encountered in the Pleistocene sequence of Sites 1 and 2, in the Pliocene and especially the Miocene of Site 3. These beds are attributed to turbidite origin; they are discussed in more detail in the section reports, and below in the section on sedimentary structures. Examples are illustrated in Plate 3 (X radiographs), and Plate 12, E & F.

Organogenic Turbidites

One of the most common sediment types encountered on Leg 1 is skeletal calcarenite to calcisiltite, with sharp base, grading upward into nannoplankton chalk. Such sediments are particularly characteristic of (1) the Pliocene and early Pleistocene of Site 3 (where they also occur in the Miocene), (2) the Upper Cretaceous of Sites 4 and 5, and (3) the Eocene of Sites 6 and 7 (with terrigenous admixture).

These graded beds closely resemble the terrigenous sequence discussed in detail in the section on sedimentary structures. Some contain essentially no terrigenous debris, while others contain some quartz grains. The skeletal composition of these calcarenites-calcisilts varies with age, location and diagenesis, but in all cases, it appears to represent a mixture of shelf-derived material with pelagic deep-sea sediment.

(1) The Miocene-Pliocene-Pleistocene calcarenites-calcisilts of Site 3 contain benthonic foraminifera (rotalids, miliolids) of presumed shallow water origin (Plate 8A), bolivinas of presumed outer shelf or slope origin (Plate 8, A, B & D), and an assortment of planktonic foraminifera (Plate 8, A-F). Sponges are represented by a variety of siliceous spicules including spheroidal tetractinellid spicules and monaxons (Plate 8C). Coelenterates are represented in a few of these beds by gorgonian spicules. The most conspicuous molluscan element consists of isolated carbonate prisms with characteristic transverse growth banding (Plate 8C). Grains of echinoderm origin include spines and elements of echinoids, as well as, rare holothurian sclerites. Tunicates are ubiquitously and abundantly represented by burr-shaped and tetrahedral sclerites of the *Didemnidae.* In addition to such readily identifiable skeletal fragments there are large numbers of carbonate grains which could not be definitely assigned in terms of origin. Among these are homogeneous fine-grained lumps which might possibly represent pieces of codiacean algae, rare fragments of finely chambered foraminifera which are probably peneroplids, a single, poorly

preserved fragment of a coralline alga, and peloids of heterogeneous texture, which probably represent faecal pellets. Skeletal constituents include both calcite and aragonite.

The main geological question regarding these resediments concerns their initial site of sedimentation. Obviously this requires more detailed study than has been possible for this report. Some shelf organisms appear to be involved; however, the absence (or rarity) of algal-bored, micritized grains, the absence or scarcity of definite algal remains, and the comparative abundance of planktonic foraminifera and of the bolivinas suggest that the outer shelf and slope contributed much more than did the inner shelf. Also, the scarcity of large planktonic foraminifera in the overlying nannoplankton chalks suggests that considerable abyssal sediment was incorporated in, and sorted by, the currents which were responsible for these beds.

(2) Graded calcarenites of rather similar overall aspect are found in the Cretaceous sequence of Sites 4 and 5. These differ in detail in that their constituent grains are much less well-preserved. Foraminifera are present in all stages from preservation of sharply defined wall structure, to micritized walls, to micritic lumps barely recognizable as foraminifera, to micritic lumps of uncertain origin (Plate 17, E & F; Plate 18, A & B). Echinoderm debris is recognizable by its unit-crystal nature, but has lost most of its microstructure by permineralization and shows syntaxial overgrowth (Plate 17, C & D). Unlike the Miocene calcarenites which contain aragonitic material, the Cretaceous calcarenites are entirely calcitic with exception of some dolomite grains. These Cretaceous calcarenites are generally cemented by calcite. This cement takes three forms: (a) most grains are covered by a thin crust of fine, radially oriented, calcite crystals (Plate 17, E & F; Plate 18B); (b) echinoderm elements are overgrown with somewhat coarser syntaxial rim cement (Plate 17, C & D); (c) scattered through the calcarenite are comparatively coarse scalenohedra of calcite (Plate 17F; Plate 18, A & B) which grow around some of the grains, and are, therefore, distinctly younger than the deposition of the calcarenite.

The matter of alteration is taken up under the section on diagenesis. The greater alteration of the Cretaceous calcarenites can either be attributed to a much longer diagenetic history, or to contact with notably different solutions—presumably fresh water.

(3) A third type of largely organogenic turbidite occurs in the Eocene of the Bermuda Rise (Sites 6 and 7). One of these has been described in some detail by Beall (below). The primary constituent particles of these sands and silts are a mixture of quartz grains, glauconite grains, siliceous sponge spicules, and benthonic and planktonic foraminifera, with a minor admixture of diatoms, Radiolaria, ostracodes, and echinoderm debris. Some reworked Cretaceous foraminifera are present. Sands and silts of such composition are illustrated in Plates 14 and 17, A & B. They may become silicified to form cherts (Horizon A), illustrated in Plate 20. Such sands or silts grade upward into nannoplankton chalks rich in siliceous tests (Plate 6, E & F; Plate 7, A, B, E & F), which are assumed to represent the resedimentation of calcareous oozes, originally deposited on the slope or on shallower parts of the abyssal floor. Such sediment is overlain in turn by non-calcareous, diatom-bearing clays, which have been discussed above, and may represent true pelagic sedimentation at this site in Middle Eocene time. The turbidity currents responsible for these sedimentary patterns would seem to have originated on the North American shelf, where quartz sands and glauconites were being deposited through much of late Cretaceous, Paleocene and Eocene time.

Pebbly Mudstones

Pebbly mudstones of two types were recovered in the cores. In the intraformational type, harder lumps of material—generally mudstone—are embedded in a more watery matrix of otherwise similar composition. Such occurrences (Plate 5A) are probably attributable to disruption of the mudstone in the course of drilling—an interpretation documented on Leg 2 (Peterson and Edgar, personal communication).

In the exotic type of pebbly mudstone, clasts of foreign rock—mainly hard limestones, much more strongly altered than any of the deep water carbonates, and of reef to backreef origin to judge by fauna and lithic character—are scattered through a matrix ranging from nannoplankton chalk to clay. Such pebbly mudstones occurred at Sites 4 and 5, from the Albian upwards (see site reports). They seem best explained as rubble which caved off the edge of the Bahama Bank, became mixed with clay or nannoplankton ooze on the slope, and traveled seaward in the form of a mudflow. These pebbly mudstones are illustrated in Plate 12, F, H, & J, and in X radiographs in Plate 5, C-D.

Paraglacial Terrigenous Sediments

The Pleistocene drab-color mudstones and the associated silts and sands, cored almost throughout the hole at Site 1 and in the upper part of Site 3, are a peculiarly distinctive set of sediments. They range from massive to laminated ("laminite facies") at Site 1 (Plates 16 and 3), but contain good turbidite sands at Site 3 (Plates 4 & 5, described in detail by Beall, below). They are characterized by an almost total lack of fossils, and by their peculiarly immature mineral content, being essentially unweathered rock flour. The high carbonate content (normally one-quarter to one-third of the total) is not skeletal debris, but is detrital carbonate derived from the continent, X-ray analysis (Figure 5)

PLATE 1

Radiographs of selected cores, × *1.*

A Sample 4-1-4, 79.5-104 cm: Pleistocene brown deep-sea clay. The granular appearance of the radiograph is caused by the abundant ferric and pyrite granules in the clay, while the larger dark bodies are larger iron and manganese nodules.

B Sample 4-1-6, 80.5-105 cm: Pliocene or Pleistocene brown deep-sea clay, with Fe-Mn nodules of intermediate and large size.

C Sample 2-4-2, 49.5-74 cm: Early Pliocene coccolith ooze, faintly bedded, and strongly burrowed by small "worms". The burrows are X-ray opaque because of lining or filling by pyrite or marcasite. The segmentation of this sulfide filling may be partly due to localized growth of the mineral, and has no doubt been enhanced by some breakage and dislocation during compaction and mass movement of the sediment. The large amount of sulfide in this core (also expressed in a strong H_2S odor) is probably related to its proximity to the cap rock of the underlying salt dome.

D Sample 2-3-2, 80-104.5 cm: Late Pliocene coccolith ooze. The X-ray opaque grains are probably pyritic, and are probably localized in part in burrows, in part in cross-laminations?

PLATE 1

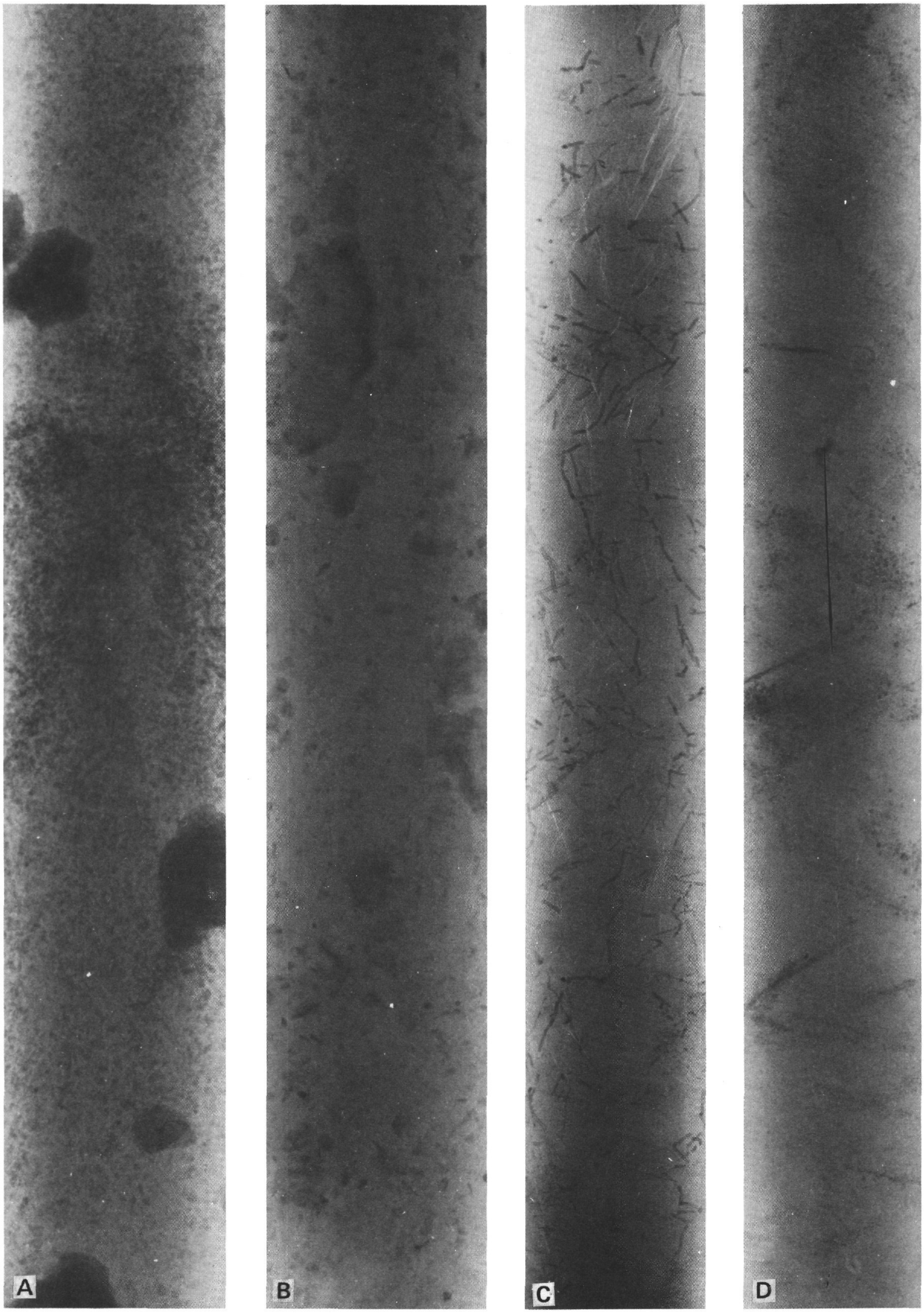

PLATE 2

X radiographs of cores × 1.

A Sample 3-6-2, 90-114.5 cm: Late Pliocene turbidite sequence, of calcarenites and calcisiltites derived from shallow water–Campeche Bank–(dark), grading upward into nannoplankton marl (light).

B Sample 3-6-2, 75.5-100 cm (partly overlaps A): Same as A, with calcarenite-filled burrows shown below base of upper turbidite.

C Sample 4-4-1, 78.5-103 cm: Firm Neocomian nannoplankton chalk, showing a faint graded bedding in upper part of picture (which was not apparent by visual inspection). A cross-laminated interval below middle. Dark blobs and segmented lines are pyritized worm burrows (cf. Plate 1, C).

D Sample 3-9-5, 114.5-129 cm: Late Miocene volcanic-rich mudstone, showing laminations partly disrupted by burrows which are generally not apparent in the X radiograph. Two thoroughly pyritized burrows are apparent near middle of picture, and the dark spots and lines in echelon, to the upper left, are probably one or more discontinuously pyritized burrows, partly collapsed by compaction.

PLATE 2

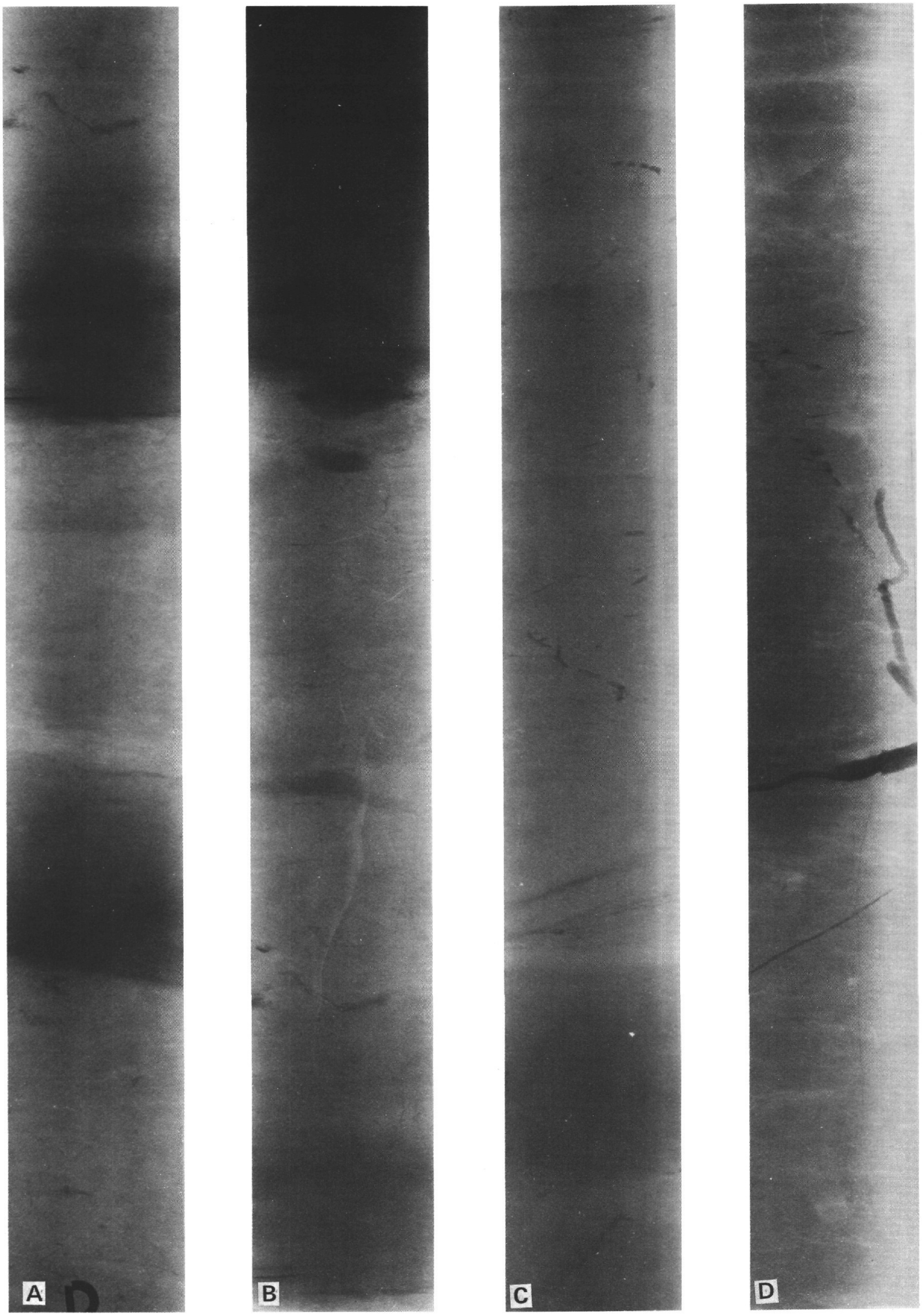

PLATE 3

X radiographs of Pleistocene mudstone cores, × *1.*

A Sample 1-1-6, 8.5-33 cm: Pleistocene muddy siltstone showing alternately more muddy (mudstone) and cleaner (siltstone) beds; thrown into recumbent fold, with horizontal axis below middle of picture (cf. B).

B Sample 1-2-2, 12-37.5 cm: Pleistocene mudstone-siltstone sequence much like A, thrown into recumbent folds, with a horizontal fold axis shown near bottom of picture.

C Sample 1-2-2, 80-104 cm: Pleistocene mudstone showing sets of fractures (white) partly in, partly near plane of bedding and near the axial plane of recumbent folds (A&B). Is this incipient fracture cleavage, or a feature induced by drilling?

D Sample 3-2-3, 85-109.5 cm: Pleistocene turbidite sequence of sand and muddy silt. The sand which is very watery and soft is represented by the speckled basal part of the picture, the somewhat firmer muddy silt by the streaked sequence of the middle and upper parts. We suspect that the light specks and streaks represent gas pockets which developed in the core as it was raised to the surface; nothing remains of them in the sand, but the muddy silt pulled apart along such bedding-parallel streaks as the core was split. The white blob in upper part is a piece of fossil wood.

PLATE 3

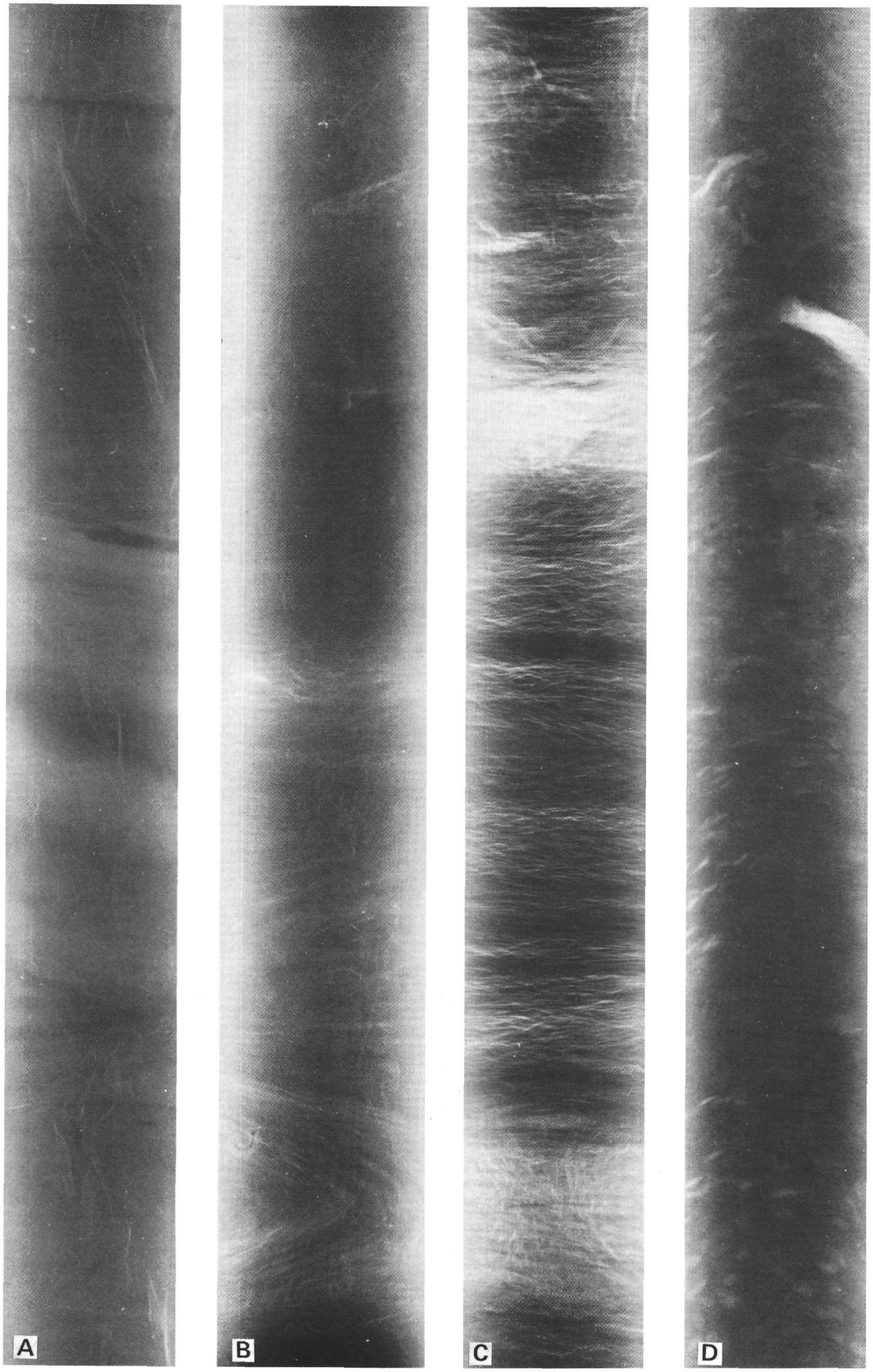

PLATE 4

X radiographs of cores, × *1.*

A	Sample 6-3-4, 85-113.5 cm: Middle Eocene turbidite siltstone showing well-defined lamination and cross-lamination.
B	Sample 6-6-1, 75-119.5 cm: Middle Eocene turbidite siltstone showing well-defined lamination.
C	Sample 5-3-1, 42.5-57 cm: Upper Cretaceous volcanic-rich clay, containing a distinctive platy X-ray opaque mineral.
D	Sample 6-2-2: Eocene montmorillonitic (?) clay, containing distinctive X-ray opaque mineral grains.

PLATE 4

PLATE 5

X radiographs of cores, × 1.

A	Sample 6-3-3, 101-125.5 cm: Eocene clay, showing intense intraformational brecciation, with harder (and more X-ray opaque) clasts in a more water matrix. Interpreted as a result of drilling.
B	Sample 5-1-2, 2-26.5 cm: Oligocene pebbly sandstone with terrigenous carbonate clasts ranging from sand grain to pebble size.
C	Sample 5-1-3, 13-37.5 cm: Oligocene pebbly mudstone underlying nannoplankton chalk. Pebbles are of terrigenous limestone, the matrix is clayey to marly.
D	Sample 4A-2-1, 10-34.5 cm: Mid-Cretaceous pebbly mudstone, of terrigenous limestone clasts in nannoplankton marl matrix.

PLATE 5

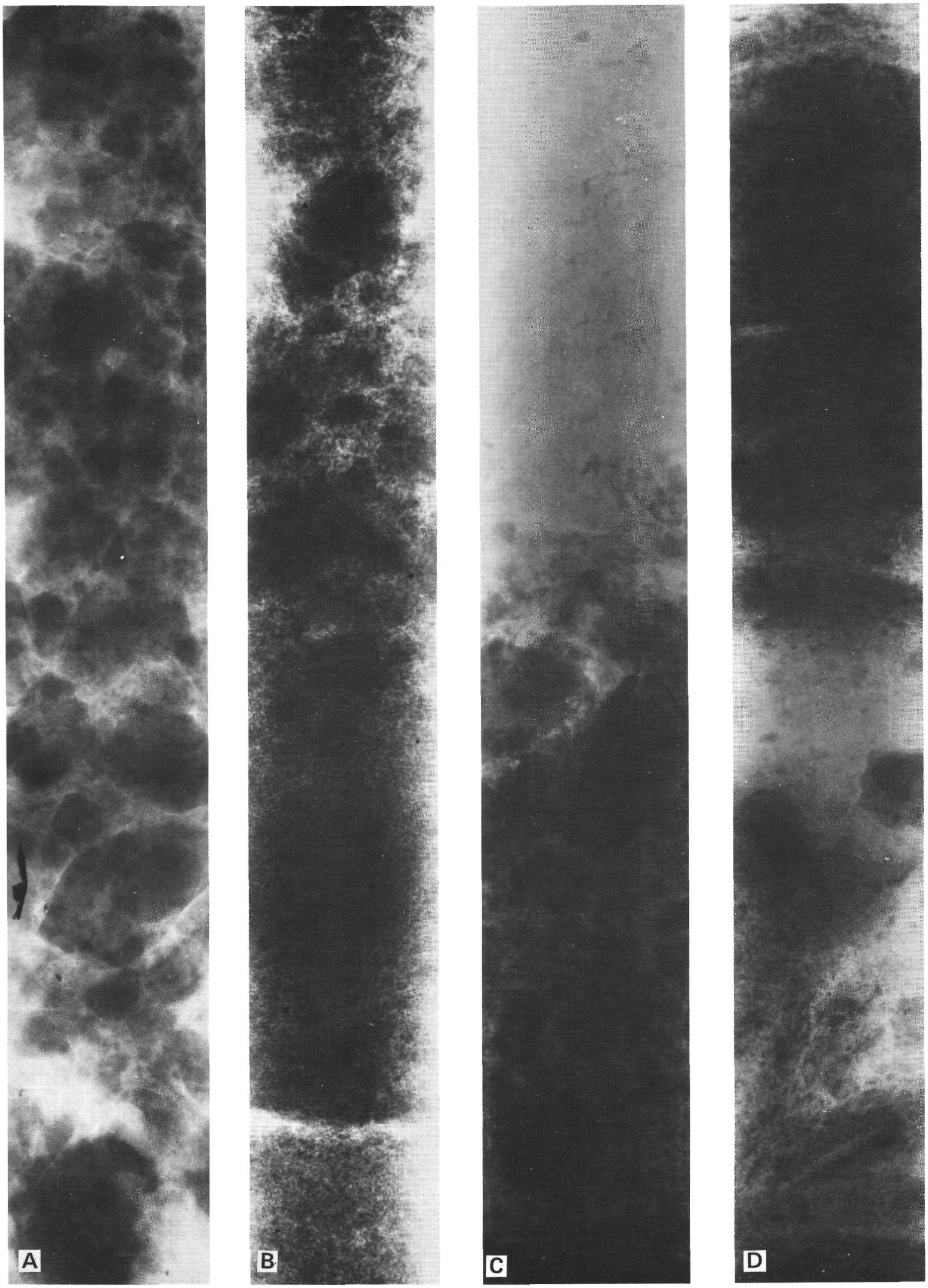

PLATE 6

Various smear slides.

A Sample 1-3-2, 7 cm (plain light, X 250): Pleistocene terrigenous mudstone. Quartz, carbonate, opaque minerals, and clay, in simple and compound grains.

B Sample 6-1-1, 50 cm (plain light, X 1000): Pleistocene brown deep-sea clay. Clay, with rounded grains of pyrite, smaller aggregates of limonitic material, and, at lower right, a problematical body of birefringent rods crossed at right angles.

C Sample 5-1-1, 109 cm (plain light, X 540): Nannoplankton chalk. Discoasters of several species; in upper right quadrant a thoracosphere; the larger coccoliths are resolved as oval bodies, the smaller ones compose the granular ground mass.

D Sample 4-4-1, 6 cm (cross-polarized, X 250): Lower Cretaceous (Hauterivian) nannoplankton chalk. The pentagonal body in the center is a pentalith of *Braarudosphaera,* and many if not most of the smaller particles are disaggregated segments of such pentaliths. Several ovoid coccoliths (extinction cross) are also visible.

E&F Sample 6-3-3, 62 cm, X 540: E in plain light, F cross-polarized. Middle Eocene diatom-coccolith marl. The isotropic particles with grid structure are diatom frustules, the birefringent ones are coccoliths. Probably the fine upper part of a turbidite.

PLATE 6

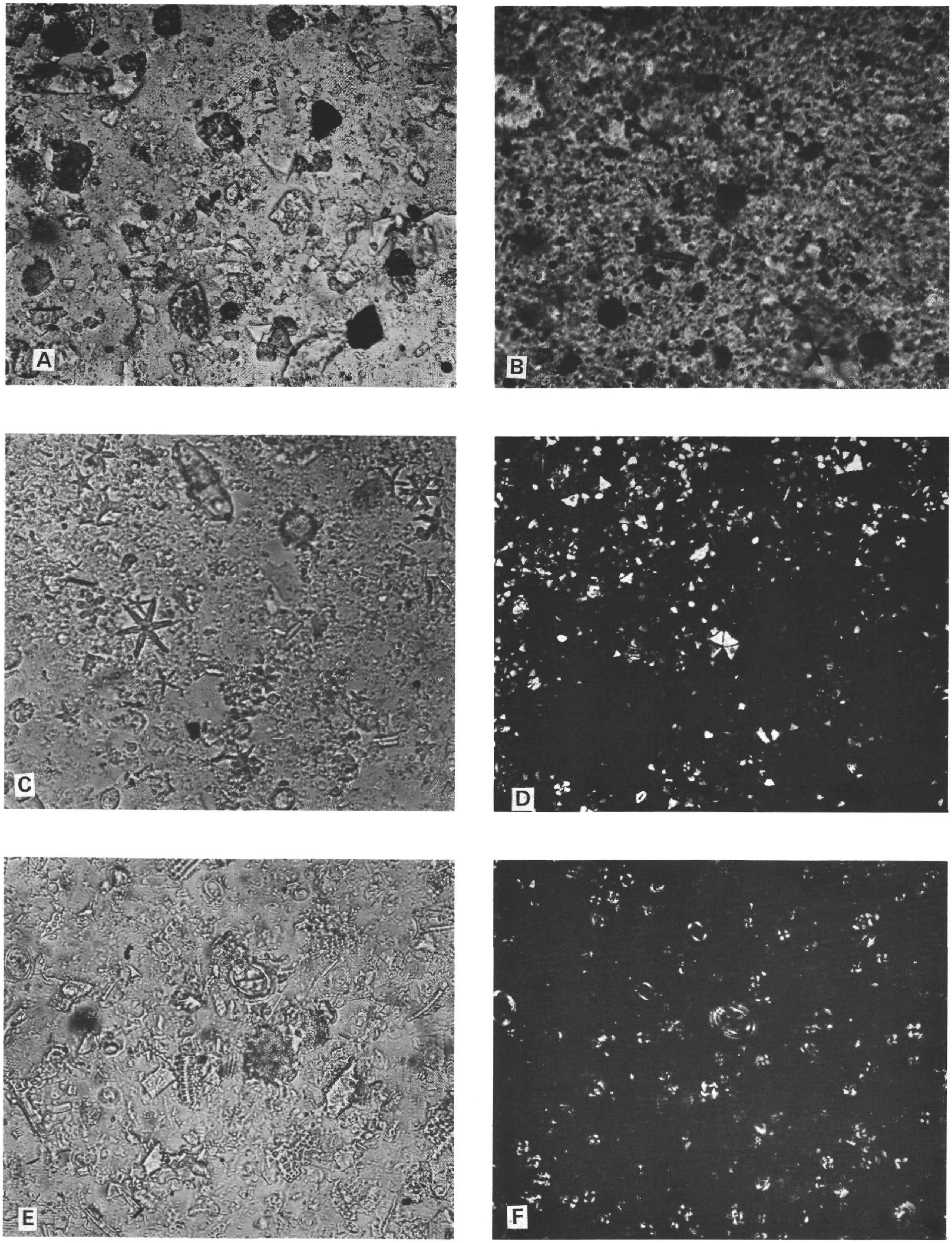

PLATE 7

Smear slides of siliceous Middle Eocene sediments.

A&B Sample 6-3-4, 64.5 cm (plain and cross-polarized light, X 250): The circular isotropic structures are diatoms, the isotropic rods are sponge spicules, the elliptical birefringent bodies coccoliths. Probably fine upper part of a turbidite.

C Sample 7-4-3, 95 cm (plain light, X 250): In addition to abundant diatom fragments this picture shows a silicoflagellate (the buckle-shaped structure in lower right quadrant). Carbonate is essentially absent from this siliceous clay, which may represent the true pelagic background sediment of the Mid-Eocene in this area.

D Sample 6-4-3, 57 cm (plain light, X 250): Siliceous clay, similar to C, with diatoms, radiolarian fragments and fine sponge spicules.

E&F Sample 6-4-2, 50 cm (plain and cross-polarized light, X 250): A silt-grade sediment of sponge spicules (isotropic, straight, hooked and tri-radiate fragments), foraminifera (birefringent), diatoms (isotropic circular disks and grid-patterned fragments), a dolomite rhombohedron, and a scattering of coccoliths (birefringent). Lower part of a turbidite.

PLATE 7

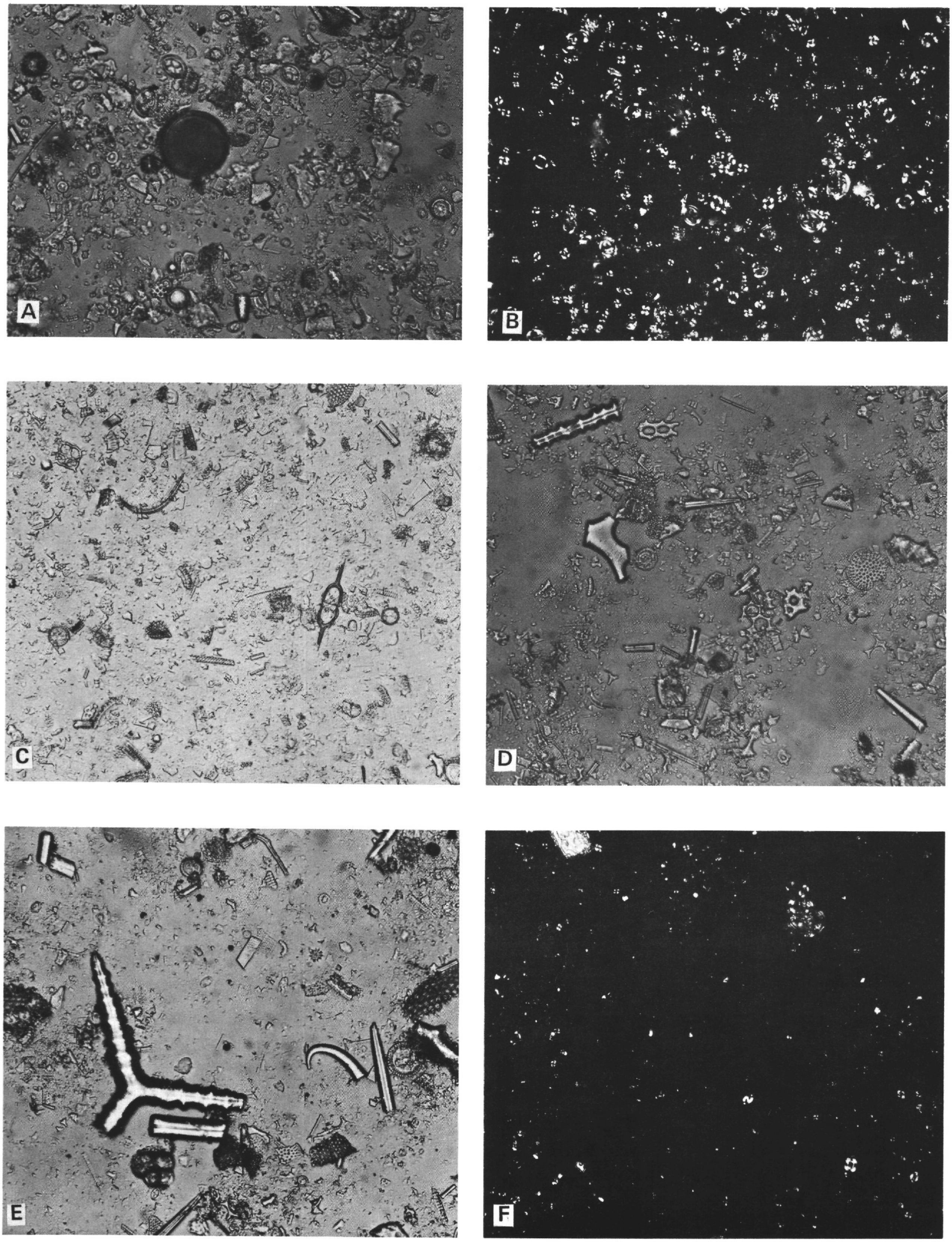

PLATE 8

Smear slides of Pliocene-Pleistocene siltstones presumed to be of turbidite origin, Site 3.

A&B Sample 3-1-1, 114.5 cm: Pleistocene, plain and cross-polarized, × 250. Besides indeterminate carbonate grains and small quartz grains (clear, upper left) this slide shows a spheroidal sponge spicule *(Tetractinellidae)* in upper left; foraminifera *(Bolivina* at left, a miliolid at right, a juvenile globigerinid at bottom center); and four didemnid tunicate spicules (burr-shaped and birefringent).

C Sample 3-1-1, 114.5 cm: Pleistocene, plain light, × 250. A curved but non-perforate opaline sponge spicule in center; a long prism of a pelecypod shell with typical transverse growth lines, in lower right; indeterminate grains, and two didemnid tunicate spicules.

D Sample 3-6-1, 93 cm: Pliocene, plain light, × 250. Various indeterminate carbonate grains; at right a juvenile globigerinid with pyrite in some chambers, next to it a *Bolivina.* Two didemnic tunicate spicules at left.

E&F Sample 3-6-2, 36 cm: Pliocene, plain and cross-polarized, × 540. The large perforate grain in center is a fragment of a perforate foraminiferal test; a single foraminiferal chamber (upper right) shows typical pseudo-uniaxial extinction cross; several other juvenile foraminifera, and indeterminate carbonate shell debris.

PLATE 8

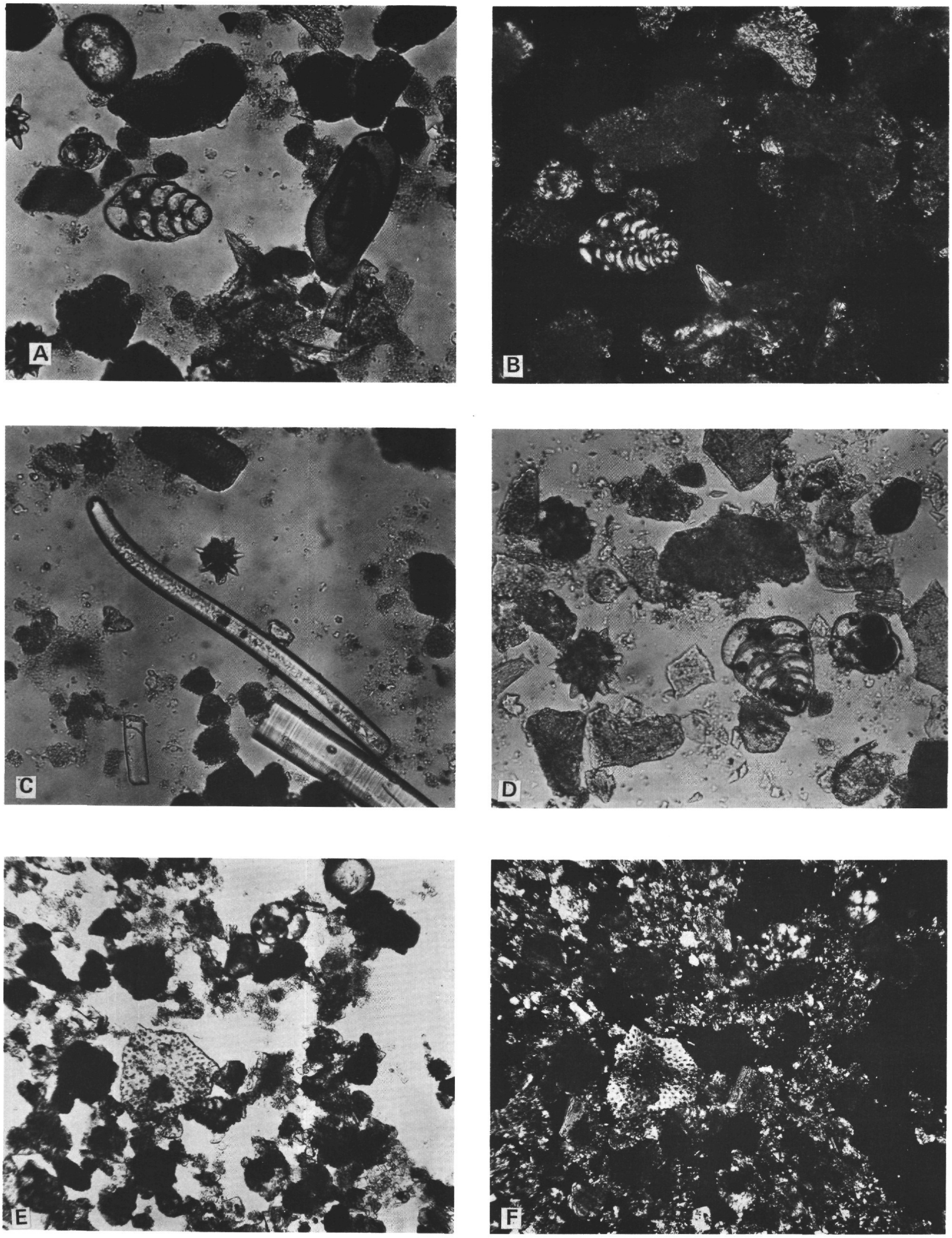

shows that dolomite predominates over calcite, in contrast to nearly all other sediments of Leg 1. Quartz and feldspar content is high compared to that of the deep-sea clays (Figure 3); the feldspar content relative to quartz is high, and is marked by a slight but consistent preponderance of plagioclase over K-feldspar (Figure 4). The quartz/dolomite ratio is rather constant (Figure 6), with a mean value of about 1.5. Beall is inclined to seek the source of these sediments mainly in the lower Mississippi drainage basin. In view of the extraordinarily high detrital carbonate content, Fischer interprets these sediments differently, as largely glacial flour derived from the ice sheets and their tills.

Brown and Red Deep-Sea Clays

Brown deep-sea clays characterize the uppermost (Pliocene-Pleistocene) sediments of the Atlantic sites, and red deep-sea clay was cored below Middle Eocene sediments at Site 7. The main mineral constituents are clay minerals and quartz. The color results mainly from iron and manganese minerals. The predominant brown color is due to hydrous ferric oxides ("limonite"), generally present in the form of minute granules of unknown origin. Flakes of red hematite are visible under the microscope in some of the brown clays, but are rare; they assume a larger proportion (perhaps up to 50 per cent of the ferric iron) in the red Eocene clays of Site 7. Pyrite is ubiquitously present in small spherules, but has escaped X-ray detection in most samples. Manganese oxides are present in small nodules in the red clays of Site 7, and may well be more widely distributed; rhodochrosite appears to be present in the same cores (see below). Cosmic nickel iron spherules were seen in some of the washed residues made in the search for foraminifera. Rods and twins of rutile appear to be common, and the occurrence of delicate cross twins suggests that some of this rutile is authigenic (Plate 6B).

These deep-sea clays are illustrated in Plate 15; Plate 1, A & B; and Plate 6B. The X radiographs commonly show a distinct granular texture, presumably because of the X-ray opaque limonite and pyrite grains, as shown in Plate 1. Also shown here is a deep-sea clay with larger ferruginous and possibly manganiferous nodules, some of which appear to be mineralized pumice fragments. With certain exceptions, the general composition of the brown and red clays cored on Leg 1 (the presence of much kaolinite and quartz, and scarcity of zeolites) suggests a largely terrigenous origin.

Other Sediments–Mainly Volcanic

In addition to the sediments described above, the Leg 1 coring program recovered some sediments with strong volcanic influence–chiefly montmorillonitic and chloritic clays, with and without notable shard relicts and zeolites. Such sediments were found in the Miocene of Site 3, in the Cretaceous of Site 5, and in the Eocene of Site 6, and they are dealt with under the core descriptions and site reports.

TEXTURAL COMPOSITION OF THE SEDIMENTS

Textural data on Leg 1 sediments have been derived from three sources: (1) sand-silt-clay percentages determined by Dr. Pimm and assistants at Lamont-Doherty Geological Observatory; (2) observations of the shipboard scientific staff while preparing visual core descriptions; and (3) a limited number of detailed sieve analyses carried out by Beall. The mechanical analyses are discussed first.

Percentages of sand, silt, and clay are summarized in Figure 1 for all sites. Since the samples were preferentially taken from the finest-grained intervals, the textural trends in Figure 1 reflect composition of the fine-grained portions of the sequences involved. Note that all Gulf of Mexico samples contain less than 10 per cent sand, and that only a few samples from the Atlantic have high sand percentages. Inclusion of these coarser sediments, which consist of graded carbonate sands and pebbly muds, was due to lack of fine-grained interbeds. Were the sampling to be extended to include all sediment types, it is expected that the coarser portion of the textural diagram would be more clearly defined as to textural trends.

Gulf of Mexico samples, while showing considerable overlap, show a trend towards the silt portion of the textural diagram. These latter samples were taken from the laminite facies of Sites 1 and 3. Pelagic foraminiferal clays and coccolith oozes from Site 2 tend to have high sand percentages, a reflection of high percentages of planktonic foraminifera and pyrite.

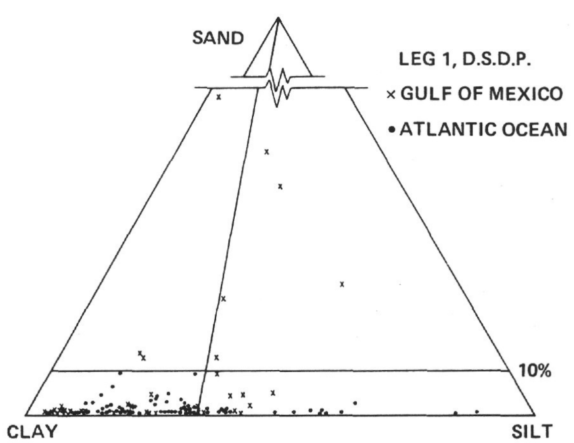

Figure 1. *Textural summary.*

Pelagic deep-sea red clays from Sites 6 and 7 tend to group near the clay end member with minor fluctuations. Authigenic (?) minerals and faecal pellets complicate textural composition of the red clays by raising sand and silt percentages. Overall, most of the pelagic sediments (as interpreted by various criteria) tend to be texturally classified as clay (using Folk's terminology, Folk, 1959) or very fine-grained silt. Textural differentiation of environmental types is somewhat obscure as revealed by some detailed photos (not shown here).

On the basis of visual descriptions of cores, two somewhat thick and ideally graded beds were selected for detailed textural analysis. A specially designed wet sieve nest ranging from 1.32 ϕ to 5 ϕ was used in the analysis. Results taken from the two graded units are shown in Figure 2. Figure 2A shows the spread of size-frequency distribution for twelve samples from Hole 3, Core 2, Sections 1 and 2. The coarsest size distributions were taken from the lower portion of the graded unit. These data are summarized, along with other measurements, in Plate 13. From inspection of Figure 2A, it is obvious that the sands are poorly sorted with a high percentage of material finer than 4 ϕ (the sand-silt boundary).

Figure 2B shows the spread of size-frequency distribution for 12 samples from Hole 6, Core 6, Section 1. This graded unit is comprised dominantly of biogenic carbonate and siliceous debris with subsidiary quartz in contrast to the graded unit from Site 3, which is primarily comprised of terrigenous quartzose grains. Figure 2B clearly shows a poorly sorted series with a high percentage of material finer than 62 microns. The upper limit of this graded unit was not recovered for sampling, and thus the pelagic interbed could not be represented. Pelagic units lower in the cored sequence generally consist of diatom-coccolith ooze and diatom-spicule clay. These data are summarized in Plate 14 and will be discussed in a following section.

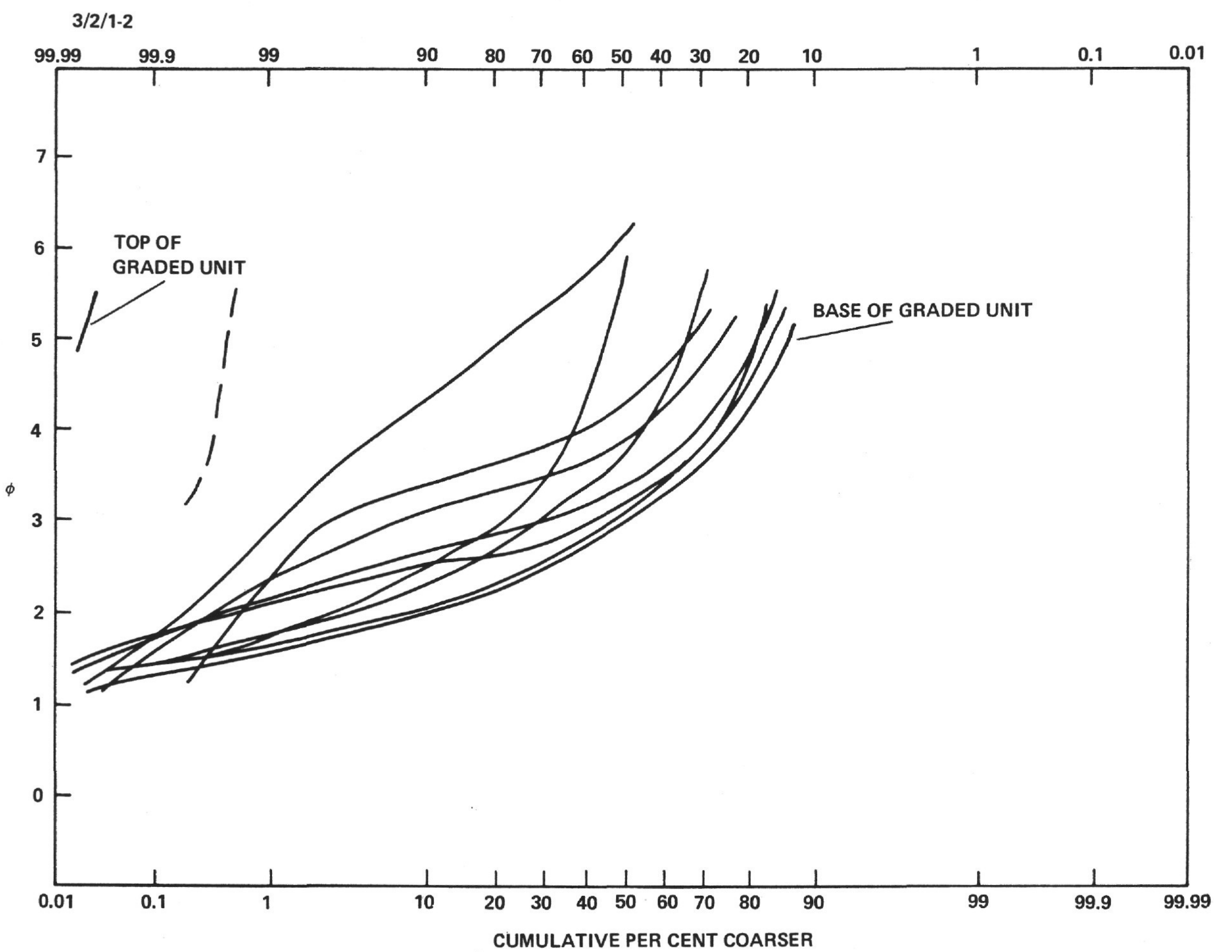

Figure 2A. *Textural analyses of samples from Core 3-2, Sections 1 and 2.*

Comparisons of the textural data from the two graded units sampled demonstrate that the quartz-rich sequence from Site 3 has a generally better sorted sand fraction and slightly finer average median diameter. The coarse silt fraction is somewhat truncated in both units, being more so in Core 6-6, Section 1, which also has a generally coarser tail. Differences in grain types and effective settling rates are difficult to evaluate on the basis of these data. Judging from binocular microscopic examination, most of the apparent textural difference between the two units is due to differences in particle type and shape.

The primary aim of the detailed sampling described above was to document textural grading as described in the shipboard visual core description. Additional detailed sampling is needed to more completely evaluate the presence and type of grading in units described as turbidites in the various drilled sequences.

Visual core descriptions commonly describe graded beds from the cored sequences penetrated on Leg 1. Grading is most easily discerned in the thicker beds. Thin beds or laminae, on the order of a few millimeters thick which were described as graded, generally exhibited a sharp base and gradational top. Experience derived from detailed textural analysis of similar sediments previously taken in the Gulf of Mexico suggests that the grading described is real. Some of the thinner, medium silt laminae are only a few grain-diameters thick. Origin of these distinctive textural units is somewhat controversial and will be discussed in a later section.

An attempt to estimate textural composition of the pelagic interbeds (as well as the coarser sediments) using smear slides was attempted. (Fischer discusses this in a subsequent section.) On the basis of the limited number of sand-silt-clay analyses previously discussed, it is suggested that analysis of the smear slides tended to overestimate the sand-silt component. Figure 1 demonstrates the preponderance of clay-rich sediment as determined for the finer-grained units.

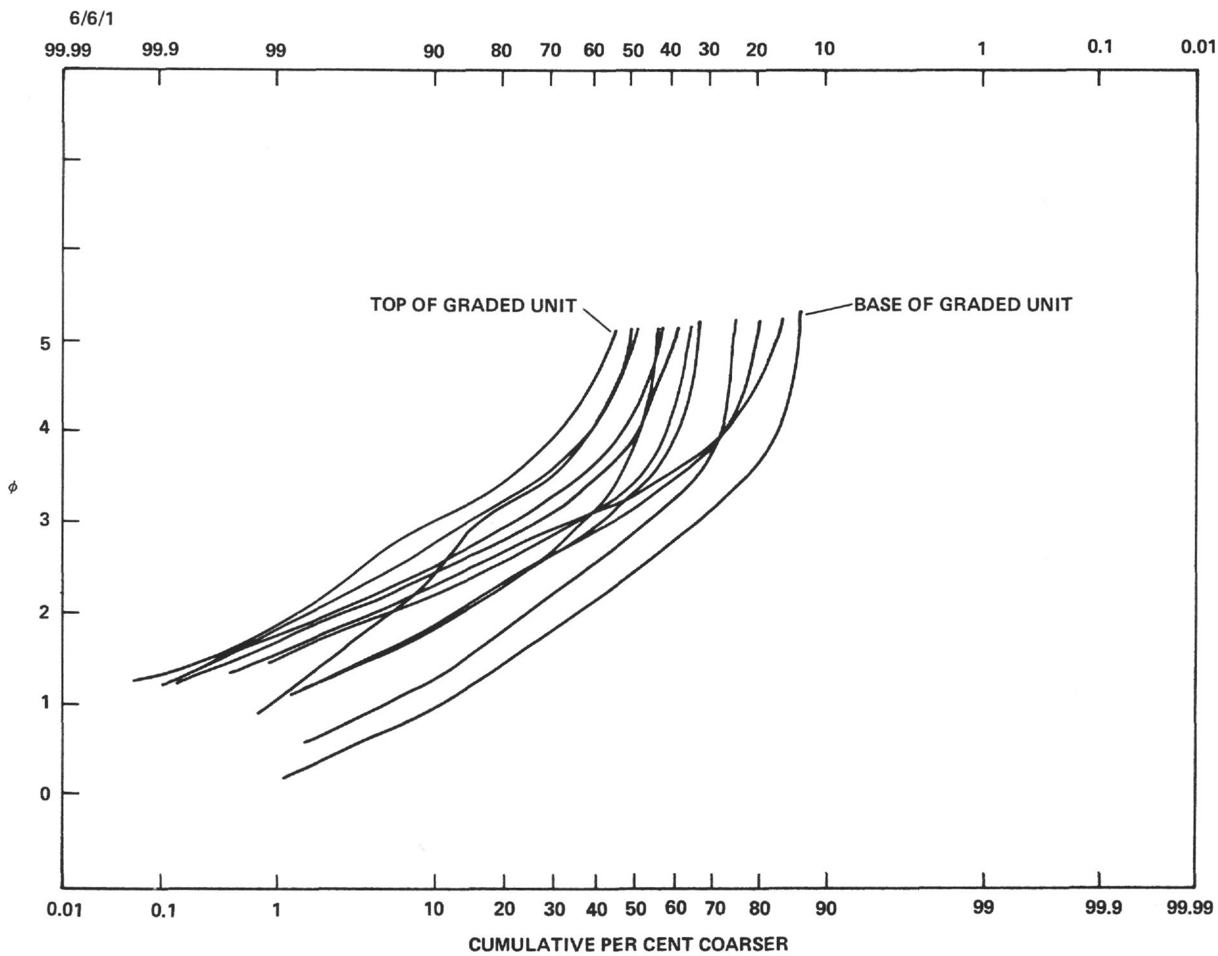

Figure 2B. *Textural analyses of samples from Core 6-6, Section 1.*

MINERAL COMPOSITION OF THE SEDIMENTS

While the general composition of the sediments has been discussed is foregoing sections, specific aspects of the mineralogy are here discussed in more detail.

The mineral composition of sediments was approached in four ways: (1) Shipboard study of smear slides under the petrographic microscope; providing a good approximation of overall composition, and serving as a basis for core description and sediment classification. (2) Semi-quantitative optical analysis of the inorganic coarse-fraction residue, taken from the grain size analysis samples. This work, carried out on shore by Beall, was especially illuminating for sediments containing small quantities of coarse grains, not revealed by smear slides and X-ray analysis. The results are summarized below, in Table 1. (3) Organic carbon-carbonate determinations carried out on shore by Pimm and associates, and recorded here in Chapter 11 as well as on the individual core section descriptions. (4) Bulk X-ray diffraction analyses provided by Rex (Chapter 13).

Detrital Silica

Detrital quartz is almost ubiquitous, but shows wide quantitative fluctuations. Quartz dominated sands and silts are common in the Neogene sections drilled in the Gulf of Mexico, but not in the Atlantic sites. The most quartz-rich sediments encountered there are the brown clays, in which the X-ray studies show up to 50 per cent quartz in the crystalline fraction, and the Eocene turbidites on the Bermuda Rise, in which quartz sand and silt commonly comprise a third or more of the coarser beds. The lowest quartz values, dropping to zero, were encountered in the calcareous chalks and oozes. Study of the coarse fraction shows that many of the quartz grains in the Pleistocene sequence of Site 1 show secondary overgrowths (Plates 9 and 10), but these are believed to predate the last deposition.

Rex's bulk X-ray analyses have been used to compare the quartz and feldspar contents of certain of these muds with the kaolinite and mica values (Figure 3). Figure 4 shows a similar comparison of quartz with feldspars. The deep-sea clays contain less quartz than the paraglacial mudstones, quartz content being lowest in the Eocene red clays of the Bermuda Rise.

Detrital chert is an abundant constituent in the sands of Site 1, and it occurs in the pebbly mudstones of Sites 4 and 5.

Detrital Silicates Other Than Clays

Discussion of these minerals is based mainly on Beall's optical coarse-fraction studies. Detrital silicates are conspicuous in the sandy beds of the Gulf of Mexico Neogene (Sites 1 and 3). Examples are shown in Plates 9 and 10, and further details are given in the plate legends and in Table 1. The assemblage is typical of Gulf Coast suites, and it appears to represent a mixed-multicycle, stable assemblage plus a volcanogenic assemblage.

The stable silicates include biotite, hornblende, rutile, tourmaline, zircon, garnet, and sphene. In the coarse fraction these minerals were found especially well represented in the lower cores of Site 1. The smear slides show a fairly diverse suite of such "heavy minerals" in the terrigenous sands throughout Site 3.

The unstable silicates include glass, feldspar, and volcanic ash fragments. The feldspars appear to be mainly plagioclase. At Site 1, the unstable silicates are particularly conspicuous in the upper part (Core 1-2, Section 3, and Core 1-3, Section 4), decreasing steadily downward. Here the volcanic fragments are mainly plagioclase with subsidiary amounts of glass and unidentified inclusions; individual plagioclase grains show simple twins and low extinction angles, and appear to be albite. The bulk X-ray analyses by Rex (Figure 4) indicate that the potash-feldspar content as a whole generally amounts to 5 per cent. A trace of microcline is also present. Unstable volcanic silicates are also abundant in the bottom cores (10 and 11) of Site 3 below bentonitic ash beds, and glass shards are common in the ash layers of other sites. Coarse fractions of the brown and red clays of the Atlantic contain significant amounts of albitic plagioclase, evidence of volcanic input. The clays as a whole, however, seem to be largely of terrigenous detrital origin, to judge from their clay-mineral composition and the scarcity of zeolites.

The feldspar content of the sediments in general, as obtained from bulk X-ray analyses by Rex (Chapter 13), shows wide variations in the potash-feldspar to plagioclase ratio. Some of these values are plotted against quartz in Figure 4. No evidence for authigenic development of feldspar in the samples from Leg 1 has been observed.

The Common Clay Minerals

Present knowledge of the clay mineralogy, being based entirely on the bulk X-ray analyses by Rex is still rather rough. Kaolinite and micas (including both coarser detrital micas and the illitic clays) are generally dominant. Montmorillonite occurs in the Holocene clays of the Gulf of Mexico, in the spicule and diatom-rich Middle Eocene of the Bermuda Rise area, and sporadically in ash beds. Chlorite was nowhere identified in this X-ray program.

Authigenic Silicates

Zeolites were recognized in numerous smear slides in association with other evidences of volcanism; phillip site was identified by X-ray in Miocene ash beds of Site 3;

TABLE 1
COARSE-FRACTION MINERALOGY

Predominantly Inorganic

Sample # incl. depth in core	Qtz	Feldspar		Rock Fragments					Heavy Minerals							
		Plag.	K-	Glas	VRF	Undif.	Chrt	Carb	Biot	Apat	Hrnbld	Rut 1	Tourm.	Zren	Grnt	Sphn
1P/1/1 - 135-137 cm.						tr										
1P/1/2 - 131-133 cm.																
1P/1/3 - 114-116 cm.																
1P/1/4 - 7 cm.	12			12					tr							
1P/1/5 - 135-137 cm.																
1P/1/6 - 132-134 cm.	tr								2							
1/1/1 - 6-8 cm.	5			1	tr				5							
1/1/2 - 7-9 cm.	22	2		2	tr			1	1						tr	
1/1/3 - 5-7 cm.	2			1	1											
1/1/4 - 7-9 cm.	2				tr											
1/1/5 - 8-10 cm.	2				1				tr							
1/1/6 - 5-7 cm.	62	1		5	5			5	5		tr					tr
1/1/7 - 6-8 cm.	90	2			tr				2		tr				tr	
1/2/1 - 52-54 cm.	80	tr	tr	2	3			2	1		1					
1/2/2 - 3-5 cm.	80	tr	tr	2	3			2	1		1					
1/2/3 - 9-11 cm.	46	1		10	10		2	5	tr		tr					
1/3/1 - 7-9 cm.	50			10	10		2	2	1		tr					
1/5/1 - 41-43 cm.	81	5	tr		5		tr	2	1	tr	1	tr		tr		
1/5/2 - 22-24 cm.	78	5	tr		4		tr	2	3	tr	1	tr		tr		
1/6/1 - 11-13 cm.	89	2			2		tr	5		tr	tr	tr		tr		tr
1/6/2 - 9-11 cm.	89	2			2		tr	5		tr	tr	tr		tr		tr
1/6/3 - 4-6 cm.	86	2			2		3	5		tr	tr	tr		tr		tr
1/7/2 - 10-12 cm.	86	2			2		3	5		tr	tr	tr	tr	tr		tr
1/7/3 - 5-7 cm.	72	1			2		2	6		tr	tr	tr	tr	tr		tr

*Note: X represents presence in unspecified amounts.

TABLE 1 - *Continued*

Predominantly Organic

Dol	Pyrt	Rhodch.	Glauc	Col-Bone	Carb Aggr	Plank. Forams	Benth. Forams	Sponge Spics.	Rad/Diat	Carbonac Debris	Spore	COARSE FRACTION % of Sample
						99		tr			tr	1.2
						99						1.1
						99						1.3
						75				tr		NIL.
						99					1	0.1
						2				81	5	NIL.
tr						2		tr		60	5	0.1
						3	2			86	5	NIL.
						5				87	5	0.1
						4				87	5	NIL.
tr						1				13	2	0.3
						90				7	tr	0.2
						tr				5		0.1
tr						tr	tr			10		0.1
tr						tr	tr			10		0.1
						tr	tr			20	5	0.1
						tr	tr			20	5	NIL.
						tr				3	tr	0.2
						tr				5	1	NIL.
										1		0.2
										1		1.1
										1		?
										1		?
						3	2			10	1	0.8

TABLE 1 - *Continued*

Predominantly Inorganic

Sample # incl. depth in core	Qtz	Feldspar		Rock Fragments					Heavy Minerals							
		Plag.	K-	Glas	VRF	Undif.	Chrt	Carb	Biot	Apat	Hrnbld	Rut 1	Tourm.	Zren	Grnt	Sphn
1/7/4 - 3-5 cm.	74	1			2		2	15		tr	tr	tr	tr	tr		tr
1/7/5 - 8-10 cm.	74	1			2		2	15		tr	tr	tr	tr	tr		tr
1/7/6 - 8-10 cm.	tr								tr							
1/7/6 - 8-10 cm.									tr							
1/7/7 - 8-10 cm.	74	1			2		2	15		tr	tr	tr	tr	tr		tr
1/8/2 - 13-15 cm.	78	2			2		2	10		tr	tr	tr	tr	tr		tr
1/8/3 - 10-12 cm.	62	3			tr		20	10		tr	tr	tr	tr	tr		tr
1/8/4 - 12-14 cm.	62	3			tr		20	10		tr	tr	tr	tr	tr		tr
1/8/5 - 5-7 cm.	56	1			tr		15	7		tr	tr	tr	tr	tr		tr
1/8/6 - 10-12 cm.	56	1			tr		15	7		tr	tr	tr	tr	tr		tr
1/8/7 - 14-16 cm.	56	1			tr		15	7		tr	tr	tr	tr	tr		tr
1/9/2 - 2-4 cm.	56	1			tr		15	7		tr	tr	tr	tr	tr		tr
1/9/3 - 11-13 cm.	56	1			tr		15	7		tr	tr	tr	tr	tr		tr
1/9/4 - 11-13 cm.	56	1			tr		15	7		tr	tr	tr	tr	tr		tr
1/9/5 - 10-12 cm.	55	1			tr		14	5		tr	tr	tr	tr	tr		tr
1/9/6 - 7-9 cm.	38	5			tr		5	5		tr	tr	tr	tr	tr		tr
1/9/7 - 7-9 cm.	80	1	tr				5	6			1	tr	tr	tr	tr	
2/1/2 - 13-15 cm.																
2/1/3 - 9-11 cm.																
2/1/3 - --																
2/2/1 - 41-43 cm.																
2/3/1 - 104-106 cm.																
2/3/2 - 5-7 cm.																
2/4/1 - 47-49 cm.																
2/4/2 - 14-16 cm.																

*Note: X represents presence in unspecified amounts.

TABLE 1 - *Continued*

Predominantly Organic

	Dol	Pyrt	Rhodch.	Glauc	Col-Bone	Carb Aggr	Plank. Forams	Benth. Forams	Sponge Spics.	Rad/Diat	Carbonac Debris	Spore	COARSE FRACTION % of Sample
							2	1			2	tr	0.6
							2	1			2	tr	0.1
											95	5	NIL.
											95	5	NIL.
							2	1			2	tr	0.1
							tr				5	tr	0.5
											5	tr	2.0
								tr			5	tr	1.1
							- 10 -				10	tr	0.3
							- 10 -				10	tr	0.2
							- 10 -				10	tr	0.1
							- 10 -				10	tr	0.2
							- 10 -				10	tr	0.3
							- 10 -				10	tr	0.2
							- 9 -				15	1	0.4
							- 30 -				15	1	0.1
	2						- 1 -				2	tr	4.3
							100						9.5
							99				1		6.1
							99		tr		tr	tr	2.6
							99				tr	tr	2.4
							99				tr	tr	4.2
		tr					99				tr	tr	2.1
		20			tr		79				tr		1.4
		15			tr		84				tr		2.5

TABLE 1 - *Continued*

Predominantly Inorganic

Sample # incl. depth in core	Qtz	Feldspar		Rock Fragments					Heavy Minerals							
		Plag.	K-	Glas	VRF	Undif.	Chrt	Carb	Biot	Apat	Hrnbld	Rut 1	Tourm.	Zren	Grnt	Sphn
3/1/1 - 28-30 cm.	x			x					x							
3/1/2 - 23-25 cm.	x			x												
3/2/2 - 40-42 cm.	86	5	tr		tr		5	tr		tr	tr	tr	tr	tr		tr
3/2/3 - 14-16 cm.	5	tr		tr			2									
3/3/2 - 14-16 cm.	tr							4	tr							
3/4/1 - 6-8 cm.	1															
3/5/1 - 37-39 cm.																
3/5/2 - 24-26 cm.																
3/5/3 - 15-17 cm.																
3/5/4 - 18-20 cm.																
3/5/5 - 26-28 cm.	tr			tr					tr							
3/6/1 - 61-63 cm.																
3/6/2 - 11-13 cm.	5															
3/7/1 - 32-34 cm.																
3/7/2 - 1-3 cm.	tr			tr					tr							
3/7/3 - 66-68 cm.	tr															
3/7/4 - 131-133 cm.	tr															
3/8/1 - 101-103 cm.								5								
3/8/2 - 14-16 cm.	1								1							
3/8/3 - 11-13 cm.	1								1							
3/8/5 - 13-15 cm.	tr							19		tr						
3/8/6 - 44-46 cm.	tr			tr												
3/9/2 - 15-17 cm.	5			3					1							
3/9/3 - 10-12 cm.	3							10								
3/9/4 - 8-10 cm.	3							10								

*Note: X represents presence in unspecified amounts.

TABLE 1 - *Continued*

Predominantly Organic

	Dol	Pyrt	Rhodch.	Glauc.	Col-Bone	Carb Aggr	Plank. Forams	Benth. Forams	Sponge Spics.	Rad/Diat	Carbonac Debris	Spore	COARSE FRACTION % of Sample
										x	x	x	NIL.
							x			x	x	x	NIL.
											2	tr	4.7
	tr						50				40		NIL.
	1						90		tr		5		0.5
							- 97 -		tr		1	tr	0.8
		tr					99				tr	tr	2.8
		tr					99				tr	tr	2.7
		tr					99				tr	tr	3.8
		tr					99				tr	tr	1.0
		1					93				5	tr	0.1
		tr			tr		99				tr		3.6
		1					93				1		2.4
		tr					99	-			tr		2.1
		1					93	-			5	tr	0.2
		50					49	-	tr		tr	tr	0.9
		5					94	-			tr	tr	NIL.
						95?							0.1
		25					71	-	tr		tr	1	0.2
		25					- 71 -		tr		tr	1	0.3
		50			25		- 5 -						0.3
		94			3	2?							0.1
		1			20	10?	56		tr	1	2	tr	0.1
		10			10		- 66 -		tr	tr			NIL.
		10			10		- 66 -		tr	tr			NIL.

TABLE 1 - *Continued*

Predominantly Inorganic

Sample # incl. depth in core	Qtz	Feldspar		Rock Fragments					Heavy Minerals							
		Plag.	K-	Glas	VRF	Undif.	Chrt	Carb	Biot	Apat	Hrnbld	Rut 1	Tourm.	Zren	Grnt	Sphn
3/9/5 - 20-22 cm.	3			tr				10								
3/9/6 - 18-20 cm.	tr			tr				30								
3/9/7 - 14-16 cm.	tr			tr				15								
3/10/2 - 9-11 cm.	32	5		tr	50				5		tr					
3/11/1 - 75 cm.	33	5		tr	53						3	tr	tr			
4/1/2 - 100-102 cm.	tr					1		95								
4/1/3 - 12-14 cm.	2					5		81								
4/1/4 - 13-15 cm.	2					5		81								
4/1/5 - 50-51 cm.	10			x	87											
4/1/6 - 10-12 cm.	20	2			7	40										
4/3/1 - 6-8 cm.	tr				81			5								
4/4/1 - 74-76 cm.																
4A/1/1 - 11-13 cm.						tr		98								
4A/1/3 - 2-4 cm.	tr							97								
4A/2/1 - 34-36 cm.						tr		96								
5/1/1 - 9-11 cm.	5				10	1		63								
5/1/2 - 12-14 cm.					1			99								
5/1/2 - 60-62 cm.								15								
5/1/3 - 16-18 cm.								50								
5/3/1 - 60-62 cm.	tr				10			89	tr							
6/1/1 - 24-26 cm.	tr				5											
6/1/2 - 24-26 cm.	tr															
6/1/3 - 9-11 cm.				2	tr											
6/1/4 - 7-9 cm.				1												

***Note: X represents presence in unspecified amounts.**

TABLE 1 - *Continued*

Predominantly Organic

	Dol	Pyrt	Rhodch.	Glauc	Col-Bone	Carb Aggr	Plank. Forams	Benth. Forams	Sponge Spics.	Rad/Diat	Carbonac Debris	Spore	COARSE FRACTION % of Sample
		10			10		- 65 -			1			NIL.
		15			5	39?	- 10 -		tr	tr			0.1
		60			3	15	- 5 -		tr	tr			0.1
							tr				5	tr	NIL.
		1					- 2 -				2		0.5
	1						- 2 -				tr		2.0
	1	1					- 10 -						12.8
	1	1					- 10 -						13.6
					tr				1	1			0.8
					30		tr						2.2
					3		- 10 -						NIL.
		100											0.2
	tr						- 1 -						51.9
							- 2 -						12.9
	3				tr								43.5
	20								tr				4.8
													8.9
		40				15	- 30 -						2.0
							- 50 -						4.1
									tr		tr		4.4
		10	tr		82		2			tr			NIL.
		35	44		20		tr			tr			NIL.
		10					87						1.1
		30	48		20		tr						0.2

TABLE 1 - *Continued*

Predominantly Inorganic

Sample # incl. depth in core	Qtz	Feldspar		Rock Fragments					Heavy Minerals							
		Plag.	K-	Glas	VRF	Undif.	Chrt	Carb	Biot	Apat	Hrnbld	Rut 1	Tourm.	Zren	Grnt	Sphn
6/2/1 - 44-46 cm.																
6/2/2 - 20-22 cm.																
6/2/3 - 11-13 cm.																
6/2/4 - 16-18 cm.																
6/2/5 - 25-27 cm.																
6/2/6 - 14-16 cm.																
6/3/2 - 24-26 cm.	1															
6/3/4 - 8-10 cm.		tr														
6/4/1 - 29-31 cm.																
6/4/3 - 94-96 cm.																
6/5/2 - 20-22 cm.																
6/6/1 - 11-15 cm.	25			tr												
6/6/1 - 81-83 cm.	40	-tr-						28								
6/6/2 - 3-5 cm.																
6A/1/1 - 33-35 cm.	2	1	3													
6A/1/2 - 20-22 cm.	tr							30								
6A/1/4 - 29-31 cm.								100								
6A/1/6 - 18-20 cm.					100											
7/1/1 - 29-30 cm.																
7/1/2 - 29-30 cm.	10			tr	tr											
7/1/3 - 12-14 cm.																
7/1/4 - 14-16 cm.	tr			tr	tr											
7/1/6 - 19-21 cm.																
7A/2/2 - 21-23 cm.	1			tr	4											
7A/3/1 - 30-32 cm.	tr				3											
7A/3/2 - 12-14 cm.	3				30											

*Note: X represents presence in unspecified amounts.

TABLE 1 - *Continued*

Predominantly Organic

	Dol	Pyrt	Rhodch.	Glauc	Col-Bone	Carb Aggr	Plank. Forams	Benth. Forams	Sponge Spics.	Rad/Diat	Carbonac Debris	Spore	COARSE FRACTION % of Sample
			82		10	2?			5	tr			0.5
			72		20	2?			5	tr			0.4
			72		20	2?			5	tr			0.4
			88		5	5?			1	tr			1.7
			88		5	5?			1	tr			0.5
			88		5	5?			1	tr			1.3
					tr				3	95			0.1
					tr		tr		10	89			2.0
									20	80			26.0
									2	98			0.2
									x	x			0.9
				tr	tr		- 63 -		10	1			29.7
					tr		- 10 -		20	1			72.0
		tr					- 2 -		tr	97			NIL.
		89	tr		5								0.1
		20	5		3	34	7		tr				0.1
													NIL.
													NIL.
							100						0.6
		15			20		54		tr	tr			0.1
		90			5		5			tr			NIL.
		56			3		40			tr			0.1
		99					tr			tr			0.1
			74	tr	20					tr			0.4
		5	41				50		tr				0.3
		15			52								4.9

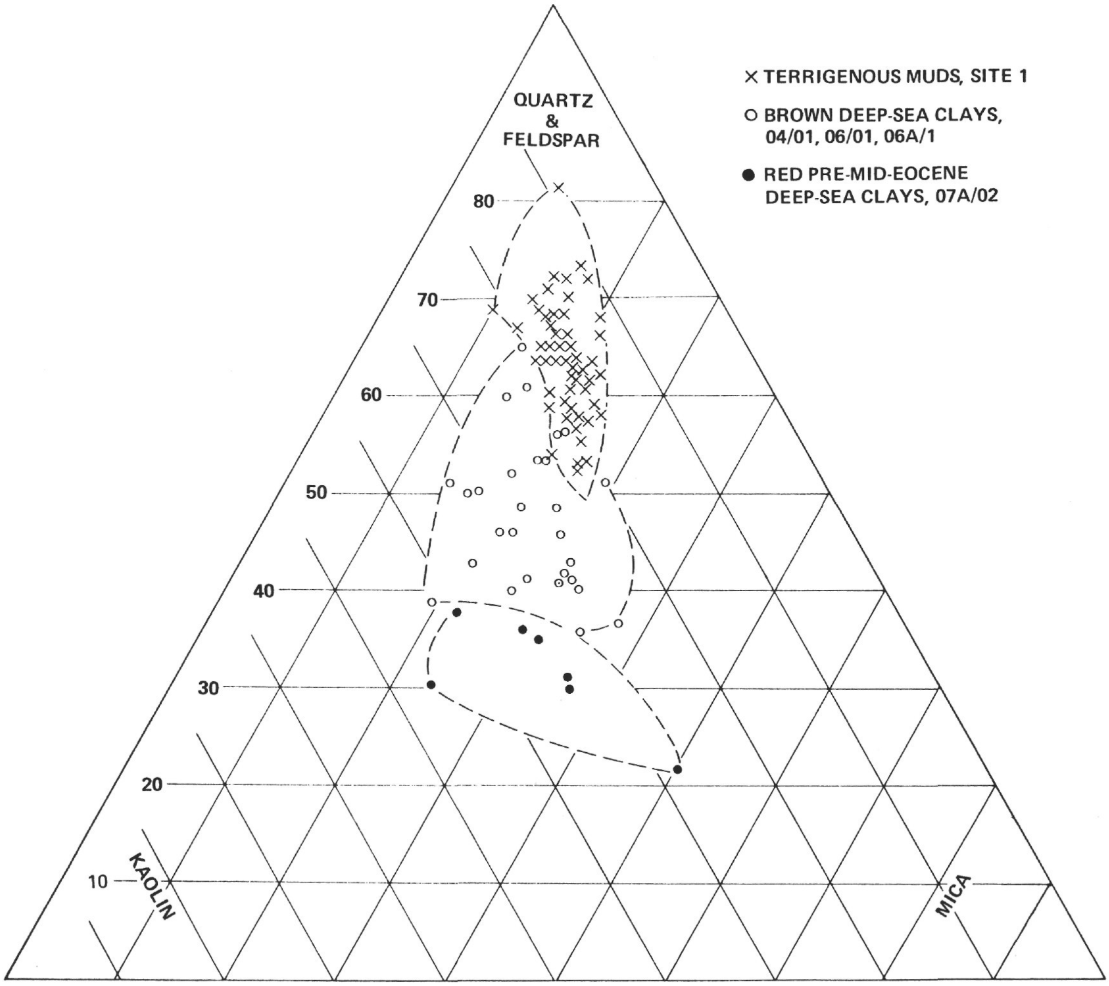

Figure 3. *Ternary plot of paraglacial terrigenous muds and brown to red deep-sea clays, indicating the relative content percentages of quartz and feldspar compared to kaolin and to mica, as shown by Rex' X-ray analyses (this report). As might be expected from their grain size, the paraglacial terrigenous muds show the highest values of quartz and feldspar. They are also notably poor in kaolin. The Eocene red clays of Site 7 show the lowest quartz-feldspar content, and may be the most truly pelagic of the clays drilled on Leg 1.*

and, clinoptilolite is widespread in the Cretaceous sediments of Sites 4 and 5. It is possible that sepiolite occurs in the Eocene of Site 6. Corrensite, rectorite, and palygorskite were searched for by X-ray, but were not found.

Authigenic Silica

Authigenic silica includes the opaline tests of siliceous organisms, inorganically precipitated opaline silica, cristobalite, and fibrous quartz which may occur in either the length-fast or the length-slow form. These minerals, which are involved in the widespread development of chert, are discussed in the section on diagenesis. According to Rex's bulk X-ray analyses, the farthest off-shore brown clays (Core 1 at Site 6 and Core 1 at Site 7) contain as much as 25 per cent cristobalite, not recognized under the microscope.

Carbonates

The carbonate minerals encountered include calcite, aragonite, dolomite, siderite, and rhodochrosite. Some of these carbonate grains are of terrigenous detrital origin. Others were precipitated on shelves or slopes or the deep-sea floor penecontemporaneous with, but at some distance from, the ultimate site of deposition; and they were eroded, transported and resedimented by turbidity currents and other currents. A third category of carbonate grains either arrived at or near the site of

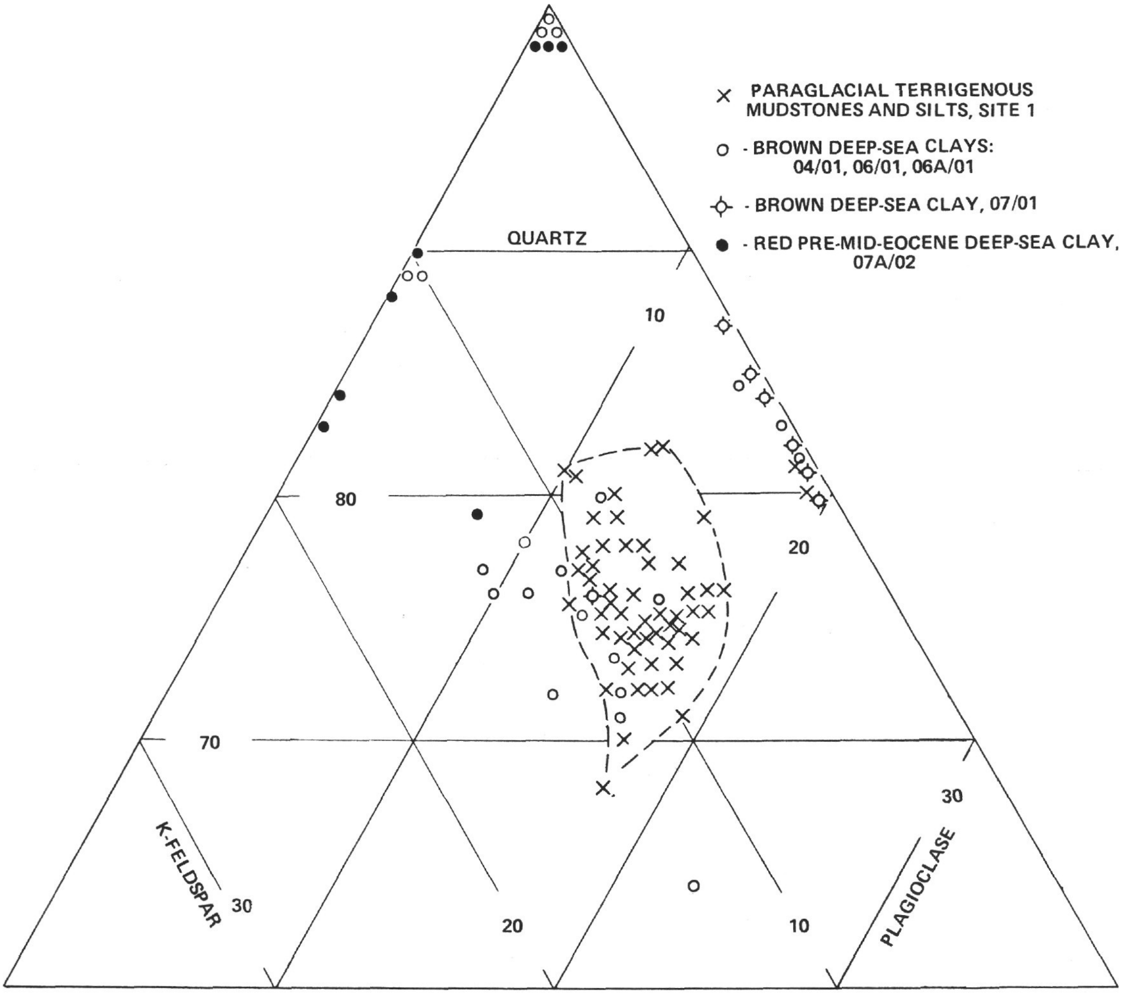

Figure 4. *Ternary plot showing relative percentages of quartz, K-feldspar, and plagioclase in paraglacial terrigenous mudstones and brown and red deep-sea clays. The terrigenous paraglacial muds of Site 1 form a well-defined group, containing all three end-members, characterized by a slight but consistent predominance of plagioclase over K-feldspar. The samples of brown and red deep-sea clays show a much wider scatter. The concentration of many values at the very edges of the diagram is an artifact resulting from the limitations of X-ray bulk analysis; most of these points should be mentally moved toward the center of diagram. Compositions from X-ray analysis by Rex (this report).*

sedimentation in the rain of planktonic skeletons out of the overlying water mass, or was contributed essentially *in situ* by benthic organisms. A fourth category owes its origin to diagenetic processes within the sediment. While such a division is good in theory, a rigorous assignment of individual particles to their category of origin is commonly not possible and, therefore, all are treated here under one major heading.

Calcite is the dominant carbonate encountered. The ratios of calcite to dolomite to quartz and silicates, as determined from Rex's bulk X-ray analyses, are plotted in Figure 5. The calcite of paraglacial mudstones (most of the points in Group I of Figure 5) is judged to be of terrigenous detrital origin, i.e., bits of ground-up limestone. The calcite of Groups II and III is partly of resedimented origin, partly contributed directly from the plankton rain, and in a small part diagenetic. The diagenetic calcite is most conspicuous in Cretaceous and Jurassic cores at Sites 4 and 5, and takes the form of a calcite cement grown *in situ*—a matter discussed further under the heading of diagenesis. A very special kind of diagenetic calcite is that found in the cap rock of the Challenger Knoll (Site 2), discussed in Chapter 2 and illustrated in Plate 17.

The calcite contributed by planktonic organisms was presumably of the low-magnesium type, as is the

PLATE 9

Microphotos

(Note: field views represent a field approximately 1.0 mm in width, whereas enlarged views represent a field approximately 0.4 mm in width.)

A Sample 1P-1-1, 135-137 cm: Field view of foraminiferal tests and debris.

B Sample 1-1-1, 6-8 cm: Enlarged view of volcanic rock fragment and organic carbon debris.

C Sample 1-1-6, 5-7 cm: Field view of dominantly quartz grains and organic carbon debris. Contrast grain-size with following figures.

D Sample 1-1-7, 6-8 cm: Enlarged view of quartz grain showing quartz overgrowth. Common occurrence of such grains suggests multi-cycle sedimentary reworking of quartz.

E Sample 1-2-3, 3-5 cm: Field view of dominantly quartz grains and organic carbon debris. Note large megaspore in upper right. Volcanic rock fragments and volcanic glass make up approximately 20 per cent of the sample.

F Sample 1-2-2, 3-5 cm: Field view of dominantly quartz grains and organic carbon debris. Inclusion-rich volcanic rock fragments again common.

G Sample 1-2-2, 3-5 cm: Enlarged view of green hornblende. Remainder dominantly quartz grains.

H Sample 1-5-1, 41-43 cm: Field view of quartz grains with several volcanic rock fragments. Note lower percentage of organic carbon debris as compared to preceeding samples.

I Sample 1-6-1, 11-13 cm: Enlarged view of detrital dolomite rhombohedron showing zoning. Dolomite is generally present in the sequence in trace amounts.

J Sample 1-6-2, 9-11 cm: Field view of large quartz grains commonly showing abraided overgrowths. Note inclusions within quartz, suggesting sedimentary origin. Dolomite rhombs in upper center of photograph.

K Sample 1-6-3, 4-6 cm: Enlarged view of multiple-quartz grains enclosed in abraided quartz overgrowth. Particle is approximately 400 μ in width.

L Sample 1-7-2, 10-12 cm: Field view of dominantly large quartz grains with minor chert. Note high percentage of inclusions within grains.

PLATE 9

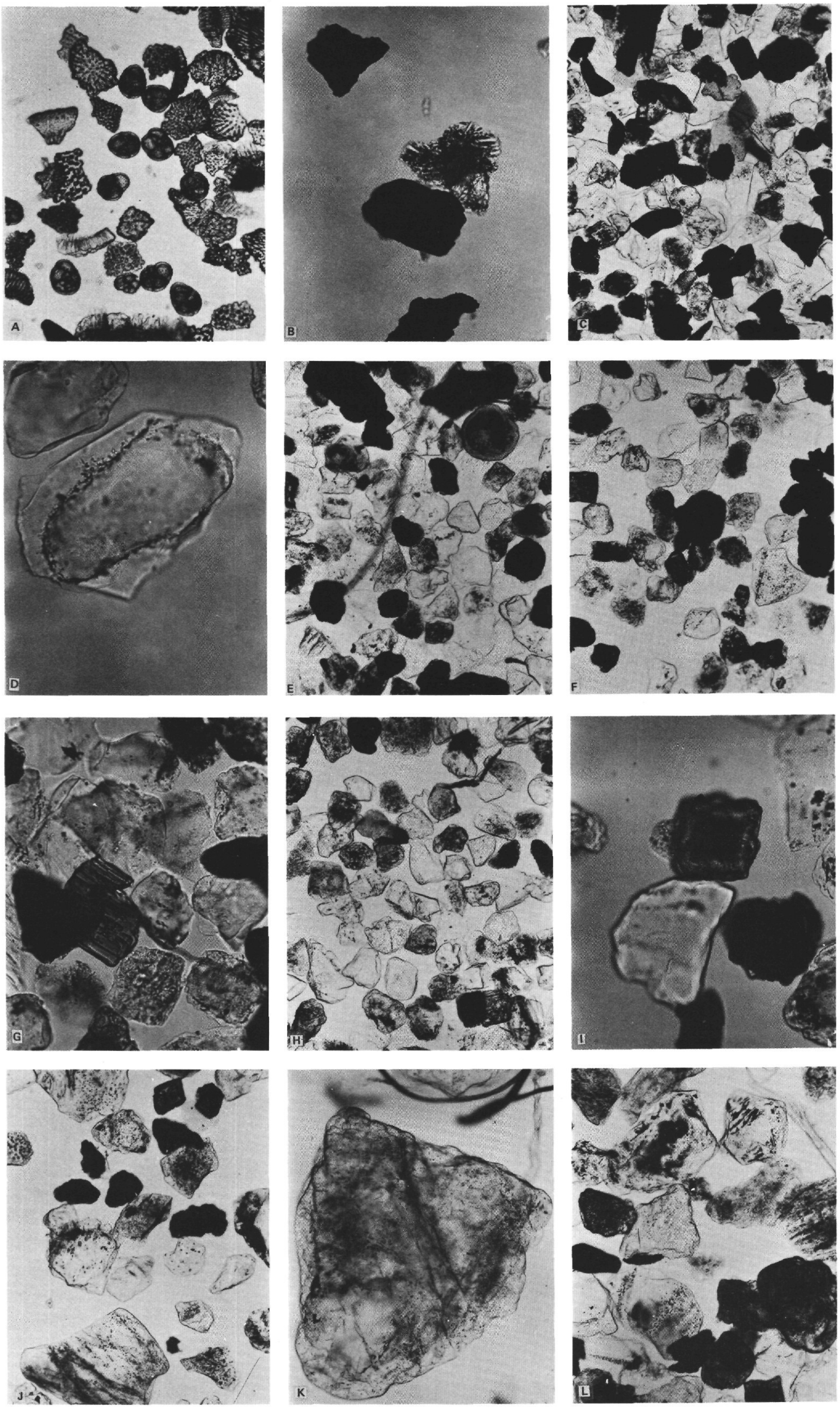

PLATE 10
Microphotos

(Note: field views represent a field approximately 1.0 mm in width, whereas enlarged views represent a field approximately 0.4 mm in width.)

A Sample 1-7-4, 3-5 cm: View of quartz grain with inclusions of carbonate (probably dolomite).

B Sample 1-8-2, 13-15 cm: View of quartz grain showing abraided overgrowth. Needle inclusions constitute a minor grain-type as noted in the sequence from Site 1. Grain is approximately 650 μ in width.

C Sample 1-8-4, 12-14 cm: Field view of dominantly quartz grains. Most of smaller, darker grains are chert. High relief particles near center of photograph are detrital carbonate. Note rounded overgrowth on quartz grain in upper right.

D Sample 1-8-6, 10-12 cm: Field view of dominantly quartz grains with subsidiary chert and organic carbon particles. Note large spicule in upper left.

E Sample 1-9-2, 2-4 cm: Field view of large quartz grains. Note benthonic foraminifera test in lower center.

F Sample 1-9-4, 11-13 cm: Large detrital quartz grain showing common type of inclusions. Well rounded.

G Sample 3-2-2, 40-42 cm: Field view of dominantly quartz grains. Compare with quartz grains from Site 1 microphotos. Note hornblende grain in lower right of center.

H Sample 3-7-3, 66-68 cm: Field view of mixed assemblage of benthonic and planktonic foraminifera. Some of the opaque particles are pyrite rods.

I Sample 3-8-2, 14-16 cm: Field view of dominantly planktonic foraminifera. Opaque particles are pyrite.

J Sample 3-8-5, 13-15 cm: Field view of dominantly pyrite spheres with subsidiary fragments of planktonic foraminifera tests.

K Sample 3-8-5, 13-15 cm: Enlarged view of twinned dolomite rhombs, possibly detrital.

L Sample 3-9-2, 15-17 cm: Field view of dominantly carbonate debris. Note radiolarian test in right center of photograph.

PLATE 10

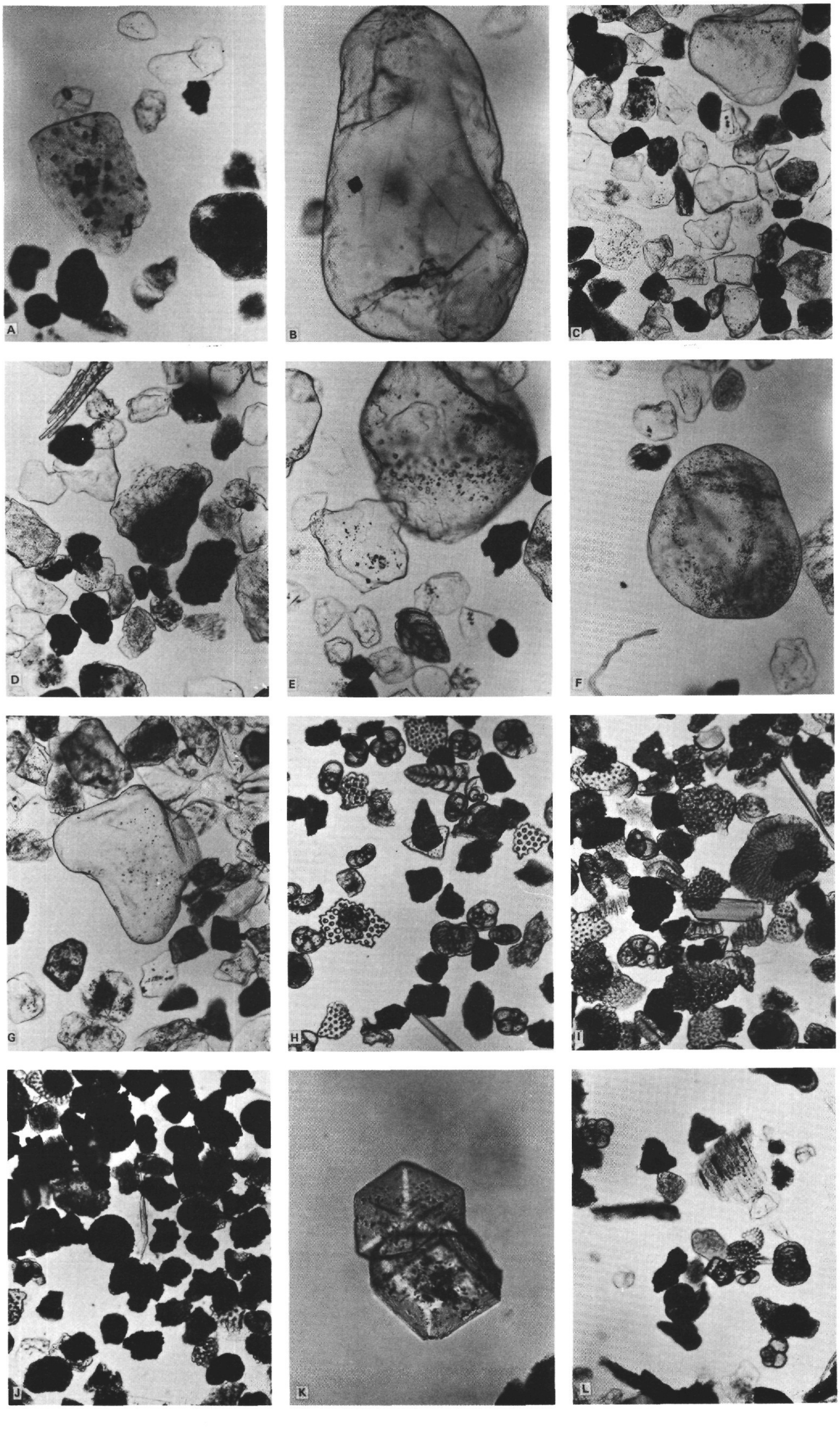

PLATE 11
Microphotos

(Note: field views represent a field approximately 1.0 mm in width, whereas enlarged views represent a field approximately 0.4 mm in width.)

A Sample 3-10-2, 9-11 cm: Enlarged view of quartz grain showing overgrowth.

B Sample 3-11-1, 75 cm: Field view of quartz, volcanic rock fragments, and subsidiary biotite (upper right of center). Note hornblende grain in lower left of photograph.

C Sample 3-11-1, 75 cm: Enlarged view of volcanic rock fragment. Grain is apparently comprised dominantly of plagioclase feldspar microlites.

D Sample 4-1-6, 10-12 cm: Field view of bone (?) plus collophane fragments, subsidiary volcanic rock fragments, and undifferentiated rock fragments.

E Sample 5-1-2, 60-62 cm: Field view of dominantly carbonate debris with subsidiary opaque grains of pyrite. Some carbonate grains appear detrital. Foraminifera test appear somewhat recrystallized.

F Sample 6-1-4, 7-9 cm: Field view of light colored collophane, intermediate grains of rhodochrosite (? of siderite) and opaque grains of pyrite.

G Sample 6-2-2, 20-22 cm: Field view of dominantly rhodochrosite (?) rhombs.

H Sample 6-4-1, 29-31 cm: Field view of radiolarian, diatom, and sponge spicule debris.

I Sample 6-6-1, 11-15 cm: Field view of mixed assemblage of sponge debris, diatom and foraminifera tests, and quartz grains.

J Sample 6A-1-2, 20-22 cm: Field view of undifferentiated carbonate, possibly similar to rhodochrosite-siderite assemblage in F & G. Subsidiary pyrite and spicules plus collophane particles.

K Sample 7-1-2, 29-30 cm: Field view of bone plus collophane grains, undifferentiated carbonate grains and subsidiary rhodochrosite (?) particles. Minor amounts of quartz are also present. Opaque grains are pyrite.

L Sample 7-1-2, 29-30 cm: View of volcanic rock fragment. Bulk X-ray of this sample resulted in high plagioclase percentage, suggesting a much higher content than obtained by visual inspection.

PLATE 11

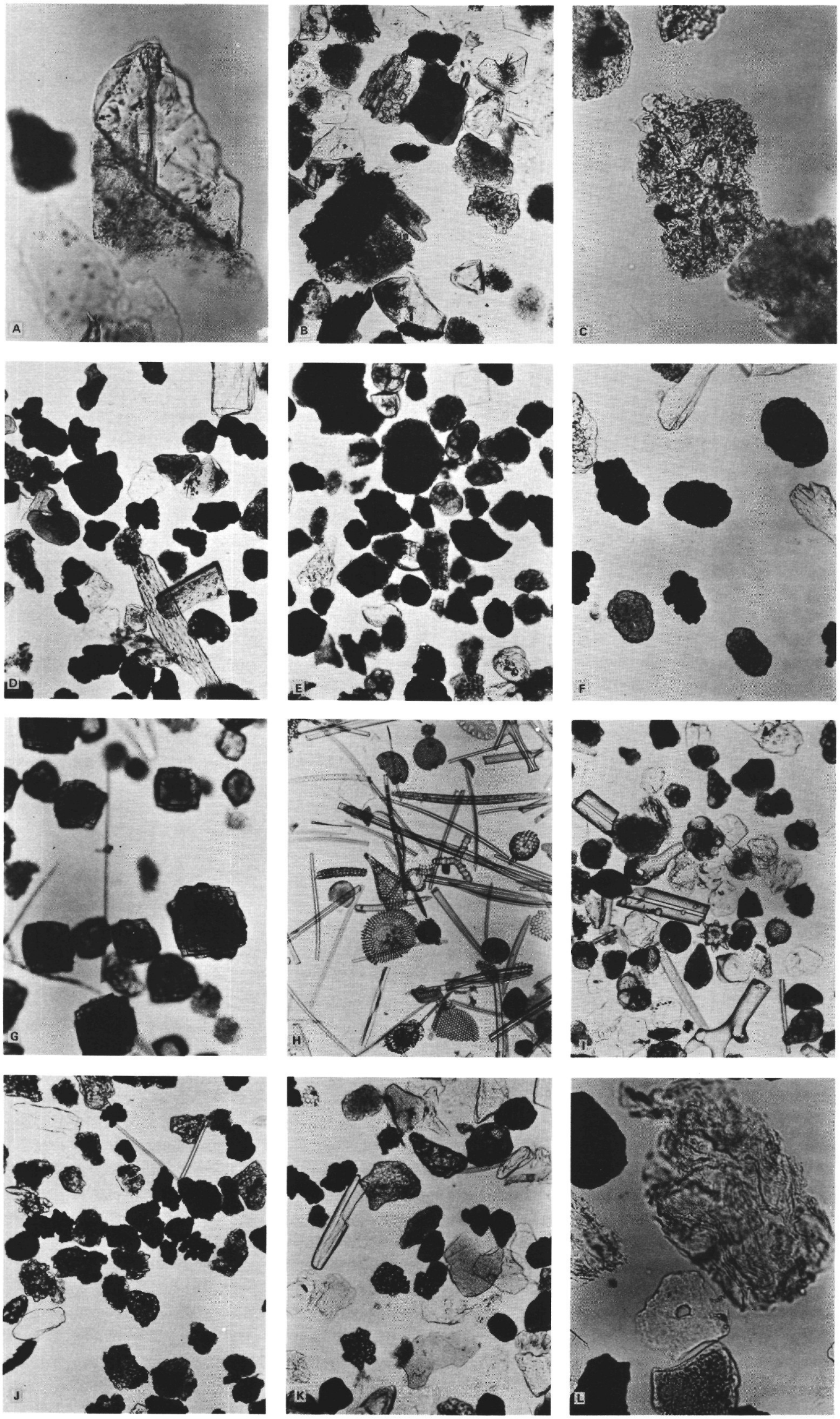

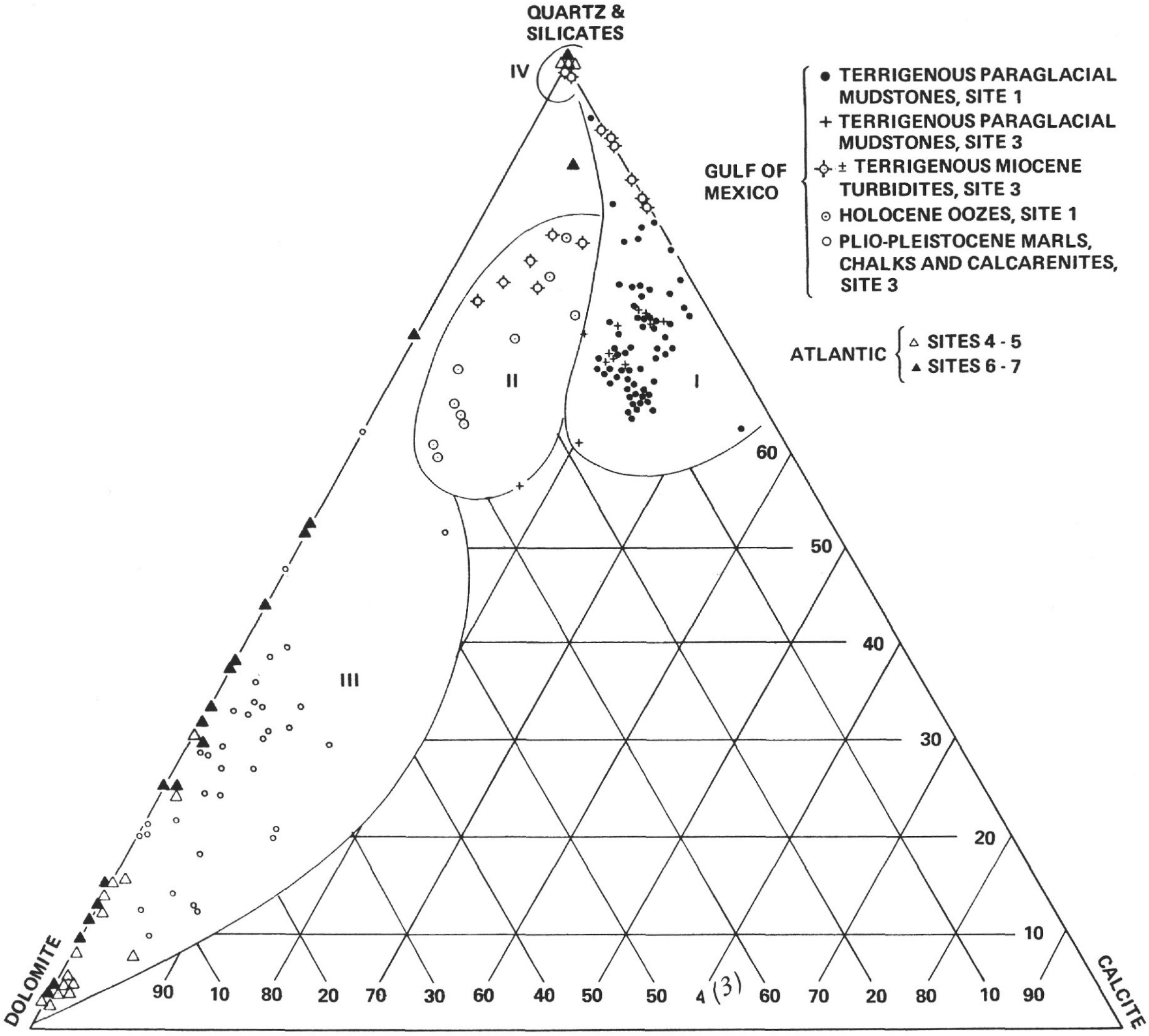

Figure 5. *Ternary plot of calcite, dolomite, and the remaining minerals (mainly quartz and silicates). Percentage compositions from Rex' X-ray data (this report). Samples fall into four distinct groups, as follows: (I) Terrigenous mudstones characterized by a high silicate-quartz content and a predominance of dolomite over calcite. Samples in this group are mainly the paraglacial terrigenous muds of Sites 1 and 3, but include a few Miocene turbidite samples from Site 3. (II) Samples of composition intermediate between (I) and (III), representing pelagic carbonate sediments with appreciable terrigenous contamination. Samples in this group include Recent muds at Site 1, and sediments associated with Miocene turbidite sands at Site 3. (III) Organogenic carbonates characterized by comparatively low content of silicates and quartz, and by a predominance of calcite over dolomite. This group includes the pelagic carbonates, as well as the shelf or slope derived carbonate turbidites. (IV) The various sediments lacking in carbonates are indicated here by a token plot only.*

terrigenous calcite. Much of that supplied by benthonic organisms, mainly in the form of resediment from the shelves, must have been of the high-magnesium type. The diagenetic calcite may be one or the other. As yet, no studies have been made of the magnesium content of these calcites.

The granules, cobbles and probably boulders of limestone in the pebbly mudstones of Sites 4 and 5 represent a special type of terrigenous carbonate, which was dealt with in Chapters 4 and 5.

Presence of aragonite in the calcareous turbidites and associated sediments of the Gulf of Mexico Neogene was suspected from the presence of tunicate spicules and molluscan debris, and is confirmed by Rex's bulk X-ray analyses. These also show some aragonite in the Eocene of the Bermuda Rise. No aragonite is recognized in the Cretaceous and Jurassic of Sites 4 and 5. It seems most probable that the resedimented Cretaceous calcarenites at these sites originally contained aragonite, and this was dissolved and reprecipitated in the form of a calcite cement during diagenesis.

Small quantities of dolomite have been reported from deep-sea sediments in numerous instances. In the samples here studied, dolomite rhombs are conspicuous in the Neogene chalks and marls of the Gulf of Mexico as well as in the Paleogene carbonates of the Bermuda Rise and the Cretaceous and Tithonian of the Blake-Bahama Basin. The oldest sediments contain the largest and most conspicuous rhombs, but not necessarily the highest dolomite content, judging from the X-ray analyses. Three modes of origin are considered: terrigenous derivation, growth of dolomite on the shelf and penecontemporaneous resedimentation into the deep sea, and authigenic origin on or below the deep-sea floor. The abundant dolomite in the paraglacial muds of Sites 1 and 3 (Figure 5, Group I) is clearly of terrigenous origin. This strongly suggests that some of the dolomite found in the other sediments is likewise derived from the erosion of older dolomites on land, even though the proportion of dolomite carried to the sea must be vastly greater at times of widespread glacial abrasion than in normal times. On a regression plot of quartz content against dolomite content (Figure 6, based on Rex's X-ray values), these paraglacial muds cluster in a distinctive group (A), while the remaining sediments scatter much more widely toward both higher and lower dolomite-quartz ratios. This suggests that terrigenous influx is not the only source of dolomite in deep-sea sediments. Resedimentation of shelf-derived, authigenic dolomite may play a role; but, if this were a major one, dolomite would be found conspicuously associated with resediments and not with pelagic chalks. Since this is not the case (Figure 5), the authors conclude that some dolomite is diagenetically produced in abyssal depths.

Siderite was sporadically encountered during optical investigation as well as in the bulk X-ray analyses. In the coarser terrigenous sediments some siderite may be of terrigenous origin, but the pelagic siderite occurrences are presumably diagenetic.

Rhodochrosite was encountered in the optical study of coarse fractions from the pre-Middle Eocene red clays at Site 7. This occurrence is surely of diagenetic origin. The records of rhodochrosite in various samples in the bulk X-ray analyses are too small to be completely trustworthy as they possibly represent dolomite (Rex, personal communication).

Iron Sulfides

The iron sulfides encountered include black stains attributed to ferrous sulfide and brassy sulfides, at least some of which are pyrite as checked by X-ray diffraction, and all of which are treated here as such. The pyrite is ubiquitous not only in the white or dark sediments but also in the brown and red ones. While optically conspicuous it generally escapes X-ray detection. Inasmuch as these minerals are of diagenetic origin, they are discussed later under that heading.

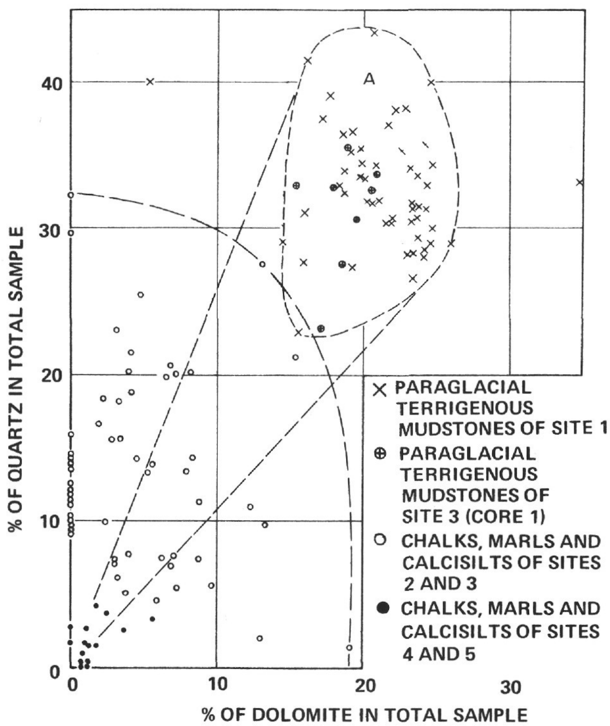

Figure 6. *Regression plot of quartz content compared with dolomite content of certain samples, from bulk X-ray analyses by Rex (this report). The paraglacial terrigenous mudstones of Sites 1 and 3 form one well-defined group (A), characterized by comparatively high content of both quartz and dolomite, with the quartz/dolomite ratio ranging from 0.9 to 2.5. The chalks and calcarenite-calcisiltites show smaller absolute values of quartz and dolomite, somewhat greater in the Neogene sediments of the Gulf of Mexico than in the Cretaceous of the Blake-Bahama Basin. The quartz-dolomite ratios in these carbonates show a much greater range than those in the terrigenous mudstones.*

Iron Oxides

Iron oxides occur in brown hydrated limonite form (presumably, in part amorphous and in part goethite), and as hematite.

The hydrated oxides occur in disseminated form, in more or less well-defined microscopic granules (Plate 6B) in larger nodules (Plates 1 and 2), in which they may be associated with manganese compounds. They are mainly responsible for the color of the brown clays so characteristic of the upper cores in the Atlantic sites and contribute much to the color of the pre-Middle Eocene red clays at the bottom of Hole 7.

Hematite occurs in the form of ruby-red flakes in the smear slides. It is an uncommon constituent in the brown Pliocene-Pleistocene clays of the Atlantic sites, but it assumes much larger importance in the red pre-Middle Eocene clays of Site 7, where occurrence is attributed to diagenetic alteration from limonite (see diagenesis).

Distinctive rhomboidal flakes of an X-ray opaque mineral are clearly seen in X radiographs of a volcanic-rich clay in the Cretaceous of Site 5 (Plate 2C). This may be an iron mineral of volcanic origin.

Manganese Oxides

Manganese minerals are not overly common in the cores of Leg 1. The occurrence of rhodochrosite has been discussed above. Black pellets from the brown Atlantic deep-sea clays, studied by Beall, failed to yield X-ray patterns of crystalline manganese minerals, but they may be mixtures of clay with amorphous manganese and iron oxides or hydroxides.

The brown limonite nodules discussed above may also contain manganese, but no studies have been made to date.

The red pre-Middle Eocene deep-sea clay at the bottom of Hole 7 contains conspicuous, small black nodules. Such a nodule, measuring 10 X 5 X 2 millimeters from Core 7A-3, Section 1, sampled at 49-51 centimeters, was studied by Beall. X-ray diffraction analysis shows the presence of $MnO_{1.88}$ and trace amounts of clay; and X-ray fluorescence analyses plus neutron activation analyses show a high manganese content and a small percentage of iron in the nodule, as well as manganese enrichment in the surrounding matrix.

Sulfates

The major occurrence of sulfates recorded is that of the Challenger Knoll cap rock (Site 2), described in Chapters 2 and 22.

The main mineral is gypsum, but traces of anhydrite were also found in acid residues of the carbonate cap rock.

The bulk X-ray diffraction analyses also record small quantities of anhydrite in a few samples at Sites 2, 3, and 6. These occurrences appear improbable on geological grounds—especially inasmuch as the stable phase is gypsum. They are treated therefore, as anomalous and suspect.

Glauconite

Glauconite is an authigenic marine silicate which is produced mainly on the continental shelf. Glauconite pellets are abundant in the Middle Eocene turbidites of Sites 6 and 7, and the authors interpret them as shelf-derived and penecontemporaneously resedimented.

Apatite and Phosphatic Skeletal Remains

Some terrigenous apatite occurs in the terrigenous sand and mud sequences, but the majority of the scattered apatite occurrences picked up by optical examination and by bulk X-ray analyses are fish remains. No systematic studies were made, but the rule that an abundance of rich remains is associated with slow sedimentation or sedimentary hiatuses is confirmed here by the observation that such remains are relatively more abundant in the thin sedimentary sequence on the Challenger Knoll (Site 2) than in the much-thicker, correlative sediments of the Sigsbee Abyssal Plain (Site 3). Fish remains also form a conspicuous feature of the residue of the pre-Mid Eocene red clays of Site 7.

SEDIMENTARY STRUCTURES

Sedimentary structures are discussed from the standpoint of visual description as well as from core X radiography. Brief summary descriptions of sedimentary structures and their interpretation have been given in individual hole summaries. This section attempts to summarize sediment types with associated sedimentary structures into three categories on the basis of dominant sedimentary processes operative during deposition. The categories are: (1) pelagic, (2) turbidity or density current and associated gravity flow phenomena, and (3) sediments intermediate between pelagic and turbidity current deposited. This last category involves sediments of various types in which interpretations are based on lack of distinctive criteria as to pelagic or turbidity current origin.

Differentiation of deep-sea sediment into two-basic end members—pelagites and turbidites—involves acceptance of concepts which have been the subject of much argument during the last decade. It is not the authors' intent to review the voluminous literature which now exists on the subject of turbidites and turbidity current mechanisms. Kuenen (1967) has presented, at some length, arguments which have not been answered conversely by critics from the "deep-sea bottom currents" school.

Deep-sea sands, several centimeters to several decimeters in thickness, showing textural grading and massive to horizontal lamination are generally accepted as being of turbidity current origin. Kuenen (1967) has discussed the general insufficiency of "normal" deep oceanic currents to yield deposits of such character.

Recognition of pelagic sediments is based on: obvious pelagic components, general fine-grained character, slow rates of deposition and associated burrowing, and lack of structures and textures associated with turbidites. Unfortunately, the inorganic clay fraction can be termed pelagic only by inference and association with the other criteria outlined above. Deep oceanic bottom currents, surface currents, and turbidity currents are all capable of transporting clay.

The fine-grained tops of turbidites are often assumed to be pelagic, yet they often lack the criteria associated with pelagic sediments. Hsu (1964) has suggested that normal bottom currents are responsible for distribution of much of the fine-grained tops of turbidites (see Kuenen, 1964, for arguments against such a mechanism). At least part of this controversy may be due to two factors: a lack of detailed textural information in the fine-grained tops of turbidites, and a failure to recognize that clay may be transported and deposited in aggregates of silt and sand size (in terms of effective settling rate).

Detailed investigations of texture and mineralogy have been conducted by Beall on Pleistocene and Recent sediments from the Gulf of Mexico Abyssal Plain. Although the data are not presented here, it can be stated that sediments deposited during glacial maxima (low sea level stage) are characterized by structures and textures associated with turbidite current origins. These sediments consist of laminated to massive quartzose silty clay with intercalated thin (commonly less than 1.0 millimeter) silt laminae and rarely found, thin (less than a few centimeters), very-fine sand laminae. Silt laminae are commonly horizontally-to-subhorizontally microlaminated and they are rarely ripple-bedded. Small scale ripple cross-lamination is generally low angle when present. Texturally, the fine-grained interbeds are characterized by significantly larger percentages of silt as compared to interglacial pelagic strata which occur in the sequence. These latter sediments are commonly burrowed and vaguely laminated, light-colored, foraminiferal lutites. Extraction of the foraminiferal tests leaves a very fine-grained clay. The pelagites, as defined here, are consistently enriched in montmorillonite whereas the laminated, silty clays and laminated silts are enriched in illite plus kaolinite (in generally coarser size fractions).

The term "laminite" (Lombard, 1963) has been ascribed to the laminated clays and silts described above; and, in this context, such sediments are described as a laminite facies of continental rise and abyssal plain sedimentation and are thought to represent turbidity current deposition. The arguments previously put forth by Kuenen (1967) for deep water sands can be equally well applied to these finer-grained deposits. Apparently, less energy is required to transport such fine-grained sediments, but the same general mechanisms should apply. Short period waxing waning normal bottom currents appear unlikely on the abyssal plain of the Gulf of Mexico. As Ewing *et al.* (1958) have shown, absence of laminites of the Sigsbee Knolls can be taken as strong evidence for a turbidity current origin of the abyssal plain.

It is suggested that much of the fine-grained material deposited in an abyssal plain setting is delivered to that site by a turbidity current mechanism. It is further suggested that much of the clay is delivered in the form of clasts of silt and sand size. Absence of criteria normally used to establish a pelagic origin for such sediments, high rates of deposition as judged by various criteria, presence of sedimentary structures and textures reminiscent of thicker turbidity current deposits, and extensive distribution of such sediments on abyssal plains are taken as support for the interpretations as applied herein.

Turbidites

Examples of various turbidity current deposits are shown in Plate 12. These sediments, easily ascribed to emplacement by turbidity currents, vary in mineralogical composition and characteristically show textural grading; they are sometimes massive, often horizontally-laminated and uncommonly small scale ripple-bedded in the upper part. Ripple cross-stratification is rarely present near the base of a graded unit. Presence or absence of convolution is difficult to assess because of distortion of the core during coring. Additional descriptions are given in the legend to Plate 12.

Plates 13 and 14 show detailed illustrations of turbidities in which results of textural analysis are combined with physical measures of bulk density and natural gamma-ray activity. In an accompanying section, there is further comment on the physical measurements.

Core 3-2, Sections 1 and 2 (Plate 13) show a more or less massive, vertically texturally graded unit with suggestions of horizontal lamination. The basal contact of the sand is very sharp with the underlying faintly mottled mud. Irregularity of the basal contact of the sand is suggestive of current scouring although distortion during coring may be responsible. Textural analyses show a consistent upward fining in grain-size and a concomittant increase in the per cent finer than 31 microns. The only exception to this is in the lower 10 centimeters of sand, where a slight fining is present, possibly corresponding to the basal reversely graded unit noted by various workers as sometimes occurring in ancient turbidite sequences.

The textural boundary between silt and mud at approximately 84 centimeters corresponds to a marked irregularity, suggesting the presence of the upper bounding surface of a ripple-stratified unit. This bounding surface is also reflected by natural gamma-radiation measurements, showing a marked inflection of the curve at approximately 85 centimeters. High gamma-radiation counts above this level reflect the increasing clay content of the sediment, whereas the lower readings below are a function of increasing quartz (decreasing clay) content. Thus, lowest gamma-radiation readings are seen near the base of the sand unit where textural analysis demonstrates a coarser grain-size and lower matrix content. Note also that the highest values of

PLATE 12

Sedimentary structures–turbidites and pebbly mudstones

A Core 3-2-3, selected intervals from 28 to 147 cm: Texturally graded unit, ranging from muddy, medium grade sand at base up to muddy, very fine sand or sandy silt at top. Disturbance during cutting prevents a detailed discussion of sedimentary structures. Approximately, horizontal lamination at 130 cm. Smeared interval from 37 to 46 cm suggests small scale ripple lamination overlain by faintly horizontally laminated mud (as described in original core description). Note sharp basal contact of sand.

B Core 3-1-1, 78-100 cm: Texturally graded unit showing abrupt upper and lower contacts with mud. Despite disturbance during core cutting, basal convolution within sand unit (not due to coring) is apparently overlain by horizontal lamination. Note that thicker intervals in uppermost portion of unit are comprised of fine mud or clay.

C Core 3-10-2, 26.5-29 cm: A mixed assemblage of quartz silts showing some small-scale ripple laminae and sharp basal contacts intercalated with mottled and burrowed mudstone overlying a slightly graded silty calcilutite (43-48 cm): The calcilutite contains a high percentage of detrital carbonate rock fragments of shallow water origin. The lower contact is considerably more abrupt than the upper, although the photograph does not clearly show such.

D Core 3-11-1, selected intervals from 84-120 cm: Badly disturbed (during coring), texturally graded, highly carbonaceous, quartzose sand unit intercalated with burrowed to massive mudstone. Although not shown in the photograph, basal contact of the sand is quite sharp, showing oriented striae/poorly developed microgroove casts, suggesting sole markings. The upper portion of the sand unit is highly disturbed, suggesting either convolution or inclusion of large clasts of mudstone. The relationship is obscured by subsequent burrowing, as most clearly seen around 90-92 cm.

E 3-7-3, selected intervals from 27-75.5 cm: Texturally graded carbonate sands (light-colored units from 30-62 cm and below 70 cm) intercalated with burrowed coccolith calcilutite. Carbonate sand in center consists of mottled finer-grained unit below overlain by horizontally laminated carbonate sand grading up into mottled finer-grained calcilutite. This unit is interpreted to represent the super-position of two or more flows.

F Core 4-2-1, selected intervals from 2-50 cm: Pebbly muds consisting of limestone rock fragments and coccolith ooze clasts in a soft coccolith ooze matrix, interlayered with a graded detrital, carbonate sand from 13-22 cm (partially cemented). Another graded calcarenite is present approximately 25 cm below the base of this photograph.

G Core 4-1-2-6, selected intervals: Consists of upper, massive, graded carbonate sand overlying zone of mixed carbonate sand and clasts of mud. This lithology overlies highly distorted silty clay containing scattered granules of detrital carbonate and occasional altered pumice (?) rock fragments. The sediment gradually becomes finer-grained and lighter-colored downward as well as becoming totally plastically deformed and mixed appearing. The upper carbonate sand unit is interpreted as a turbidite overlying a plastically deformed (mudflow?), volcanogenic, hemi-pelagic clay.

H Core 5-1-2, 5.5-23 cm: Massive, pebbly calcarenite comprised of limestone rock fragments of shallow water origin.

I Core 6-4-2-3, selected intervals from 127-147 cm and from 27-74 cm: Demonstrates texturally graded quartz and calcareous plus siliceous biogenic debris sharply overlying burrowed diatom-coccolith ooze. The sand unit is basically horizontally laminated although there is a suggestion of divergent dips in the upper portion (ripple bedding?). Small clasts of biogenetic ooze are present in the central portion (27-37 cm) of the sand.

J Core 4-3-1, selected intervals from 90.5-118.5 cm: Massive appearing pebbly mudstone comprised of limestone rock fragments of granule size in a matrix comprised dominantly of calcareous debris and coccoliths above and clay minerals below.

K Core 4A-1-1, selected intervals from 28-50.5 cm and from 128-150 cm: From the base, consists of mottled coccolith calcilutite overlain sharply by a thin unit of white, silty calcilutite (139-145.5 cm). This unit is overlain by an unconsolidated, white, more or less massive calcarenite, which is in turn overlain by a partially consolidated, texturally graded calcarenite which contains clasts of mudstone at various horizons, suggesting multiple grading.

L Core 6-3-4, selected intervals from 78-126 cm: Texturally graded and horizontally-to-subhorizontally laminated sandy/clayey silt comprised of quartz and calcareous/siliceous biogenic debris. Sharply overlies (109.5 cm) mottled diatom ooze grading downwards into another graded unit below.

PLATE 12

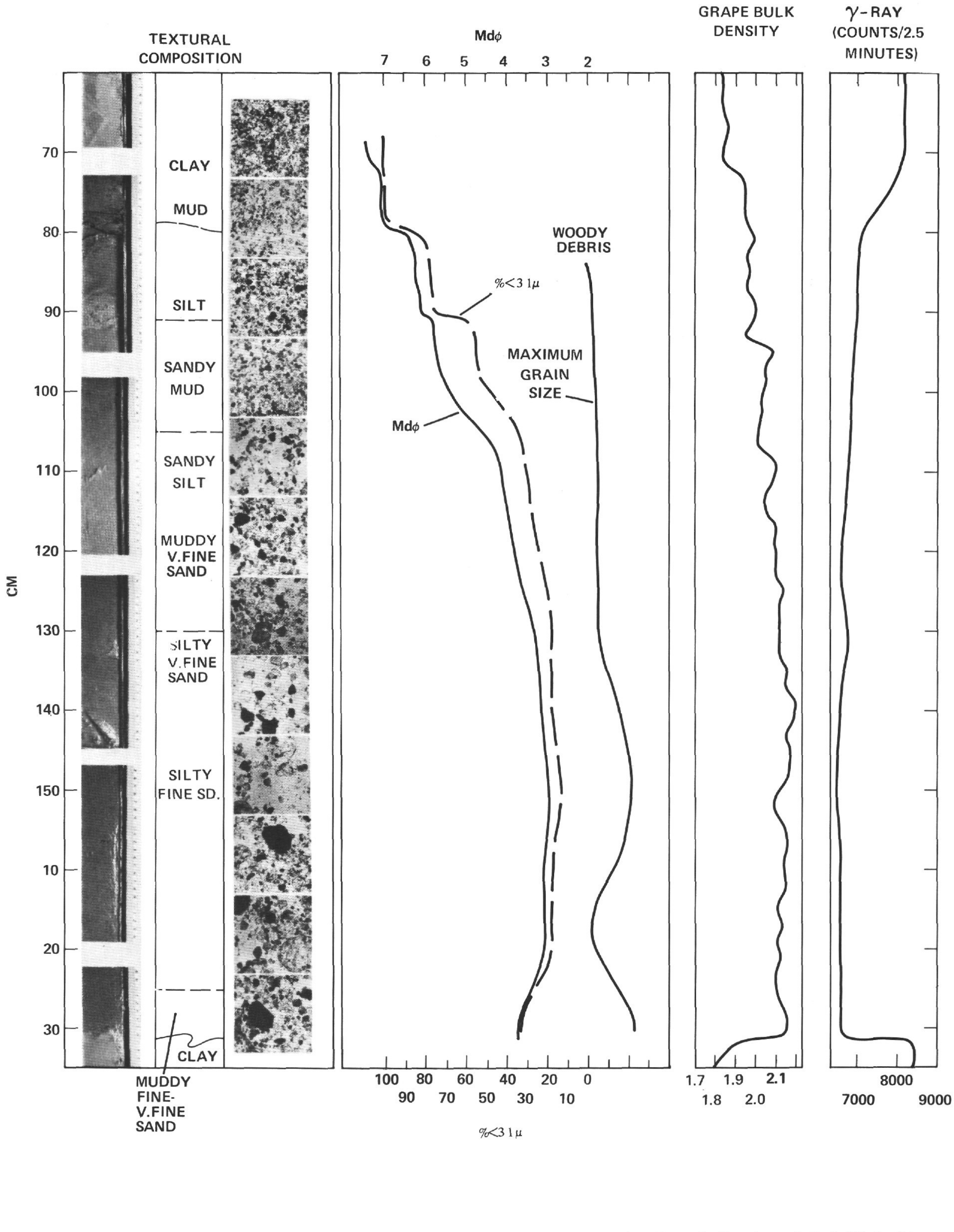

Plate 13. *Relationships between lithology and physical properties for Core 2, Sections 1 & 2 (Hole 3).*

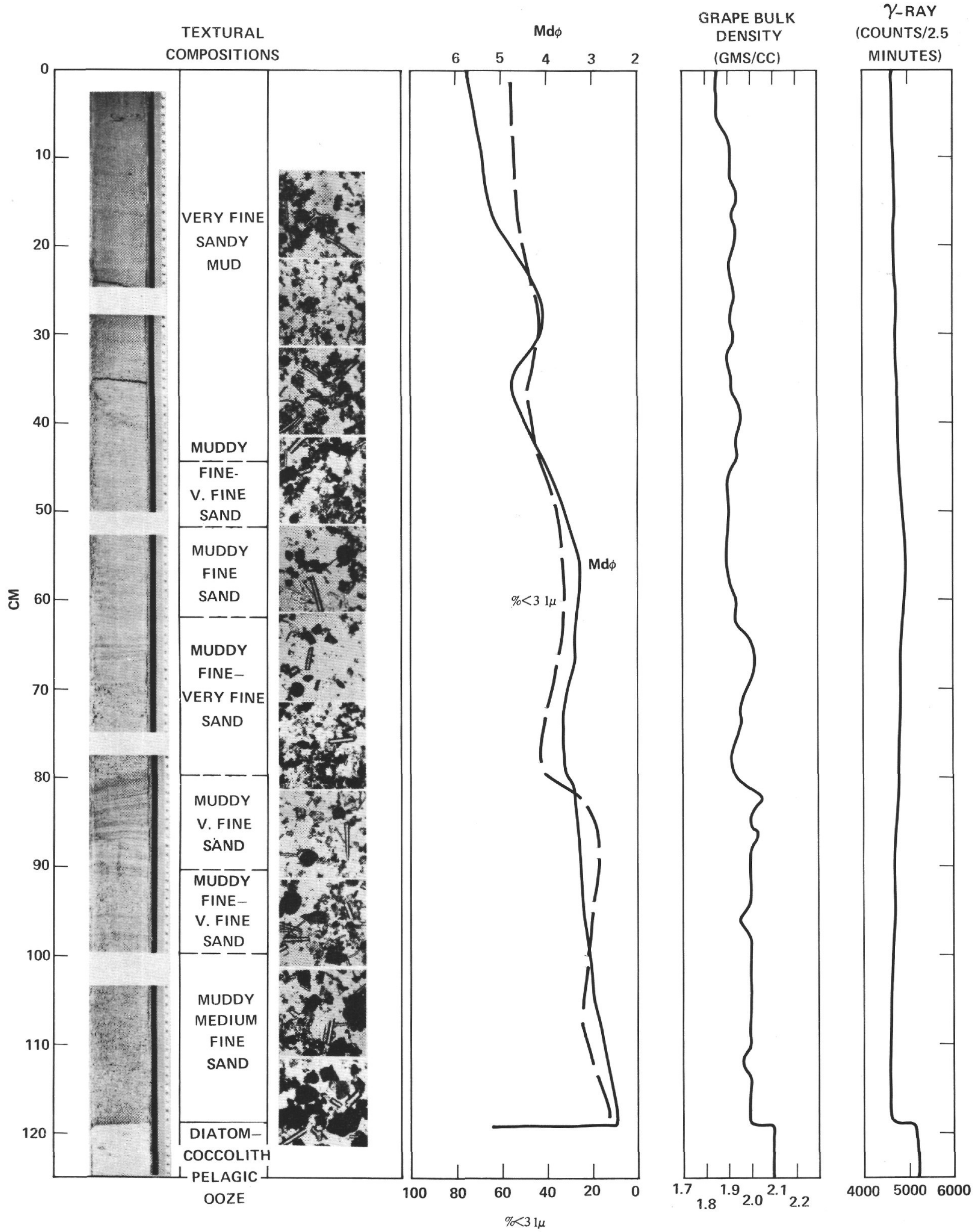

Plate 14. *Relationships between lithology and physical properties for Core 6, Section 1 (Hole 6).*

bulk density are recorded in the coarsest portion of the bed, reflecting a lower "effective" porosity as compared to the unconsolidated clays above and below. These types of physical relationships are to be expected in unconsolidated sediments.

Core 6-6, Section 1 (Plate 14) was chosen as an ideal example of a turbidite of considerably different composition as compared to Plate 13. Sharply overlying semi-consolidated diatom-coccolith pelagic ooze, this unit is dominantly massive-to-horizontally laminated, rarely subhorizontally laminated, and vertically texturally graded.

High percentages of clasts (comprised of pelagic ooze) occur between 70 and 80 centimeters, and at, approximately, 50 to 57 centimeters. This is suggestive of a multi-graded unit.

Detailed textural analysis shows that the unit grades from muddy, medium fine sand up to very fine sandy mud. Note that the curve representing median grain-size shows an inflection between 70 and 80 centimeters, opposite from the previously mentioned interval of clay clasts. This probably reflects disaggregation of the clasts during textural analyses. It is suggested that this interval represents the basal unit of a superimposed turbidite, thus accounting for the slightly coarser material between 50 and 70 centimeters.

Compositionally, detritus in this unit represents a mixed assemblage of source terrains. Quartz, carbonate grains, foraminifera tests, and sponge spicules comprise most of the sand fraction near the base of the sand unit. Foraminiferal tests increase in abundance upward, making up approximately 65 per cent of the sand fraction near the top of the graded sequence. The finer-grained matrix material is comprised dominantly of coccolith, diatom, and radiolarian debris, with minor amounts of clay minerals.

The high percentage of pelagic debris of deep water origin suggests either a considerable amount of assimilation of deep water debris while the turbidity current was en route to the site of deposition, or initiation of the flow at a site where abundant pelagic debris was initially available. Considering the thickness of the graded unit and the remarkable distance from known sources of terrigenous debris, the first alternative is favored. Such a turbidite would correspond to the predictions of Kuenen (1967), as to the ultimate terrigenous versus pelagic composition of a distal turbidite.

In Core 6-6, Section 1, the correspondence of physical measurements to lithic character is good, though not as dramatic as in Core 3-2, Sections 1 and 2. Gamma-ray values are comparatively monotonous through the sand sequence, and slightly higher in the pelagic ooze below, theoretically due to a higher clay mineral content. Bulk density shows a general decrease upward, corresponding to an increase in finer-grained sediment with higher effective porosity. Note that the semi-consolidated pelagic ooze below the sand unit has the highest bulk density, suggesting a state of overconsolidation when compared to theoretical porosity based on bulk densities obtained at the top of the graded sand unit. This is yet another example of unsolved problems related to consolidation of diverse sediment types.

Also shown in Plate 12 are various examples of what might generally be called pebbly mudstones. Plate 12, F and J show different sediment types which are characterized by coarse clasts in a fine-grained matrix. Both examples, described in the legend of Plate 12, are from Site 4 and apparently reflect proximity to the carbonate banks of that region. A related sediment type is shown in Plate 12G. This assemblage of sediment types has been interpreted to represent a carbonate turbidite overlying a plastically deformed (mudflow?) volcanogenic clay.

Pelagic and Hemi-pelagic Sediments

Examples of various types of pelagic and hemi-pelagic sediments are shown in Plate 15. These sediments characteristically are: very fine-grained, often burrowed, rich in pelagic debris, and lacking in terrigenous detritus. Where terrigenous detritus is present in significant amounts, the sediments are arbitrarily termed hemi-pelagic. Most of the arguments pertaining to differentiation of pelagic sedimentary processes as contrasted to turbidity current processes were discussed in a previous section.

Presence or absence of burrowing was often used to support interpretations of depositional rate. Although not frequently noted in this study, examples of moderately burrowed turbidites are known from the literature. A considerable variety of burrow types was noted during description of the cores taken in the present discussion. The presence of faecal (?) pellets, several types of pyrite tube-shaped fillings (?), and a broad range in burrow fill and morphology suggest a wide range of burrow origins. Cores collected during Leg 1 would form a good base for a detailed study of burrow types as deduced from sedimentary structures and composition.

Laminites

Plate 16 shows a somewhat broad range of sediments which are interpreted as intermediate between truly pelagic sediments and what are conventionally interpreted as turbidites. These sediments, as previously described, basically consist of laminated silts (and, rarely, sands) and muds or clays, sometimes intimately associated with either burrowed pelagic sediments or with turbidites.

PLATE 15

Sedimentary strucutres–pelagic and hemi-pelagic sediments

A Core 2-1, Section 2–selected intervals from 38-72 cm: Vaguely to moderately color-banded, burrow-mottled, foraminiferal, clayey calcilutite. Compare to following three figures of same sequence.

B Core 2-2, Section 1–selected intervals from 97.5-121 cm: Vaguely color-banded to irregularly laminated, burrow-mottled to mottled, slightly foraminiferal, coccolith calcilutite.

C Core 2-3, Section 2–selected intervals from 68-95 cm: Strongly burrow-mottled churned, and slightly foraminiferal, coccolith calcilutite.

D Core 2-4, Section 1–selected intervals from 79-116 cm: Vaguely color-banded, moderately burrow-mottled, slightly foraminiferal, coccolith-discoaster calcilutite. Scattered dark areas (eg., 86 cm, 105 cm) reflect presence of concentrations of pyrite tubes and concretions of various descriptions.

E Core 6-1, Sections 1 and 2–selected intervals from 6-24 cm and from 13.5-24.5 cm: More or less massive, (burrow?) mottled, dark brown, slightly silty clay.

F Core 6A-1, Section 3–28-50 cm: Massive, somewhat mottled, dark-brown, slightly silty clay.

G Core 7-1, Sections 1 through 7–selected intervals: Somewhat burrow-mottled and mixed-appearing, slightly foraminiferal, clayey, coccolith calcilutite interbedded with more clayey zones which grade downwards into massive, highly distorted appearing, possibly slightly burrowed, clay. Lower lithology contains small, dark, faecal (?) pellets, concentrated locally.

H Core 7A-2, Section 1–selected intervals from 31.5-67.5 cm: Vaguely color-banded and laminated, mottled, slightly silty clay. Local discontinuities (possibly formed during coring?) present at irregular positions in core.

I Core 7A-3, Section 2–selected intervals from 31.5-90.5 cm: Color-banded and irregularly laminated, locally mottled (concretionary as well as burrow), silty clay. Darker bands appear to be high concentrations of iron oxide and manganese oxide.

J Core 6-2, Sections 1 through 5–selected intervals from 14-21.5 and 103.5-115 cm: "Clasts" of radiolarian/diatom-rich clay and unfossiliferous clay "clasts" in a matrix of clay. Originally interpreted as a "pebbly mudstone," an alternate interpretation of disturbance during coring has been suggested.

K Core 6-5, Section 2–59.5-74.5 cm: Massive, diatom ooze with local, lighter-colored concretionary appearing masses. Composition of the lighter-colored areas is unknown.

L Core 1-8, Sections 2, 3 and 4–selected intervals: Deformed and irregular laminae and bands of slightly silty clay. Much of deformation appears to be result of recumbent folding with fold axes approximately horizontal. Deformation of laminae, along with local discontinuity, suggesting slip movement horizontally in a plastic state.

M Core 1-9, Section 6–selected intervals from 36-68.5 cm: As above, deformation and discontinuity more pronounced.

N Core 3-8, Section 5–selected intervals from 28.5-74.5: Strongly burrow-mottled, intercalated bands and laminae of light-colored coccolith calcilutite which grades downwards into darker-colored, clay mineral-rich coccolith calcilutite, sometimes grading downwards into quartzose, calcisiltites and/or silty calcilutites with a high clay mineral content. Burrows consist of several apparently different types, origins unknown.

O Core 3-9, Section 5–80.5-101 cm: Vaguely banded and irregularly laminated, strongly burrow-mottled clay. Note pyrite concretion at 91.5 cm.

P Core 3-9, Section 7–52.5-75 cm: Much as above with thin bed of darker-colored bentonite (?) at 66-71 cm overlain by a thin bed of lighter-colored calcareous, volcanogenic-debris-rich, slightly sandy, clayey silt. The latter unit appears somewhat burrow-mottled and mixed with the overlying sediment.

PLATE 15

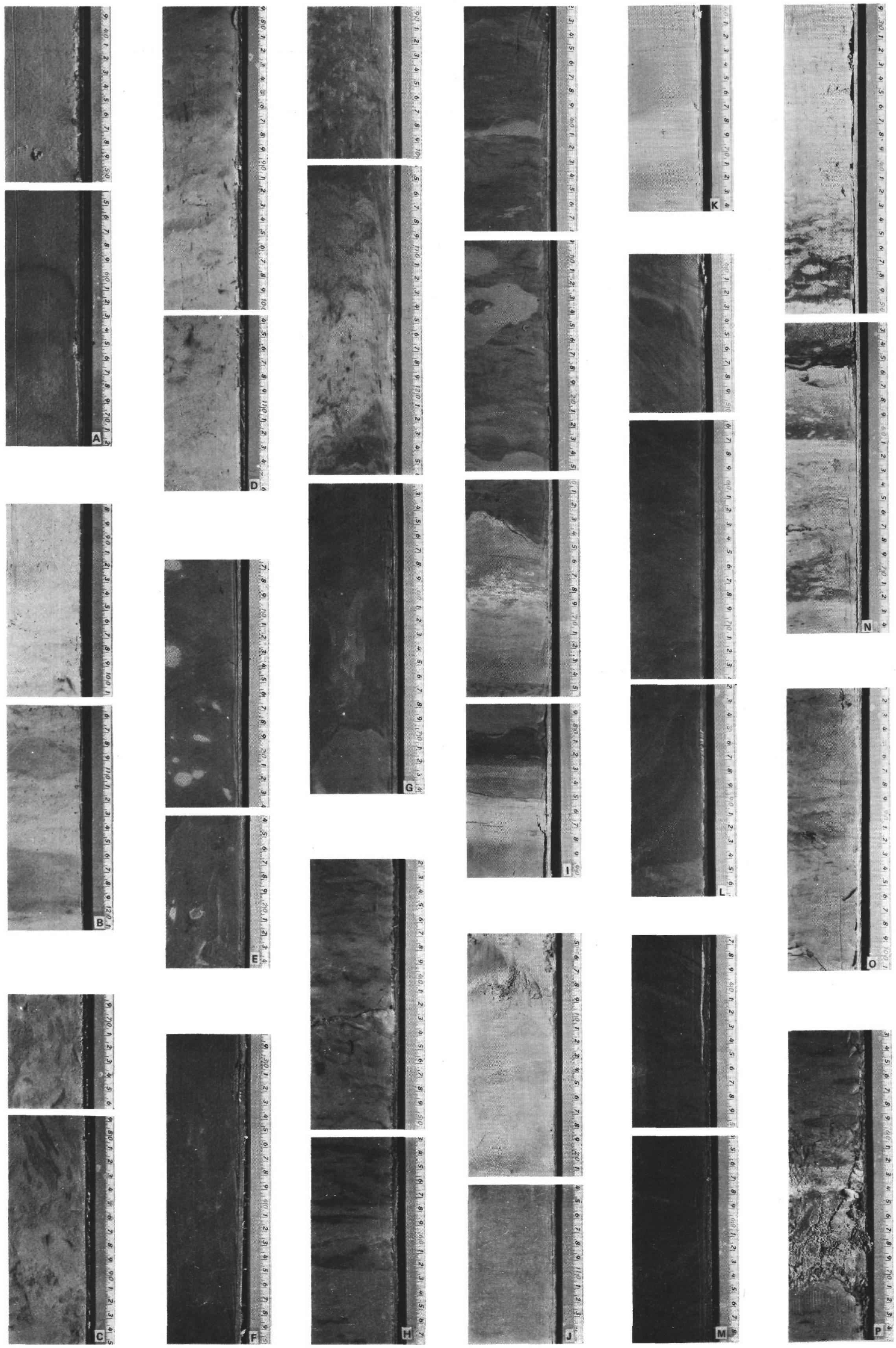

PLATE 16

Sedimentary structures–intermediate types/laminites.

A Core 1-1, Sections 2 through 6–selected intervals from 2-7 cm and from 104-119.5 cm: Demonstrating lithological contrast between the upper and lower portions of Core 1. Drag marks in the upper segment are related to the abundance of foraminifera, which make up a few per cent of the dry sediment. Horizontally oriented markings were made during core cutting, as the sediment was originally described as burrowed clay. The lower segment is noticeably but vaguely laminated and banded, showing little evidence of burrowing and lack of large foraminifera tests. Generally described as silty clay.

B Core 1-1, Section 2–58.5-75 cm: Massive to slightly burrow-mottled (with silt-filled burrows) silty clay with occasional thin silt laminae (63.3 cm). The silt laminae generally exhibit a sharp base and gradational upper contact.

C Core 1-1, Section 3–selected intervals from 108-138.5 cm: Intercalated, more or less massive to vaguely laminated silty clay and silty or clayey silt. This segment of core is strongly deformed by recumbent folds, the fold axes approximately horizontal as seen at 111 cm. Crumpling within silt laminae is pronounced (135 cm), suggesting translation along zones of weakness.

D Core 1-2, Section 1–109-120 cm: Strongly plastically deformed silty clay and silt. Note especially the overturned and truncated silt lamination at 117 cm.

E Core 1-2, Section 3–selected intervals from 27-74 cm: Thin intercalations of laminated silty clay and silt laminae, apparently largely overturned (?). Deformation is most noticeable from 27 to 40 cm, where folding and crumpling of laminae can be seen. The thicker silt laminations are seemingly internally cross-laminations on a small scale, probably as low angle ripple-laminae. Although not easily seen, most of the silt laminae appear to have more sharply defined tops than bases, converse to that normally observed, suggesting that the sequence is overturned.

F Core 1-3, Section 1–27.5-45 cm: Strongly folded (recumbent folds with horizontally oriented fold axes) interlaminated silty clay and silt. Note the removal of sediment along the outside of the core, evidently produced during drilling.

G Core 1-3, Section 7–3-25 cm: Interlaminated silty clay and silt, as above. Note deformation and truncation of laminae from 3-7 cm, suggesting horizontal translation of sediment during folding. From 13-15 cm, note convoluted-like appearance of stratification, suggesting plastic deformation in a dominantly horizontal plane.

H Core 1-5, Section 2–selected segments from 9-40.5 cm: Thin intercalations of laminated silty clay and silt, relatively undeformed as compared to preceeding views. Note presence of internal cross-lamination (small scale) in the silts. Much of the discontinuity of individual laminae, similar to that seen in other views, is thought to be depositional. See text for a move through discussion of this phenomena.

I Core 1-9, Section 6–128-140.5 cm: Section showing isolated "blob" of sand within a section of strongly deformed claystone. Nature of original stratification has been totally obscured, but mineralogy of the sand indicates a terrigenous source, probably delivered to the site of deposition via turbidity current processes.

J Core 3-3, Section 2–82-101.5 cm: Somewhat mottled, interlaminated silty calcarenite, vaguely laminated coccolith calcilutite, and calcareous silty clay. The calcarenites (and calcisiltites) are dominantly comprised of foraminifera tests and biogenic carbonate fragments of shallow water origin.

K Core 3-4, Section 1–selected intervals from 64-92.5 cm: Interbedded, massive to vaguely laminated, clayey foraminiferal calcarenite overlain by burrow-mottled to very irregularly laminated silty, calcareous clay grading upwards into a clayey, coccolith calcilutite.

L Core 3-5, Section 2–29-51.5 cm:
M Core 3-5, Section 3–78-100.5 cm:
N Core 3-5, Section 5–27-74.5 cm:
O Core 3-6, Section 1–78-100 cm:
P Core 3-6, Section 2–53-100.5 cm:

A comparison of vertical sequence as demonstrated by L through P. Note the following lithologies: (1) light-colored calcilutites, calcisiltites, and foraminiferal calcilutites; (2) intermediate shades representing clay-rich coccolith calcilutites; (3) dark shades representing calcareous, coccolith-rich silty clays and quartzose-calcareous silts. Two general types of graded sequences are thus represented: calcarenites grading upwards into coccolith calcilutites, and quartzose calcareous silts grading upwards into silty clays and then into coccolith calcilutites. Burrowing varies from slight to severe, suggesting depositional rates varying from moderate to slow.

PLATE 16

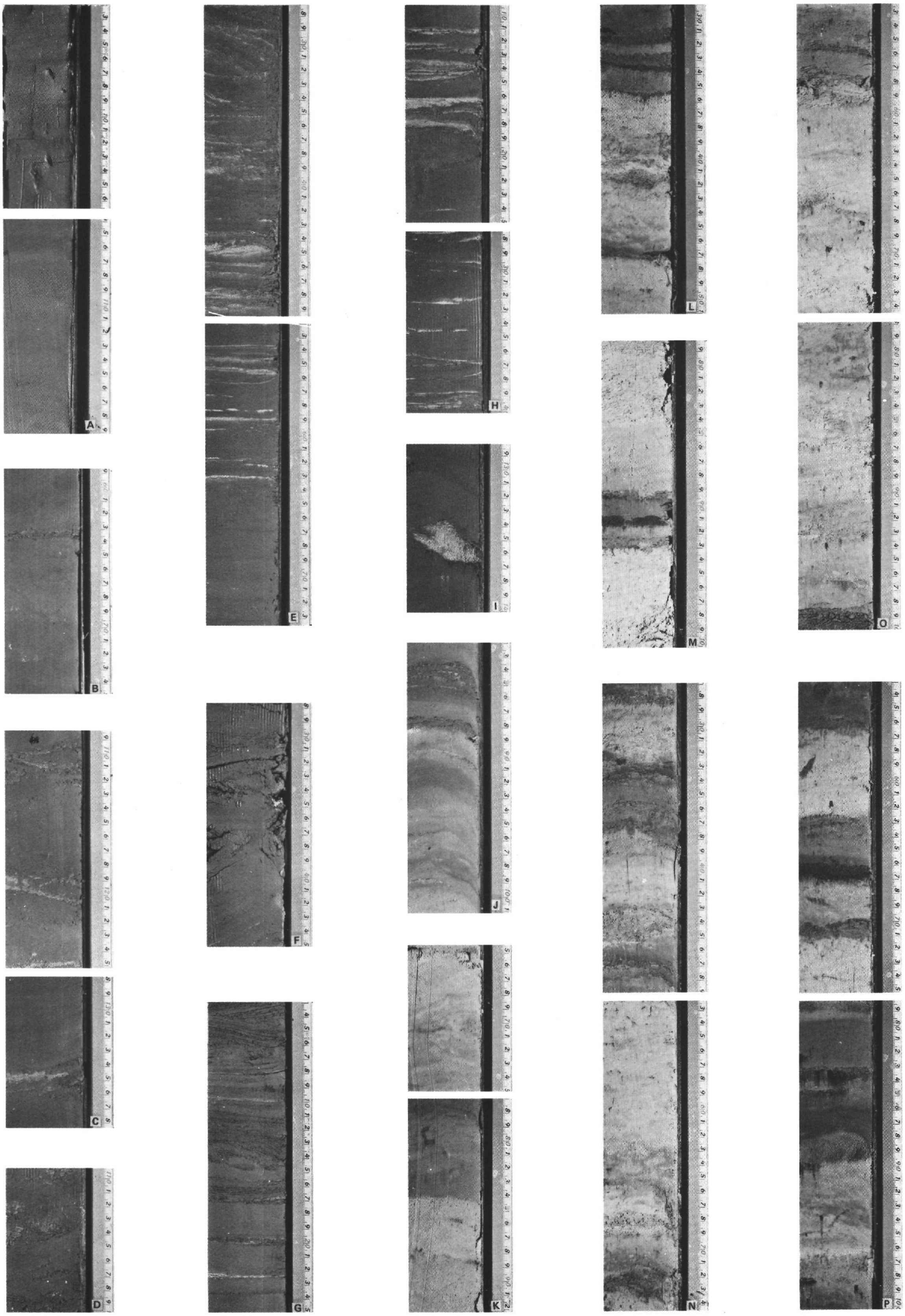

Examples A through I, all from Site 1, are thought to be most representative of the laminite concept. Paleontological age determinations support a high rate of deposition, as does lack of burrowing and identifiable pelagic debris. Examples J through P are from Site 3. These sediments are interpreted as the carbonate laminite analogue to similar non-carbonate laminites from Site 1. The laminites from Site 3 are intimately associated with burrowed, pelagic interbeds. The presence of thin, graded, quartzose silts or thin, graded carbonate silts and sands with high percentages of shelf carbonate debris supports the general interpretation of turbidity current processes. This interpretation is enhanced by the presence of graded carbonate turbidite sands within the sequence.

The conclusion can be reached that a complete spectrum exists between pelagic sedimentation and turbidity current sedimentation. It is beyond the scope of this discussion to present rigid criteria for absolute discrimination between these two end members. A detailed investigation of thickness of individual lithic units from Core 3-6 was made by Burk and Beall to attempt to determine percentages of pelagic versus turbidity current deposited sediment. In a five foot sequence of core, approximately 50 per cent of the sediment was interpreted as pelagic; thirty per cent was interpreted as turbidity current deposited; and, the remaining 20 per cent was indeterminate. Thus it is concluded that as much as 50 per cent of the sequence could have been deposited initially by a turbidity current mechanism. A more detailed study of composition should be undertaken to determine what percentage of the sediment can be absolutely ascribed to pelagic processes of sedimentation.

PHYSICAL PROPERTIES OF SEDIMENTS

Broadly speaking, the topic "physical properties of sediments" can include descriptive parameters of sediments ranging from type of stratification and textural composition to less common measurements such as natural radioactivity or engineering properties. One aim of the project has been to obtain as many diagnostic measurements as deemed scientifically practical within the overall objectives of the mission. This section deals with the specific sediment properties described below and then offers some preliminary interpretations. As more data becomes available, results should become somewhat more refined.

The following physical properties were selected for discussion here: (1) bulk density and natural gamma-ray emission measurements of the cores, (2) results of penetrometer tests on the fine-grained portions of the cores, and (3) a limited discussion of down-hole measurements of formation resistivity, natural gamma-ray activity, and bulk density.

Gamma-Ray, Density, and Penetrometer Measurements

Three physical measurements were made on the cores in the shipboard laboratory either before or immediately after cutting the core. The properties measured are generally considered somewhat ephemeral. These measurements consisted of (1) continuous natural gamma-ray emission, measured as counts per 2.5 minutes, (2) continuous bulk density and derived porosity as determined by a GRAPE (Gamma-Ray Attenuation Porosity Evaluation) device, and (3) intermittent penetrometer tests which utilized measurement of depth of penetration of a weighted needle into sediment. This last measurement, a simple engineering-type of determination, was taken as an empirical measure of degree of consolidation.

Continuous measurement of gamma-ray and density was used to differentiate lithology on a rather detailed basis as well as demonstrating broader variations in composition and consolidation. Figure 7 shows examples of detailed variation of sediment properties as revealed by gamma-ray and bulk density.

Figure 7A, from a depth of 130 feet below the sea floor, represents a typical relationship found in unconsolidated sediments; that is, sands which show a higher bulk density (and thus lower theoretical porosity) than intercalated muds. A maximum "effective" porosity approaching 40 per cent in unconsolidated quartzose sandstones is well documented in the literature. Effective porosity refers to intergranular porosity and does not include clay infill. As consolidation proceeds and water is expelled from the more easily compacted muds, a point is gradually reached where bulk density of the muds is higher than that of interbedded effectively porous sands. These relationships were especially important in interpreting down-hole measurements in shallow bore holes.

The graded sand represented in Figure 7A is one of the better examples of a turbidite from the Gulf of Mexico Abyssal Plain. The more or less massive graded unit, with suggestions of horizontal lamination, shows a very sharp basal contact and gradational top. Grain-size varies from silty, fine sand at the base to mud and clay in the uppermost portion shown. Response of gamma-ray and bulk density curves to variations in textural and mineralogical composition is marked. Gamma-ray is most sensitive to variation in clay content, whereas bulk density reflects higher porosity in the clay-rich zones. Note that the density curve reflects the presence of a thin silt near the base of the core whereas the gamma-ray does not; this is primarily due to the more specific level of sensing of the GRAPE device.

In the second example, Figure 7B, lithology is again reflected by curve response, although not so clearly as above. Here the finer-grained, coccolith pelagic oozes

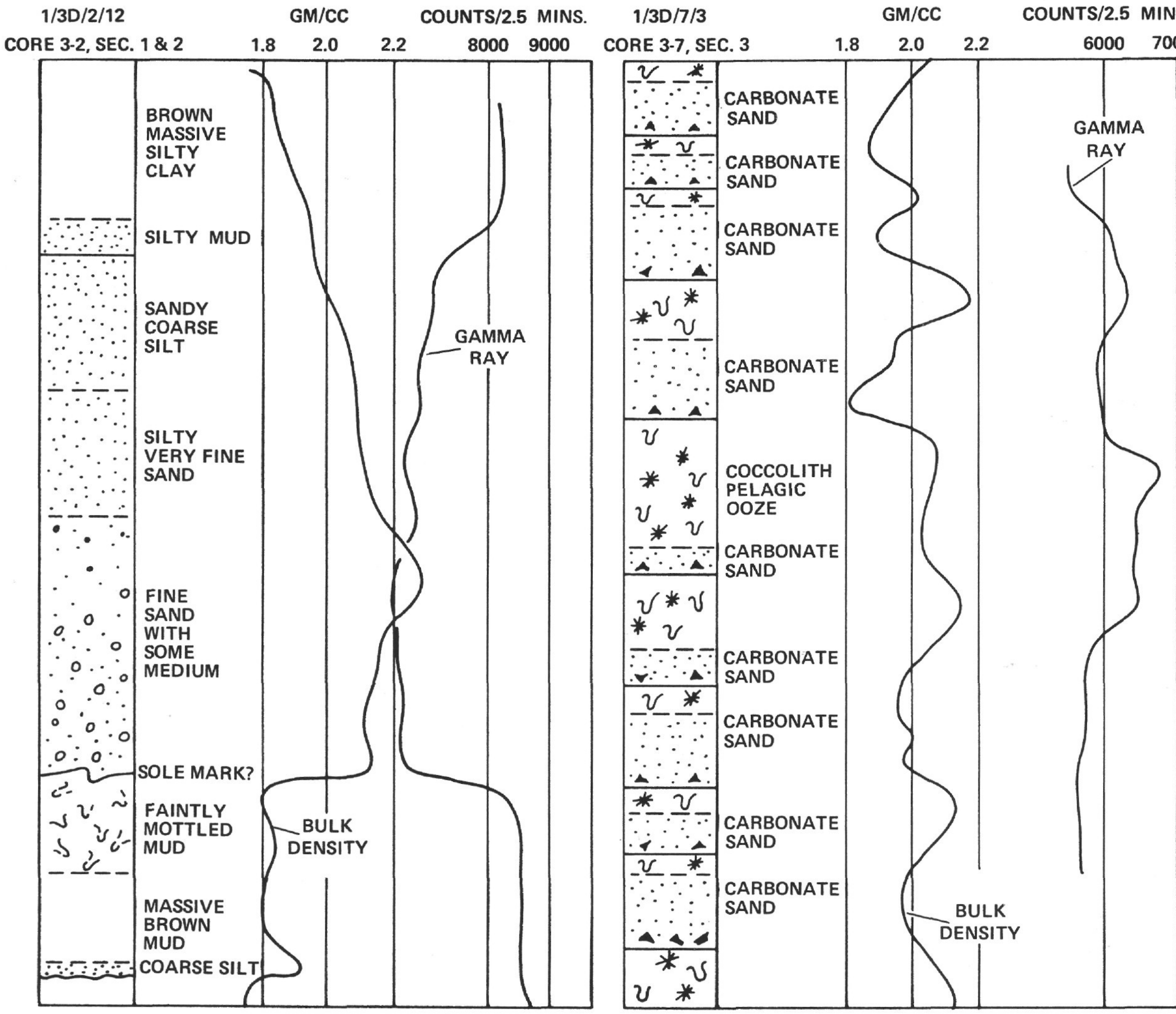

Figure 7. *Relationship between physical properties and lithology.*

have a higher bulk density and higher gamma-ray count than the intercalated, graded carbonate (turbidite) sands. Thus, density relationships are reversed in this example. This core, taken from a depth of approximately 1260 feet below the sea floor, is considerably more consolidated and exhibits less mineralogical variation than the first example (Figure 7A). Thus curve discrimination of lithology becomes considerably more interpretive.

Examples from the Atlantic sites are shown in Figure 8. Figure 8A (from Site 4), shows differences in bulk density values for three basic lithological types: (1) pebbly mud, (2) graded calcarenite (turbidites), and (3) coccolith pelagic ooze. Note that the lower calcarenite is partially cemented, thus accounting for the higher bulk density as compared to the upper calcarenite. Differences in bulk density of the two units of pebbly mudstone are a reflection of higher concentration of limestone rock fragments in the lower part. The pelagic ooze is unconsolidated and has a bulk density approximately equivalent to uncemented carbonate sand. Although not shown here, gamma-ray values are somewhat uniform through this sequence, as might be expected.

The second example, Figure 8B, from Site 6, shows a mixed terrigenous–pelagic, quartzose, multi-graded (turbidite), calcarenite sand, with local concentrations of mud clasts. This turbidite unit overlies a higher density, diatom-coccolith pelagic ooze with thin intercalations of silt and occasional fragments of displaced chert. This core might be considered an example of semi-consolidated sediments where intercalated muds have a higher bulk density than the uncemented sands. Gamma-ray values, not shown here, show consistent values through the sand, rising sharply in the coccolith ooze as a reflection of clay content. Note that the thin carbonate silts are indicated by low density values.

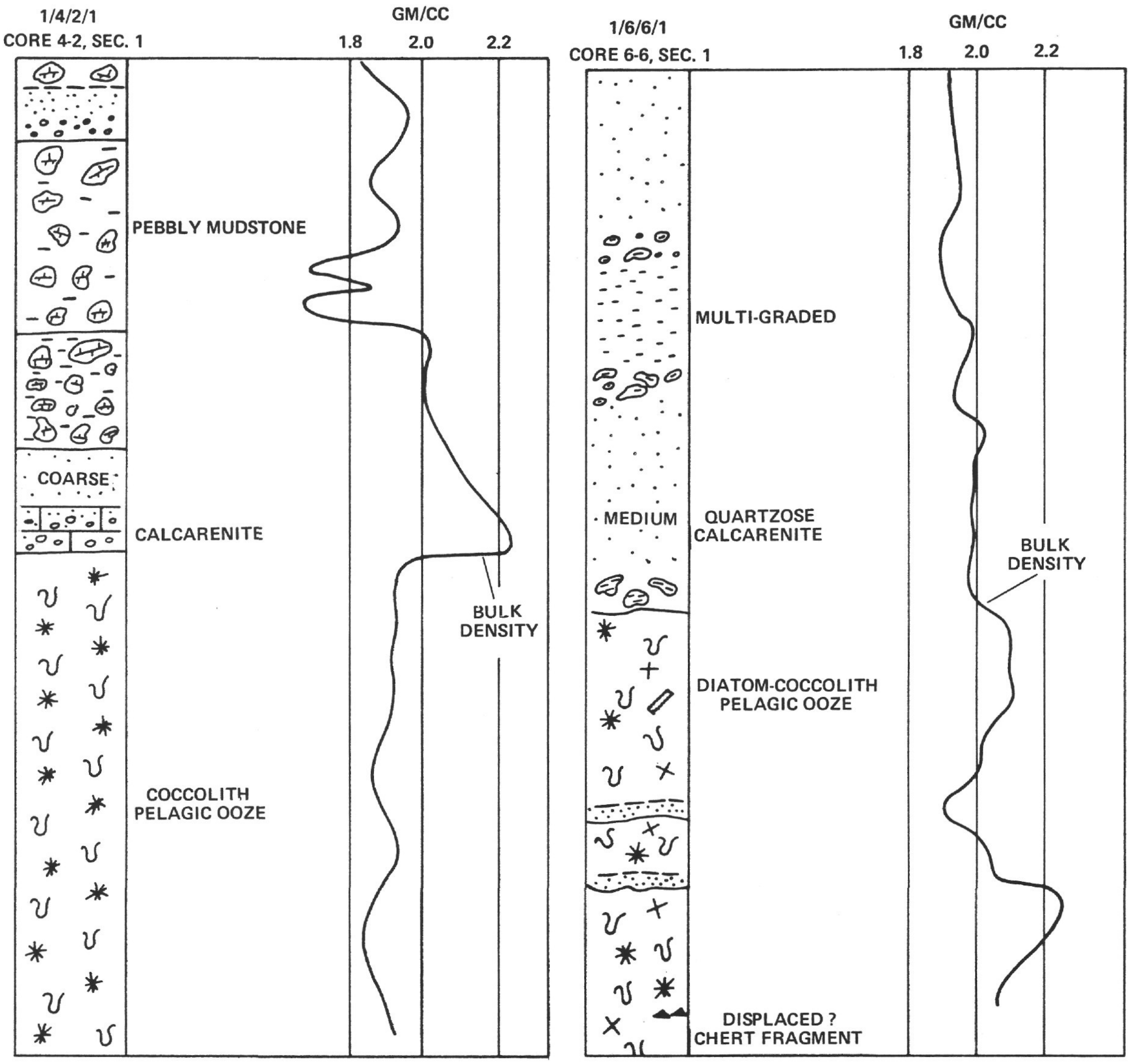

Figure 8. *Further examples of the relationship between physical properties and lithology.*

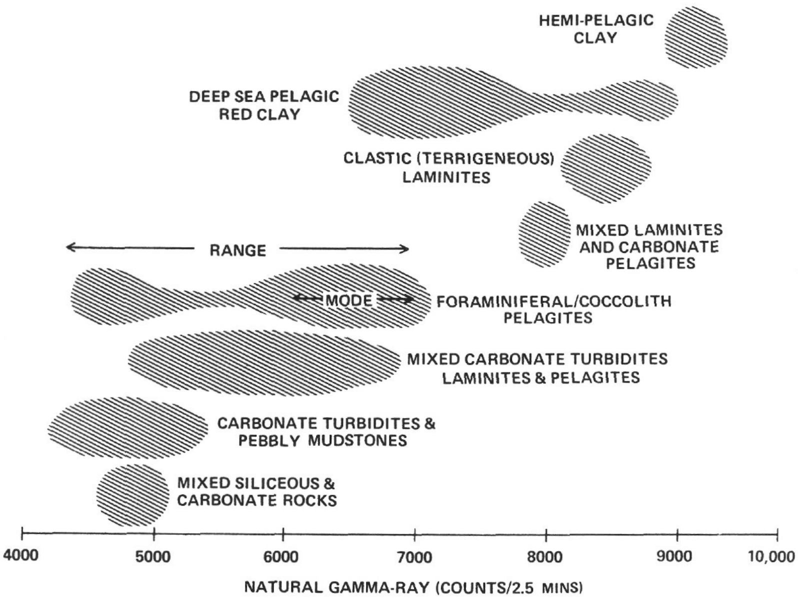

Figure 9. *Groupings of various sediment types on the bases of natural gamma-ray emission counts.*

In the examples described above, detailed information on lithology and mineralogical composition are related to gamma-ray and bulk density values. Figure 9 shows a plot of various lithologic and genetic sediment types grouped on the basis of natural gamma-ray emission counts. As described previously, increasing clay content correlates well with high gamma-ray count. Although well-logging service companies have used this concept for many years, this present compilation establishes, as far as is known, the first time these types of deep water sediments have been so characterized. As more information arrives from subsequent drilling operations, compilation of this type of information should enable us to make more specific assignments of lithology to gamma-ray response.

With the exception of the pelagic deep-sea red clay, all of the samples shown by bold lettering in Figure 9 are from the Gulf of Mexico. Thus, this data supports the general observations on the clay-rich nature of sediments recovered from the Gulf of Mexico as compared to the Atlantic sites. Although not shown here, the influence of consolidation tends to broaden the fields shown. A plot of bulk density versus gamma-ray tends to remove some of the overlap, but much remains due to the overlap in other physical properties and in composition. In general, the carbonate turbidites from Site 4 have the lowest gamma-ray counts, and the thin bentonites from Site 3 have the highest counts.

Penetrometer readings were taken on each 5 foot (1.5 meters) segment of core, generally in the finer-grained sediment within the sequence. Penetrometer readings refer to the depth (in tenths of millimeters) which a weighted needle is able to penetrate freshly cut sediment core. The relationship between penetrability and other engineering tests or physical measurements is still purely empirical. Nevertheless, the test is surprisingly reproducible and fits well with observation and experience. Toward that end, this writer has proposed a scale of consolidation, in which penetrometer values of 0 to 10 qualify a sediment as a stone; readings between 10 and 30 categorize sediment as semi-consolidated; and readings greater than 30 refer to unconsolidated sediment. These terms refer to fine-grained sediments or muds only. Variability and reproducibility in coarse-grained sediment reduce usefulness of the measurement. Attempts to standardize penetrometer readings will undoubtedly be made when this test becomes more generally applied.

Figure 10 shows a comparison of penetrometer values plotted against depth for the seven sites studied. Sites 4 and 5 are combined and so are Sites 6 and 7.

Site 1 can be interpreted as less consolidated, especially below 300 meters, as compared to the other sites shown on Figure 10. Sediments at Site 1, basically a turbidity current deposited sequence, apparently were deposited more rapidly than sediments recovered at the other sites. These sediments can be readily contrasted with sediments from Site 3—the abyssal plain of the Gulf of Mexico—which also contain a high percentage of carbonate pelagic sediment (since the penetrometer measured the fine-grained interbeds of the turbidite sequence); this suggests either slower rates of deposition or differences in the consolidation rates of carbonate muds as compared to muds dominantly comprised of clay minerals. As the terrigenous component increases near the base of Site 3, the penetrometer

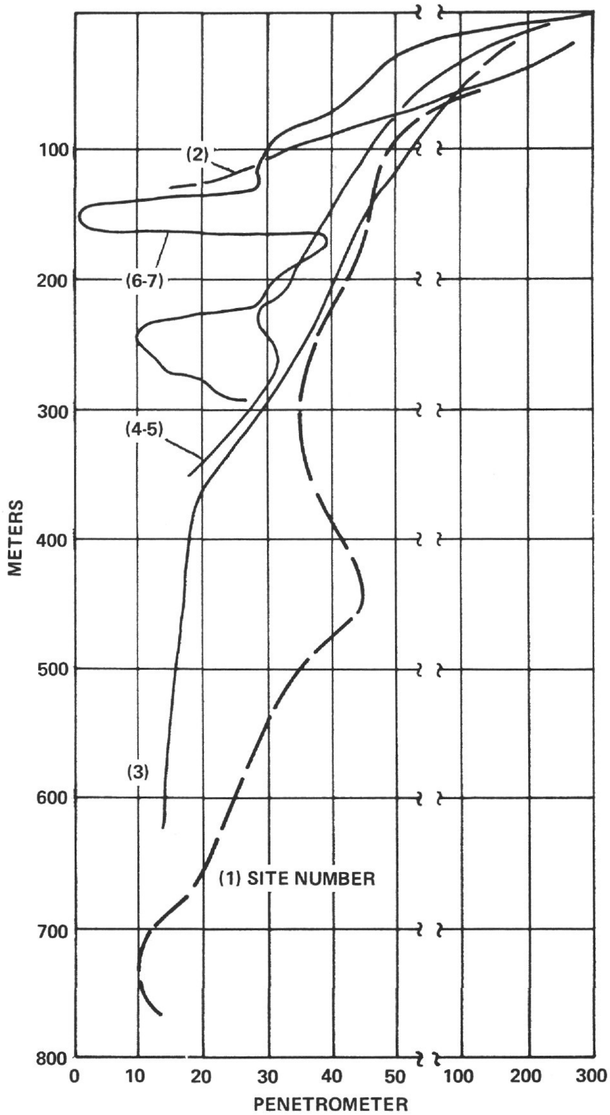

Figure 10. *Penetrometer values plotted against depth of penetration.*

values more closely approach penetrometer values attained at Site 1.

The two sites described above can be contrasted with Site 2, a pelagic sequence drilled on the crest of one of the Sigsbee Knolls (described as "Challenger Knoll"). Sediments from Site 2 are basically clay mineral-rich, carbonate oozes or clays. Based on paleontological criteria, these sediments were deposited quite slowly as compared to Site 3 (see Berggren, Chapter 25). Penetrometer values suggest a considerably higher rate of consolidation as compared with Sites 1 and 3, and may be interpreted as reflecting either differences in composition or in depositional rate.

Several writers (see Richards and Hamilton, 1967), have suggested that age or possibly cementation will tend to generate a state of over-consolidation. Measurement of engineering properties of Gulf of Mexico sediment by Bryant and Wallin (1968), McClelland (1967), Fisk and McClelland (1959) showed that continental slope sediments tended to be over-consolidated. Abyssal plain sediments, studied by Bryant, tended to be normally consolidated. Assuming that Site 2 sediments correspond to Bryant's over-consolidated category, these sediments compare most favorably with slope sediments. This can be interpreted as their representing slow rates of pelagic sedimentation without the diluting influence of turbidity current deposits and accompanying high rates of deposition. The underlying parameters responsible for these phenomena have not been clearly delineated. Age alone is obviously not an explanation.

Atlantic sites show considerably more variation of penetrometer values with depth, in part due to the presence of cherts and highly silicic pelagites. The sharp re-entrants for these sets of data occur in siliceous zones. Pelagic coccolith oozes at intermediate depths are somewhat comparable to Site 2. The deep-sea red clay pelagites of Sites 6 and 7 are more comparable to Gulf of Mexico inorganic clays from Sites 1 and 3.

Vertical profiles of natural gamma-ray measurements are shown in Figure 11. Again, Site 1 is distinctive, maintaining a consistently high value due to high clay mineral content of the sediment sequence. This can be contrasted with Sites 4 and 5, which represent a carbonate-rich sedimentary sequence.

Lithological variation is evident from inspection of the various gamma-ray curves shown in Figure 11. The carbonate turbidite-laminite-pelagite sequence in the mid-portion of Hole 3 is well delineated by relatively low gamma-ray values. Bentonites near the base of Site 3 give local values in excess of 10,000 counts per time increment. Deep-sea red clays from the upper and lower parts of Sites 6 and 7 also show relatively high gamma-ray counts.

Gamma-ray values for Site 2 are somewhat intermediate between Sites 4-5 and 6-7, suggesting that composition is more like that of Atlantic sediments than Gulf of Mexico. This is primarily due to the low percentage of clay present in this sequence. No data was obtained from the cap rock material at the base of the Site 2 sequence. It is suggested that gamma-ray values would be low in that interval.

A down-hole gamma-ray log was obtained at Site 1, furnishing an opportunity to compare values as determined by core measurement with down-hole determinations. It should be noted that gamma-ray values for the

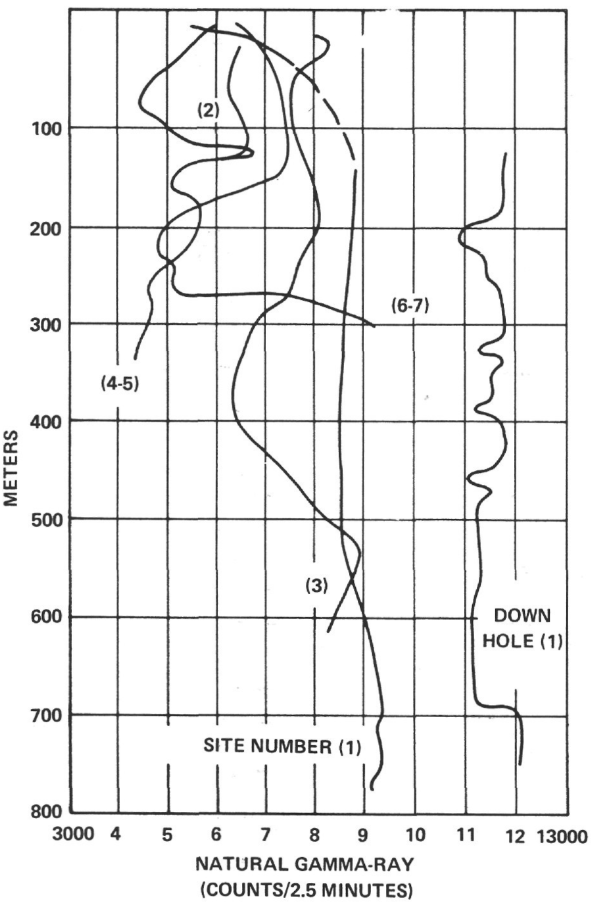

Figure 11. *Natural gamma radiation plotted against depth of penetration.*

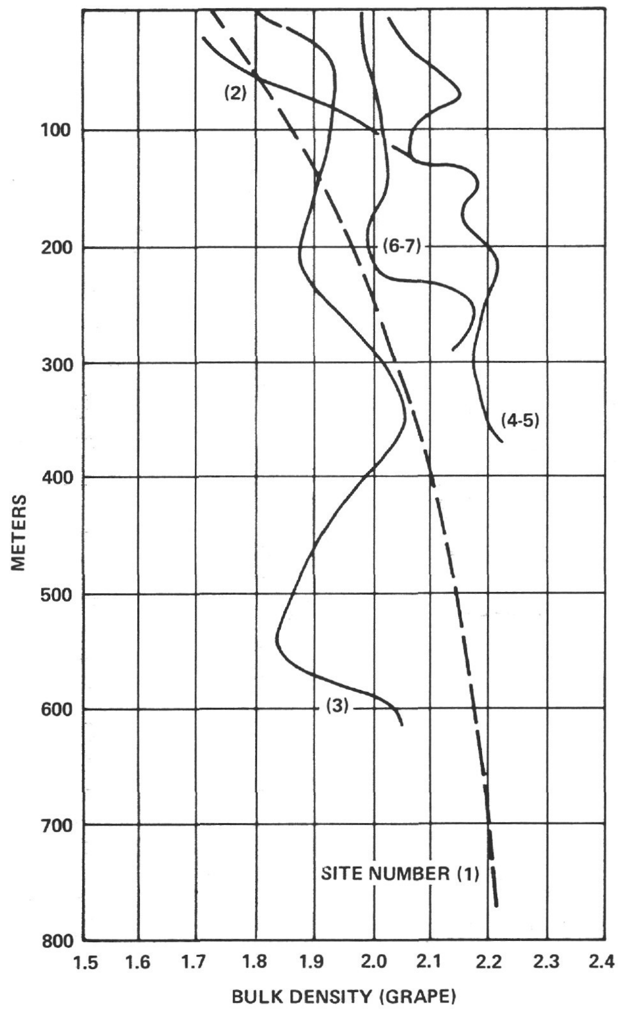

Figure 12. *Bulk density plotted against depth of penetration.*

down-hole log are not in the same units as natural gamma-ray values determined on the cores. Maximum gamma-ray values at the top of the logged interval are about 76 API units, increasing to about 87 API units at the base. These values are somewhat comparable to mudstone sequences measured on the Louisiana continental shelf.

Analysis of the logged interval, in conjunction with other down-hole logs and other lines of evidence, has been summarized elsewhere. Large scale variations in bore-hole diameter furnish most of the "log character" noted in the down-hole log of Site 1. The general increase of gamma-ray with depth corresponds with the curve generated by measurement of cores, and is thought to represent consolidation of the section. The basal segment of Site 1, a clay-rich, hemi-pelagic lithology, is apparently somewhat overconsolidated as judged by penetrometer values (Figure 10). Deformation is also quite extensive in this part of the section, suggesting that the two are related.

Results of bulk density determinations (utilizing the GRAPE device) are shown in Figure 12. A limited number of measurements were available for Site 1, therefore, the results are highly interpretive. The derived curve for Site 1 shows .a relatively simple increase with depth, and correlates well with gamma-ray and penetrometer determinations. This is to be expected, since the lithology is relatively consistent with depth as compared to the other sites. Site 3, in comparison to Site 1, appears somewhat anomalous, especially in lower portions of the sequence. Low density values at depths around 500 meters at Site 3 are evidently related to very clay-rich (high gamma-ray), bentonic, pelagic sediments. The carbonate turbidite wedge previously described around 350 meters is well displayed by the density curve. The basically tripartite configuration of density at Site 3 corresponds well with seismic interpretations (see Site 3 report, this volume).

The pelagic sequence at Site 2 shows a high rate of bulk density increase, which corresponds to a high rate of penetrometer value increase (Figure 10). Bulk density determinations near the base of Site 2 suggest a comparison with Sites 4 and 5, where carbonate sediments dominate the sequence. It could thus be assumed that density determinations in carbonate sediments are somewhat affected by differences in grain-density or matrix effects plus possibly cementation as compared to Gulf of Mexico borings. The deep-sea red clays of Sites 6 and 7 are somewhat intermediate, as are gamma-ray and penetrometer values. Siliceous sediments near the base of this latter sequence show high bulk densities, part of which is due to consolidation into deep-sea red clay.

Comments on Overconsolidation of Deep Water Sediments

The sediment parameters described above can be interpreted in terms of the state of consolidation as well as in compositional or textural terms. It should be emphasized that, on the basis of penetrometer measurements as well as by other types of data, the sediments recovered on the first leg of the project are primarily unconsolidated to semi-consolidated. Exceptions to this are diagenetically cemented carbonates and cherts, which classify as "stones."

By comparing the depth profiles described previously with shelf sequences and with data in the literature (Figure 13), the concept of over-consolidation of deep marine sediments is reinforced. For purposes of discussion, Site 1 has been compared to an averaged bulk density versus depth curve for southern Louisiana offshore sediments (continental shelf, northern Gulf of Mexico). Data for this latter curve includes bulk density determinations from gamma-gamma logs for shales only, and does not include sands. Furthermore, only normally hydrostatically-compensated sequences are represented herein. Inasmuch as both curves represent clay mineral-rich sediments, a comparison of density versus depth is probably more meaningful. Assuming that the two sequences are approximately correct with respect to absolute bulk density, the deep water sequence appears overconsolidated.

For the sake of comparison, results of Hedberg's (1936) determinations of Venezuela sediments as well as results of laboratory consolidation of artificial clay mineral-rich sediment (Warner, 1964) are shown. It is thought that these curves more or less establish a range of bulk densities for rapidly deposited muds. The question can then be asked as to what is overconsolidated and what is underconsolidated. The curve derived for Site 1 is

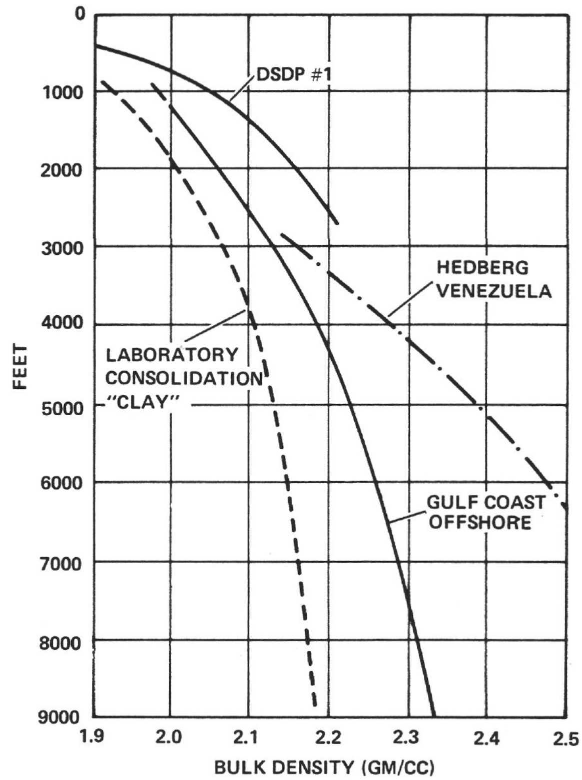

Figure 13. *Consolidation curves for several sediments compared with the curve for samples from Leg 1.*

obviously overconsolidated with respect to shelf sediments not too far removed spatially. Since other sites drilled during the first leg of the project are of an even higher density or consolidation state, it would appear that deep marine sediments tend to be overconsolidated.

It is beyond the scope of this chapter to answer the questions raised above. The general problem of how sediments consolidate is still far from solved, as pointed out in a review by Meade (1966). It would appear that compared to quickly deposited shelf sequences, deep water sediments attain absolute hydrostatic equilibrium more quickly, possibly due to slower depositional rates. In addition, cementation effects in fine-grained sediments are possibly encouraged in a deep water environment, although reasons for this seem obscure. Finally, more opportunity exists for readjustment to take place, especially on the continental slopes and rises, either by gravity transport or simple slumping. Differences in the behavior of carbonate muds as compared to clay mineral muds are still in an early stage of investigation. Recent work in mud rock fabrics may provide at least part of the answer (Meade, 1966).

Summary

Physical measurements performed on sediments recovered from the first leg of the Deep Sea Drilling Project correlate well with conventional lithologic parameters. Mineralogical composition variations are best expressed by gamma-ray measurements, whereas bulk density determinations appear somewhat less sensitive. Penetrometer measurements appear least sensitive to composition. Textural composition is best expressed by bulk density determinations, especially in the upper, unconsolidated portions of the sequences studied. Since textural composition and mineralogical composition are not mutually exclusive, gamma-ray determinations also reflect textural composition, although less definitively than bulk density. Penetrometer measurements most clearly reflect state of consolidation and effects of secondary cementation. Penetrometer determinations fit well with observation and personal experience.

Although most sediments encountered in this study were unconsolidated to semi-consolidated, comparison with shelf sediments from the northern shelf of the Gulf of Mexico would indicate that the deep water sediments are over-consolidated at any particular depth. This phenomenon has been noted frequently in the literature, but much remains to be learned before solutions to the many problems which bear on the general processes of consolidation can be offered. Further studies on the effects of slow depositional rates, authigenic and diagenetic cementation, remolding by gravity deformation, and mud fabric are recommended. The physical-chemical environment of deep marine sedimentation is still poorly understood.

CHEMICAL DIAGENESIS

In the absence of special studies the authors have recorded here such observations as were made in the course of general descriptions and analyses, but which are significant in view of the limited knowledge of diagenetic processes in the subsea environment. The problems dealt with here are of the carbonates, chert and iron minerals.

Carbonate Diagenesis

Nannoplankton oozes are thought to be wholly composed of low magnesium calcite. Their alteration with increasing burial appears to be mainly one of compaction to harder and harder chalks, and this corresponds to our observations on the Leg 1 cores. Under sufficient pressure, solution welding of coccoliths occurs, and a hard fine-grained limestone results (Garrison, 1967; Fischer, Honjo & Garrison, 1967). It is possible that the Tithonian sediments at Site 5 are just approaching the solution welding stage.

But the calcarenites and calcisiltites found at all the sites, and the chalks closely associated with them, contain a great variety of skeletal grains, and must have consisted initially of mixtures of aragonite and high magnesium as well as low magnesium calcites. We do not have data on the magnesium content of calcites, but Rex's X-ray diffraction analyses provide insight into the distribution of aragonite.

The Neogene calcarenites and calcisilts of the Gulf of Mexico appear to have suffered little alteration. The widespread occurrence of well preserved didemnid tunicate spicules is evidence that the aragonite has been largely retained, and the X-ray analyses bear this out. The absence of cementation in these beds is further evidence that very little alteration has occurred. Yet, some of the chalks immediately overlying (and gradational with) these calcisilts are somewhat cemented, and suggest that these chalks contained an unstable phase that was converted into stable cement. The authors suggest that these chalks, which they interpret as the fine upper unit of turbidites, contained aragonite needles derived from the shelf-needles which because of their minute size and large surface area were less stable than skeletal aragonite.

The Cretaceous calcarenites at Sites 4 and 5 appear to have undergone considerably more alteration. The micritic alteration of most of the skeletal particles may antedate the resedimentation on the deep-sea floor, but some alteration occurred in place. No grains of definite aragonite composition were recognized optically, and no aragonite was revealed by the X-ray analyses. But much secondary calcite has been deposited, in three different forms: as permineralizing spar and syntaxial rim cement on echinoderm remains (Plate 17, C & D); as a general crust of very fine calcite spar crystals over all the grains (Plate 17, E & F); and in much larger scalenohedral calcite crystals, growing between and in some cases around the primary grains of the sediment (Plate 17F; Plate 18, A & B). It cannot be certain that these larger crystals were wholly formed after resedimentation on the deep-sea floor, but their growth around adjacent grains makes it seem likely that at least part of their growth occurred in place. Furthermore, the general cementation of the sediment leaves no doubt that calcite growth occurred *in situ.*

The nature of the associated sediments (nannoplankton chalks, radiolarian cherts and mudstones) suggests that these calcarenites were deposited in deep water. While deep penetration of fresh waters, to provide these sediments with a touch of fresh water diagenesis, cannot be wholly dismissed, the alternative–alteration and cementation of the sediment in connate marine waters–seems more probable.

The occurrence of dolomite in the nannoplankton chalks and marls as well as in the turbidite calcarenites and silts has been discussed above. Dolomite rhombs are shown in Plate 7F and in Plate 18B. While much of the dolomite is of terrigenous detrital origin (Figures 7 and 8), the low quartz-dolomite ratios in some of the carbonate sediments strongly suggest that some of the dolomite is authigenic.

Cherts

The siliceous organic sediments have been discussed above. Wherever siliceous skeletons were abundant in the sediments, chert was encountered in the form of beds or nodules. These cherts will be discussed in order, from youngest to oldest.

Eocene Spiculites of Bermuda Rise

As discussed above, the mid-Eocene sequence of Sites 6 and 7 contains many graded units, each consisting of a calcareous sand- or silt-grade base, passing upward into nannoplankton chalk and ending in a non-calcareous clay. Each of these rock types is replete with siliceous fossils: sponge spicules, diatoms, Radiolaria and silicoflagellates. Many of these skeletons show signs of corrosion (Plate 17A). Silicification has occurred in some of the sands and silts, and has converted them into cherts which here provide the reflector termed Horizon A.

The silicified rock appears to have been originally a silt or sand of quartz (and feldspar) grains, glauconite pellets, borken siliceous sponge spicules, and calcareous foraminifera (with planktonic ones predominant); minor constituents included diatoms, Radiolaria, echinoderm debris, ostracodes, and presumably other grains. Presence or absence of a fine matrix (nannoplankton?) can no longer be ascertained. These grains are now embedded in a matrix of opaline silica (Plate 20), with flecks of chalcedonic quartz and remnants of calcite. The calcareous fossils are normally preserved as such, but are filled with silica, and show local replacement by silica. The originally opaline skeletons are preserved in a variety of ways. Some remain apparently unaltered, in the form of isotropic opaline silica (Plate 20, C & D). The majority appear to have been removed in solution leaving molds. Some of these molds have remained unfilled, but the majority show one or two generations of infilling, by fibrous quartz, as follows: A first generation of radially oriented length-slow fibers, form a uniform lining of the mold (Plate 20, B, E & F)—rarely are there two successive layers of this type; then, a second generation of fibrous quartz, length-fast (chalcedony, *sensu stricto*) fill the remaining void by growing in radiating sheaves, from several centers on the surface of the first lining (Plate 20, E & F).

Albian-Cenomanian Radiolarian Cherts

At Site 5 in the Albian and Cenomanian, a sequence of dark radiolarian mudstones was encountered which contained various silicified layers—radiolarian cherts. These are illustrated on Plate 19. They may be the reflecting horizon locally identified as Horizon β.

The Radiolaria are for the most part mere spheroidal or turbinate holes or mineralized patches in the rock, but enough of them retain microstructure (Plate 19A) to essentially identify the remainder. This appears to be normal in radiolarian cherts of all ages. The cherts are laminated on a millimeter scale (Plate 19, E & F), into alternatingly radiolarian-rich and radiolarian-poor layers.

The radiolarian-poor layers consist largely of homogeneous opaline material, full of fine carbonaceous matter; a faint reticulation suggests a spherulitic sub-structure of the opal. The Radiolaria in this matrix were generally dissolved, and the voids are now lined with distinct spherules or granules of opaline matter, some of which show spherulitic internal structure whereas others are homogeneous (Plate 19C). In most cases the remaining void stayed empty, but in some it was filled with sheaves of chalcedony (Plate 19D).

The radiolarian-rich layers show a matrix of well-defined opaline granules (Plate 19B), and the Radiolaria here are generally filled with chalcedony. The contrast is well shown in Plate 19, E & F.

Though not visibly porous, the opaline matrix in these cherts absorbs water readily. X-ray diffraction shows the presence of cristobalite.

Neocomian-Tithonian Cherts

Some of the Neocomian and Tithonian nannoplankton chalks contained abundant Radiolaria, which are commonly preserved in calcitized form (Plate 18, E & F). Though not much chert was recovered from these sediments, it appears to be a common constituent, to judge from the drilling rates and poor core recoveries. These cherts appear to be of two types: cherts formed by replacement of extremely radiolarian-rich nannoplankton chalk, and cherts formed by silicification of graded calcarenite beds. This latter type, reminiscent of the silicified Eocene turbidites of Sites 6 and 7, is familiar because of experience with the Mesozoic deep water sequences of the Alps (Garrison, 1967; Garrison & Fischer, 1969).

Iron Minerals

The authigenic iron minerals which are apparent in these sediments include (1) black iron sulfides, probably at least in part ferrous sulfide; (2) pyrite or marcasite; (3) the hydrous ferric oxides, here lumped as limonite and presumably largely goethite; and (4) hematite.

Most of the black staining in burrows, observed in near-surface sediments, is probably to be attributed to ferrous sulfide minerals. Such black stains, especially associated with chondrite-type dwelling burrows, extends to depths of more than 800 meters below the sea floor, and occur in sediments as old as Pliocene or Miocene, raising the question whether these minerals are more stable under deep submarine conditions than near sea level, or whether the black stains are due to some other substance.

Pyrite occurs in most of the cores studied, though generally beyond the limits of detection by X-ray bulk analysis. In the brown clays it normally occurs in spherules of uncertain origin. In clays, marls and carbonates it commonly fills dwelling burrows, a particularly good example of which is shown in Plate 1C (see also Plate 2D). Its abundance at Site 2 may be related to the supply of sulfur, from the underlying salt dome. Framboidal spherules of pyrite commonly occur inside tests of foraminifera (Plate 21, A & D) or Radiolaria. In the Tithonian-Neocomian sequence of the Blake-Bahama Basin these framboids are generally lodged in the bottom of radiolarian spheres, thus affording a geopetal criterion, as in the correlative beds of the Alpine deep water sequence (Honjo, Fischer & Garrison, 1965). Replacement of siliceous tests by pyrite is common in these beds, as well as in the Middle Eocene of the Bermuda Rise.

The Neogene pelagic clays of the Atlantic are all brown in color, and owe this to hydrous ferric oxides. In the older and more deeply buried Eocene clays at the bottom of Hole 7, a large part of the ferric iron is present in the form of hematite, and these cores are accordingly mottled with varying shades of red. Presumably this hematite is a diagenetic alteration product of limonite, and further drilling will provide data on the condition under which such alteration takes place.

REFERENCES

Arrhenius, G., 1963. Pelagic sediments. **In** *The Sea.* M. N. Hill (Ed.). New York (Interscience) 655.

Bryant, W. R. and Wallin, C. S., 1968. Stability and geotechnical characteristics of marine sediments, Gulf of Mexico. *Trans. Gulf Coast Assoc. Geol. Soc.* **18**, 334.

Ewing, M., Ericson, D. B. and Heezen, B. C., 1958. Sediments and topography of the Gulf of Mexico. **In** *Habitat of Oil.* L. G. Weeks (Ed.). Tulsa (Am. Assoc. Petrol. Geologists) 995.

Fischer, A. G., Honjo, S. and Garrison, R. E., 1967. *Electron Micrographs of Limestones and their Nannofossils.* Princeton (Princeton University Press). 141 pp.

Fisk, H. H. and McClelland, B., 1959. Geology of continental shelf off Louisiana: its influence on offshore foundation design. *Bull. Geol. Soc. Am.* **70**, 1369.

Folk, R. L., 1959. *Petrology of Sedimentary Rocks.* A laboratory syllabus, Univ. of Texas, Austin, Texas (Hemphill's).

Garrison, R. E., 1967. Pelagic limestones of the Oberalm beds (Upper Jurassic-Lower Cretaceous), Austrian Alps. *Bull. Canadian Petrol. Geol.* **15**, 21.

Garrison, R. E. and Fischer, A. G., 1969. Deep water limestones and radiolarites of the Alpine Jurassic. *Society of Economic Paleontologists and Mineralogists, Special Publication No. 14.* p. 20.

Hedberg, H. D., 1936. Gravitational Compaction of clays and shales. *Am. J. Sci.* **31**, 241.

Hollmann, R., 1962. Über Subsolution und die "Knollenkalke" des calcare ammonitico rosso superiore im Monte Baldo (Malm; Norditalien). *Neues Jahrb. Geol. Palaont. Monatsh.*, Heft 4, 163.

_______. 1964. Subsolutions-Fragmente (zur Biostratonomie der Ammonoideen im Malm des Monte Baldo/Norditalien). *Neues Jahrb. Geol. Palaont. Abahndl.* Bd. 119, 22.

Honjo, S., Fischer, A. G. and Garrison, R. E., 1965. Geopetal pyrite in fine-grained limestone. *J. Sediment. Petrol.* **35**, 480.

Hsu, K. J., 1964. Cross-laminations in graded bed sequences. *J. Sediment. Petrol.* **34**, 379.

Kuenen, Ph. H., 1964. Deep-sea sands and ancient turbidites. **In** *Turbidites.* A. H. Bouma and A. Brouwer (Eds.). Elsevier, Amsterdam, 3.

_______. 1967. Emplacement of flysch-type sand beds. *Sedimentology.* **9**, 203.

Lombard, A., 1963. Laminites; A structure of flysch-type sediments. *J. Sediment. Petrol.* **33**, 14.

McClelland, B., 1967. Progress of consolidation in delta front and prodelta clays of the Mississippi River. **In** *Marine Geotechnique.* Chicago (Univ. Illinois Press) 22.

Meade, R. H., 1966. Factors influencing the early states of the compaction of clays and sands—Review, *J. Sediment. Petrol.* **36**, 1085.

Richards, A. F. and Hamilton, E. L., 1967. Investigations of deep sea sediment cores, III. Consolidation. **In** *Marine Geotechnique.* Chicago (Univ. Illinois Press) 93.

Warner, D. L., "An analysis of the influence of physical-chemical factors upon the consolidation of fine-grained clastic sediments." (unpublished Ph. D dissertation, Univ. California, Berkeley, 1964.) 136 pp.

PLATE 17

Various smear-slides.

A Sample 6-4-3, 67 cm (plain light, X 250): Middle Eocene siliceous silt. The large sponge spicule extending diagonally across field shows two larger solution pits and several smaller perforations.

B Sample 6-3-4, 110 cm (plain light, X 250): Middle Eocene siliceous marl. From higher in the same turbidite bed. Note preponderance of smaller sponge spicules (some of them imperforate and ornate) and juvenile foraminifera.

C Sample 4A-1-3, 51 cm (plain and cross-polarized light, X 250): Late Cretaceous calcarenite. An echinoderm fragment with syntaxial calcite overgrowth.

D Sample 5-7-1, 25 cm (plain light, X 250): Cretaceous calcarenite. Micritized foraminifer overgrown with small calcite crystals.

E Sample 5-2-1 (cross-polarized light, X 100): Cretaceous (Santonian) calcarenite. Micritic grains overgrown with and cemented by thin rinds of sparry calcite; in upper middle a large authigenic scalenohedron of calcite (bright).

F Sample 2-5, 90 cm: Spindle-shaped calcite scalenohedra out of cap rock of Challenger salt dome, X 100.

PLATE 17

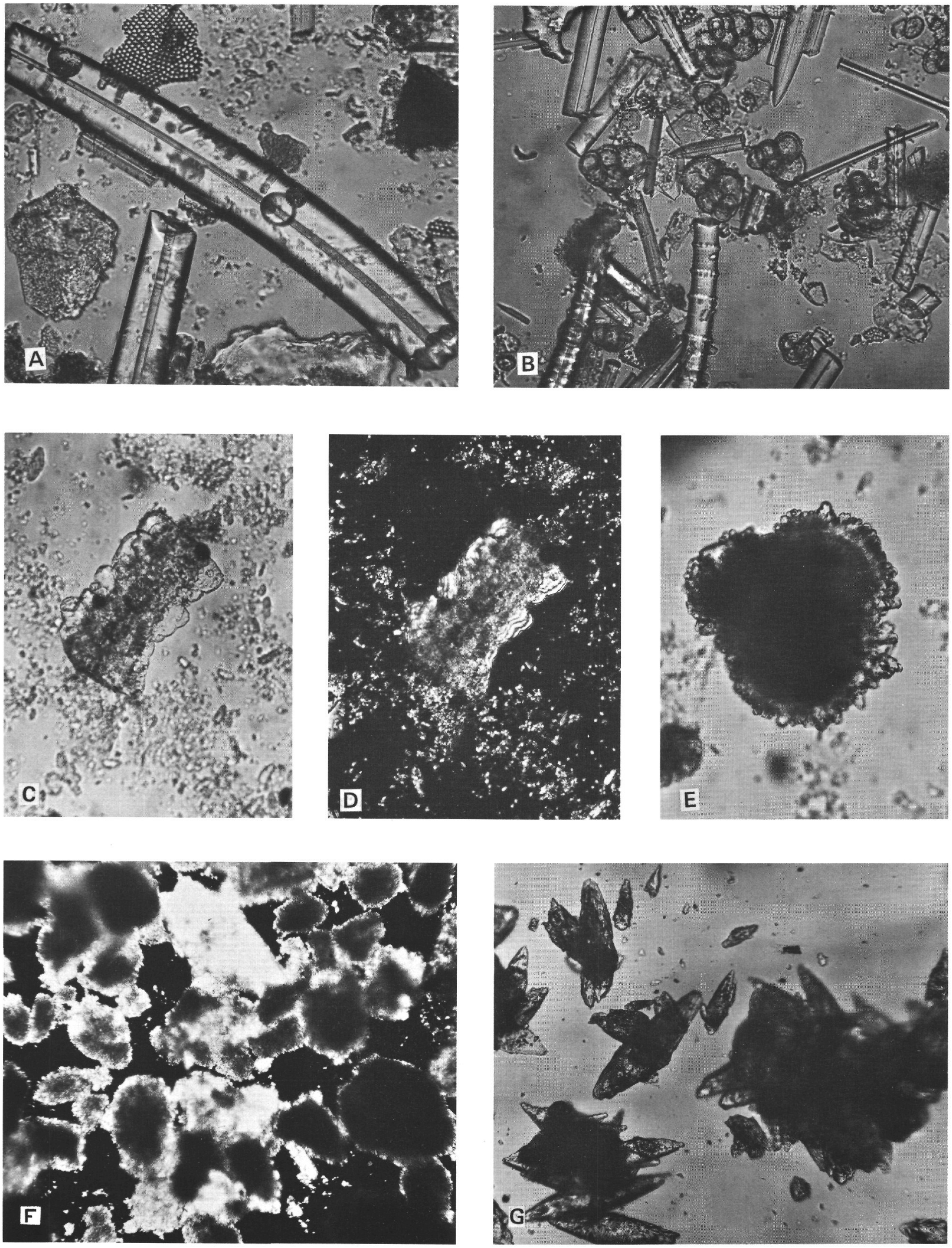

PLATE 18

Thin-sections of limestones.

A — Sample 5-2-1, 29-32 cm (cross-polarized, X 240): Upper Cretaceous calcarenite (probably turbidite) in nannoplankton chalk. Micritic grains (at least in part altered fossils) and grains of single calcite crystals, grown in place (light); pore space black.

B — Sample 5-2-1, 6-9 cm (plain light, X 240): Micritic grains of uncertain origin (dark); skeletal fragments at lower right; dolomite rhomb in upper left corner; two calcite spar grains (light) in center and one on right margin.

C&D — Sample 3-7-1, 109-112 cm (C, plain light, X 53; D, plain light, X 240): Somewhat cemented nannoplankton chalk rich in planktonic foraminifera; Pliocene. Foraminifera in unresolved nannoplankton matrix. The mottling in D suggests the possibility that this nannoplankton chalk consisted initially of faecal pellets of nannoplankton feeders, or was pelleted on the bottom.

E&F — Sample 5A-6, core catcher (E, plain light, X 53; F, plain light, X 240): Cemented radiolarian-rich nannoplankton chalk, from near Jurassic-Cretaceous boundary. Nannoplankton matrix unresolved; Radiolaria have been altered to generally structureless spheres of calcite, but note faintly preserved turret-shaped nasselarian in F.

PLATE 18

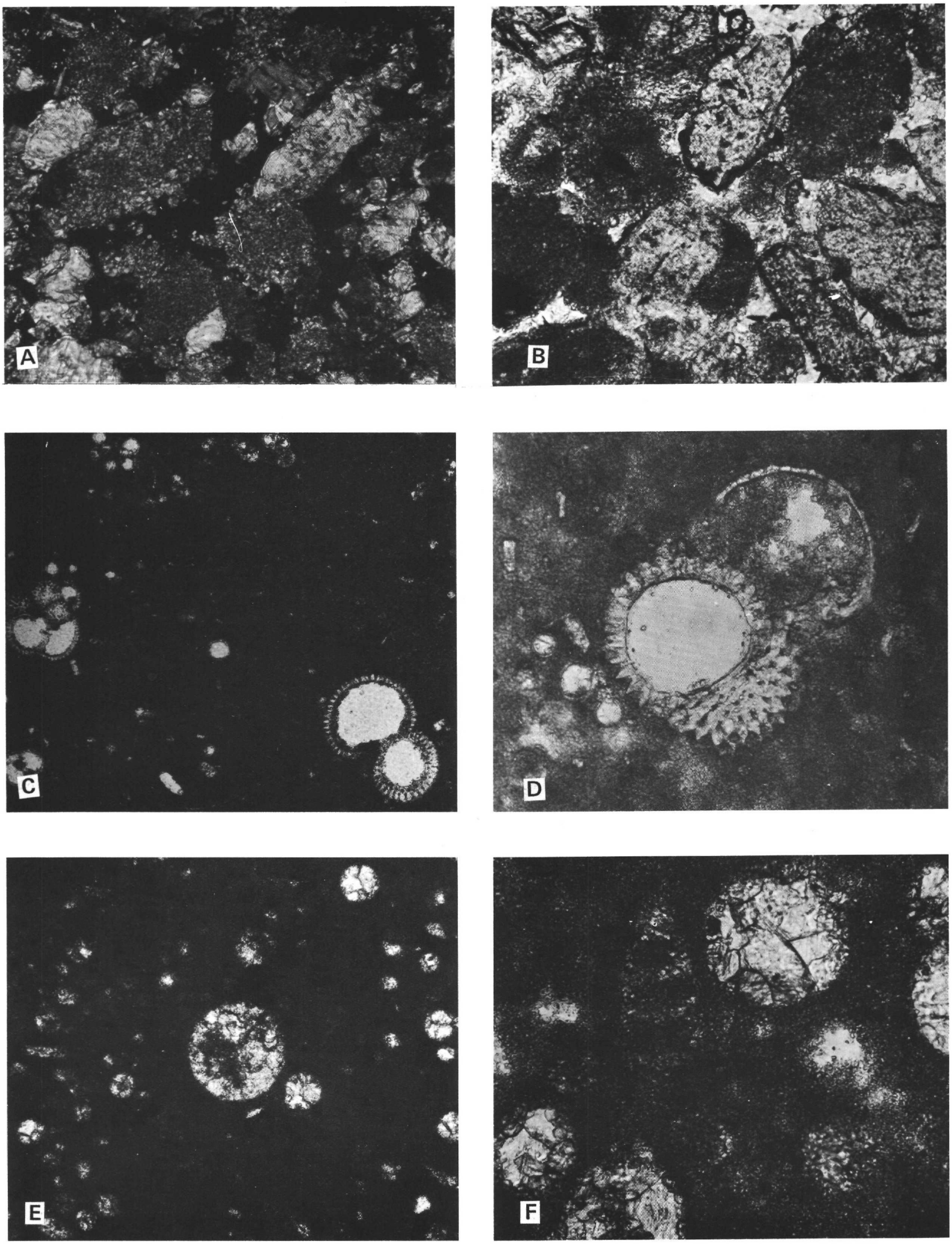

PLATE 19

Radiolarian chert of Cenomanian Age, Sample 5A-2-1, 0-5 cm, in thin-section.

A	A nasselarian radiolarian, chalcedony-filled, in opaline matrix, plain light, X 240.
B	Portion of a radiolarian-rich layer, in which the matrix consists largely of opaline spherules; in this case the pores (clear areas) are open; plain light, X 240.
C	Relict of a radiolarian (spumellarian), outer lining of opaline spherules, cavity filled by chalcedony; plain light, X 240.
D	Relict of a radiolarian (same as C), in cross-polarized light, showing chalcedony sheaves.
E	The chert in plain light, X 10, showing banding with lighter, more radiolarian-rich layers, and darker, organic rich layers of fine-grained opal. Both pore-space and chalcedony-filled areas here appear bright.
F	Identical field, in cross-polarized light, in which pores are dark and only chalcedony-filled spots are bright. Comparison with E shows that some laminae are largely devoid of chalcedony, consisting of opal and open pores, whereas other laminae have had all the coarser pores filled with chalcedony.

PLATE 19

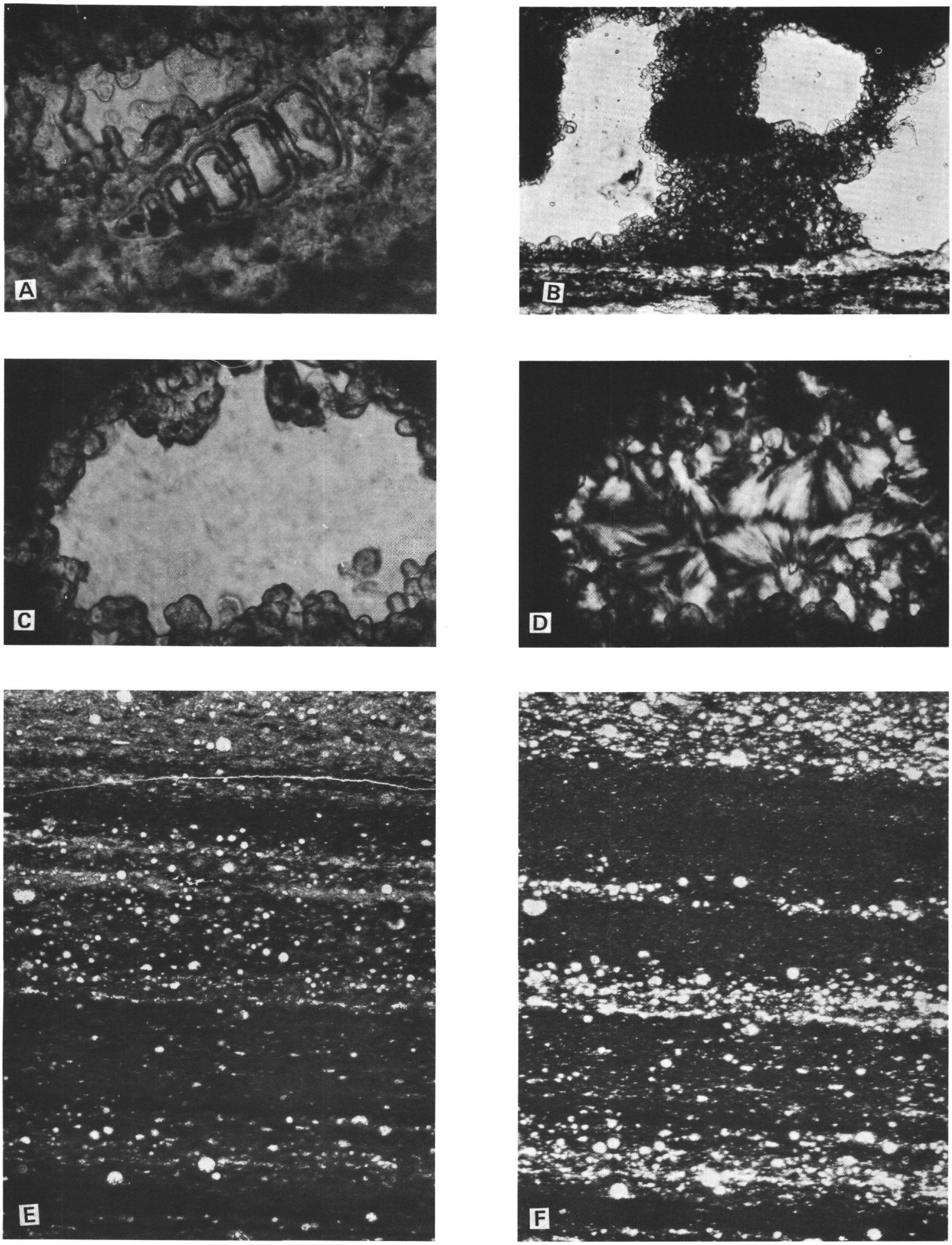

PLATE 20

Thin-sections of silicified Eocene turbidites, Bermuda Rise (Sample 6-6-1).

A Plain light, X 50: Light grains are quartz (angular) and cross-sections of sponge spicules (round). Glauconite grains are round and granular; the dark grains are carbonate (note cross-sections of foraminifera) and pyrite. Matrix is largely opaline silica, with relicts of calcite and flecks of chalcedony.

B Plain light, X 250: A quartz grain is at left, a glauconite grain at right. Cross-sections of sponge spicules show an outer rim of radially oriented length-slow quartz fibers, and a hollow interior (filled in some cases with chalcedony). Cross-sections of foraminifera at bottom and top.

C&D Plain and cross-polarized light, X 250: A quartz grain is at lower left, and a cross-section of a sponge spicule is below it; also, abundant planktonic foraminifera, showing birefringence in polarized light and an echinoderm fragment in upper right.

E&F Plain and cross-polarized light, X 250: In center a fragment of a sponge spicule, with its characteristic marginal mold-filling of fibrous length-slow quartz forming an outer rim, and chalcedony sheaves filling the interior. A quartz grain below, an echinoid spine at upper left (dark in E, light in F). Matrix mainly opaline silica, filled with tiny flecks of chalcedony.

PLATE 20